

This item is the archived peer-reviewed author-version of:

Homogeneous and heterogeneous catalysts for hydrogenation of CO₂ to methanol under mild conditions

Reference:

Bai Shao-Tao, De Smet Gilles, Liao Yuhe, Sun Ruiyan, Zhou Cheng, Beller Matthias, Maes Bert, Sels Bert F.- Homogeneous and heterogeneous catalysts for hydrogenation of CO₂ to methanol under mild conditions
Chemical Society reviews / Chemical Society [London] - ISSN 0306-0012 - 50:7(2021), p. 4259-4298
Full text (Publisher's DOI): <https://doi.org/10.1039/D0CS01331E>
To cite this reference: <https://hdl.handle.net/10067/1785070151162165141>

Homogeneous and heterogeneous catalysts for hydrogenation of CO₂ to methanol under mild conditions

Shao-Tao Bai,^{a,†} Gilles De Smet,^{b,‡} Yuhe Liao,^{a,d} Ruiyan Sun,^a Cheng Zhou,^a Matthias Beller,^{*c} Bert U. W. Maes,^{*b} and Bert F. Sels^{*a}

In the context of a carbon neutral economy, catalytic CO₂ hydrogenation to methanol is one crucial technology for CO₂ mitigation providing solutions for manufacturing future fuels, chemicals, and materials. However, most of the presently known catalyst systems are used at temperatures over 220 °C, which limits the theoretical yield of methanol production due to the exothermic nature of this transformation. In this review, we summarize state-of-the-art catalysts, focusing on the rationales behind, for CO₂ hydrogenation to methanol at temperatures lower than 170 °C. Both hydrogenation with homogeneous and heterogeneous catalysts is covered. Typically, additives (alcohols, amines or aminoalcohols) are used to transform CO₂ into intermediates, which can further be reduced into methanol. In the first part, molecular catalysts are discussed, organized into: 1) monofunctional, 2) M/NH bifunctional, and 3) aromatization-dearomatization bifunctional molecular catalysts. In the second part, heterogeneous catalysts are elaborated, organized into: 1) metal/metal or metal/support, 2) active-site/N or active-site/OH bifunctional heterogeneous catalysts, and 3) cooperation of catalysts and additives in a tandem process *via* crucial intermediates. Although many insights have been gained in this transformation, in particular for molecular catalysts, the mechanisms in the presence of heterogeneous catalysts remain descriptive and insights unclear.

1. Introduction

Global warming and other climate change issues pose significant threats to the Earth's ecosystems and the sustainable development of our civilization.¹⁻⁶ Earth's average surface temperature increased over the past century due to a rapid rise of greenhouse gases, especially CO₂. The growth of harmful CO₂ gas in the atmosphere can be clearly linked to the utilization of fossil resources. Indeed, the CO₂ concentration has increased by more than 45% since the start of the Industrial Revolution, up to a value of 415 ppm in 2019. In 2018, global emission of CO₂ was around 42.1 Gt, of which 36.6 Gt (87%) originated from a fossil resources based energy system and the chemical industry.¹ As a consequence, the rate of temperature rise has nearly doubled in the last 50 years. Keeping the increase in global average temperature this century to well below 2 °C above pre-industrial levels would substantially reduce the risks and impact of climate changes. However, the long-term temperature goal seems far from realization, despite ongoing measurements to mitigate CO₂ emissions worldwide under the Paris Agreement. Note that, for the past centuries, primarily coal and oil were used as fossil resources to produce chemicals and fuels as the main driving force for social development. Substantially reducing the global CO₂ emission is rather difficult and unrealistic based on current industries. As a result, many countries have applied CO₂ capture and storage (CCS)

processes. However, the capacity is limited, for example only around 35 Mt CO₂ is captured from power and industrial facilities (less than 0.1%), and the cost, sustainability, and safety issues of these technologies are also of concern.⁷⁻¹³ Therefore, developing new technologies for CO₂ capture and subsequent conversion of this renewable feedstock into chemicals and fuels to (partially) replace fossil resources is of long term benefit for humankind.

Catalysis is a core technology of the chemical and life science industries producing more than 70,000 products including all kinds of materials and fuels, hereby providing us a better quality of life in every aspect. Fossilization of biomass, which is produced *via* photosynthesis using solar energy, has provided us with cheap and abundant coal, gas and oil, creating the basis for global development since the Industrial Revolution. Current catalysis technologies have been largely directed to convert these feedstocks into valuable fuels and chemicals (Figure 1, see the black dotted-arrows). With increasing globalization, huge amounts of goods and energy are produced and consumed with a continuously increasing demand. This poses a double problem, namely depletion of limited fossil resources produced by nature over millions of years and concomitantly increasing CO₂ emissions by fossil resources based industries contributing

^a Center for Sustainable Catalysis and Engineering, KU Leuven, Celestijnenlaan 200F, 3001 Heverlee, Belgium.

^b Division of Organic Synthesis, Department of Chemistry, University of Antwerp, Groenenborgerlaan 171, B-2020 Antwerp, Belgium

^c Leibniz Institute for Catalysis, Rostock, Albert-Einstein-Strasse 29a, Germany

^d Present Address: Guangzhou Institute of Energy Conversion, Chinese Academy of Sciences, Guangzhou 510640, PR China.

*Emails: bert.sels@kuleuven.be (B.F.S.); Matthias.Beller@catalysis.de (M.B.); bert.maes@uantwerpen.be (B.U.W.M).

[†] S.-T. B. and G. D. S. contribute equally to this review manuscript.

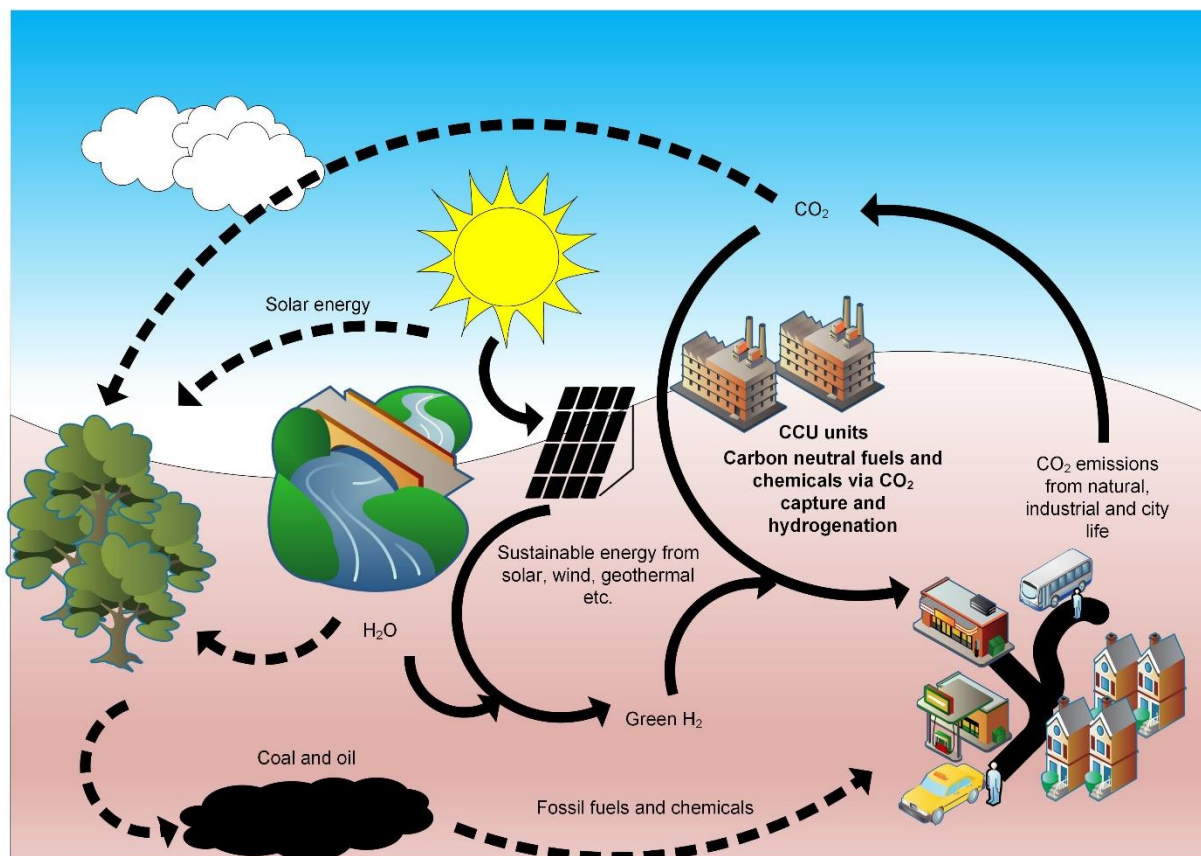
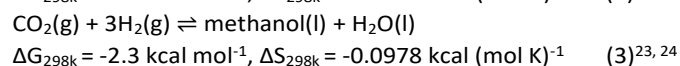
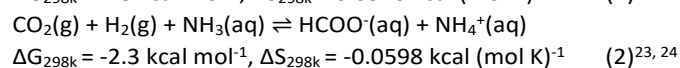
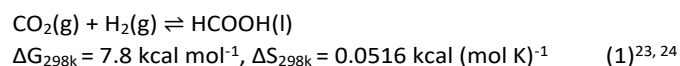


Figure 1 General concept of a future sustainable carbon neutral cycle (black arrows) based on hydrogenation industries vs. current carbon cycle (black dotted-arrows) via fossil resources based industries.

to global warming, and thus calls for renewable solutions. Development of new catalysis technologies for renewable carbon-neutral fuels, chemicals and materials is a solution towards mitigation of the CO₂ emission problem and foreseen fossil resources crisis (Figure 1, see the black arrows). In this carbon neutral scenario, CO₂ will be captured and converted to fuels, chemicals, and materials - directly at the site of emissions or at a remote site from the air using CO₂ capture and utilization (CCU) technologies - based on, for example, hydrogenation reaction technologies. In principle, green H₂ can be obtained from water using photocatalysis or electrolysis with green electricity, originated from solar, wind, atom, hydro- and geothermal energy. Such technology has been installed in China at pilot scale using sunlight energy.¹⁴ The North-C-Methanol project with a methanol production capacity of 45,000 ton methanol per year has been initiated in Flanders, Belgium.¹⁵ Furthermore, recycling rather than storage of CO₂ is more attractive provided that economically feasible catalysis technologies are available for CO₂ conversion to value-added chemicals and fuels such as formic acid/formate and methanol. CO₂ reduction to methanol *via* hydrosilylation and hydroboration using expensive silanes^{16, 17} and boranes¹⁸⁻²⁰ has been investigated by Guan, Hazari, Ying, and others. Though very interesting from a fundamental point of view such technologies are less attractive on larger scale. Electrochemical reduction of CO₂ is a more realistic possibility to generate methanol using copper based electrodes, however remains still

limited by issues such as rather low faradaic efficiencies, low current density, and high overpotentials.^{21, 22}



Hydrogenation reactions have been intensively investigated and are applied in many industrial transformations, involving the reduction of e.g. nitro, carboxylic acid, amide, nitrile, urea, ester, ketone, and alkene functionalities.²⁵⁻³⁰ In the context of CO₂ hydrogenation, catalysts for its reduction to formic acid has reached high activity (> 1,000,000 h⁻¹ TOF), productivity (> 3,500,000 TON), stability and selectivity for potential applications.³⁰⁻³⁴ However, though thermodynamically favored (equation 3), catalytic CO₂ hydrogenation to methanol is more difficult due to complicated mechanisms with kinetic and compatibility challenges of this transformation. Comparing CO₂ hydrogenation to formic acid with to methanol, the latter is thermodynamically favored due to the concomitant production of water (equations 1-3). Importantly, catalytic reduction of CO₂ with H₂ to methanol can, besides environmental benefits, also generate considerable economic advantages. In fact, 140 million tons of methanol were produced in 2018 and its production is expected to double by 2030.³⁵ Methanol is also

used to synthesize important other chemicals such as methyl *tert*-butyl ether and dimethyl ether.³⁶ These are alternatives for gasoline but methanol can also directly be used as a transportation fuel.³⁷ Besides *via* catalytic oxidation formaldehyde is obtained, with major applications in the resin business³⁸. Furthermore, coupling this technology to methanol converting technologies, i.e. well-developed acidic zeolite catalysts for MTO (methanol-to-olefins) and MTG (methanol-to-gasoline) processes, a variety of bulk chemicals such as aromatics and fuels can be provided.^{39, 40} In this context, conventional Cu based heterogeneous catalysts have been intensively applied to convert CO₂ to methanol by hydrogenation reactions.⁴¹⁻⁴⁵ However, these reactions are generally conducted at high temperatures (> 220 °C) which limits the theoretical yield due to the exothermic nature of this reaction and also leads to deactivation by catalyst sintering.^{46, 47} Recently, Zhang⁴¹ and Chen⁴⁸ reviewed CO₂ hydrogenation to methanol using heterogeneous catalysts under typical high temperature conditions. In 1993, Saito and co-workers^{49, 50} reported the first molecular complex Ru₃(CO)₁₂-KI for CO₂ hydrogenation to methanol, which was performed at 240 °C, resulting in a distribution of methanol, CO and methane *via* reverse water-gas shift reaction (RWGSR). Therefore, rational optimization of catalysts for selective CO₂ hydrogenation to methanol under mild process conditions remains a challenging and contemporary research subject. In this review, optimized molecular and heterogeneous catalysts for catalytic CO₂ hydrogenation to methanol under milder conditions (< 170 °C) will be summarized and discussed. Particularly, the gained mechanistic insights of these catalytic systems will be highlighted and analyzed, including the drawbacks and remaining challenges. Note that an additive is often used in (super)stoichiometric or catalytic amounts, transforming CO₂ in the presence/absence of H₂ *via* one pot⁵¹, one pot two steps, or two steps⁵² into beneficial intermediates, which are finally reduced into methanol.

2. Optimization of molecular catalysts

Molecular catalysts generally show high activity in CO₂ hydrogenations under relatively mild reaction conditions and have therefore received significant attention. However, compared to the conversion of CO₂ to formic acid, its conversion to methanol involves further hydrogenation steps, involving many intermediates, including formic acid, formates (formed in the presence of base or alcohol additives), formamides (formed in the presence of amine additives), methanediol (= formaldehyde hydrate) and formaldehyde, as well as possible CO. Hydrogenation of the C=O group in formic acid, formates, and formamides is more challenging than in ketones or aldehydes, in accordance with their lower electrophilicity due to lone pair electron density delocalization.^{53, 54} Hydricity of a metal-hydride (M-H) determines the thermodynamic potential of a hydride transfer ($\Delta G^\circ_{\text{H}^-}$) to the C=O bond and is highly influenced by solvents, ligands and additives (Brønsted and Lewis acids).⁵⁵ Hydrogenation of formic acid, formates and formamides intermediates requires a metal hydride species

with higher hydricity than necessary for the initial hydrogenation of CO₂. Furthermore, stabilization of transition states to reduce activation energies is required to realize catalytic transformations under milder reaction conditions. Avoiding the formation of stable resting state complexes and off cycle catalytic species also requires consideration. Tolerance of catalysts towards complex reaction conditions is another tricky issue, including catalyst deactivation or incompatibility to acidic, basic or other additives, anionic formate and carbonic acid intermediates, as well as CO. For these reasons, only a limited number of metal complexes, including iron⁵⁶, cobalt⁵⁷⁻⁵⁹, manganese^{60, 61}, and ruthenium⁶²⁻⁶⁷, have shown activity in CO₂ hydrogenation to methanol under mild conditions. Interestingly, to the best of our knowledge, molecular rhodium and iridium based metal complexes, generally highly active in CO₂ hydrogenation to formic acid, do not show observable activity for methanol formation under similar conditions.^{31, 34, 68, 69} The latter might be due to possible competition reactions with formic acid such as its dehydrogenation/dehydration or disproportionation.⁷⁰⁻⁷² The latter has been reported for iridium catalysts in an attempt to hydrogenate CO₂ to methanol. Below molecular catalysts reported in CO₂ hydrogenation to methanol under mild conditions are discussed. The field will be

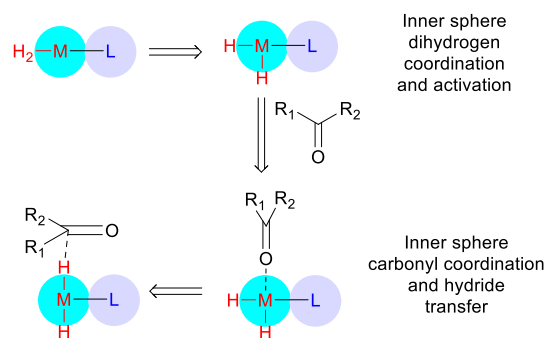
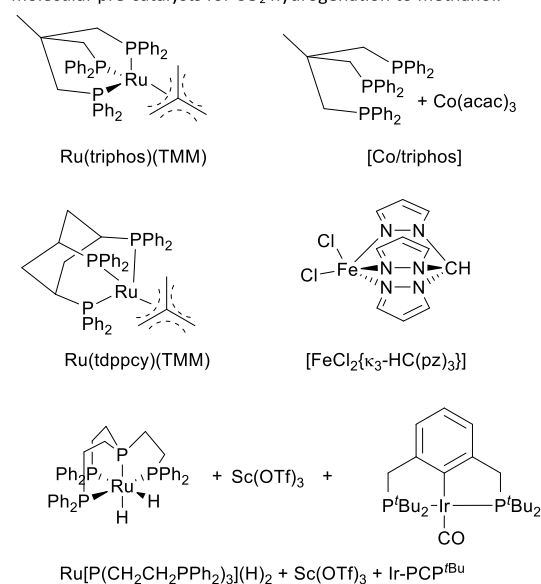


Figure 2 Monofunctional molecular catalysts in dihydrogen activation and hydride transfer steps.

Chart 1 Chemical structures of representative monofunctional molecular pre-catalysts for CO₂ hydrogenation to methanol.



subdivided into three sections based on the mode of action of the molecular catalyst applied: 1) monofunctional, 2) M/NH bifunctional, and 3) aromatization-dearomatization bifunctional molecular catalysts.

2.1. Monofunctional molecular catalysts

Figure 2 shows the crucial steps, i.e. the H₂ coordination, H₂ activation, and hydride transfer steps taking place on the metal center (inner sphere mechanism), for hydrogenation of the C=O bond using typical monofunctional molecular catalysts.⁷³⁻⁷⁷ Generally, diphosphine based metal complexes show activity in hydrogenation reactions of aldehydes/ketones, albeit with low turnover efficiencies, as reflected in the use of ~1 mol% catalyst loadings.⁷⁸⁻⁸² These complexes are not active enough in the hydrogenation of CO₂ to methanol. Tridentate ligands can enable a higher electron density on the metal center than obtained with bidentate ligands, thereby enhancing the

hydricity⁵⁵ of the formed metal-hydride species. This boosted hydricity of metal-hydride species can, in principle, facilitate hydride transfer to the carbonyl groups of CO₂ and its derived intermediates, finally resulting in the formation of methanol. Indeed, metal complexes with tridentate ligands are reported in the hydrogenation of challenging ester, carbonate, and even carbonic acid and amide functionalities.⁸³⁻⁹¹ Privileged tridentate ligands used in hydrogenation reactions are triphos [= 1,1,1-tris(diphenylphosphinomethyl)ethane]⁹², conformationally less flexible tdppcy [= *cis,cis*-1,3,5-tris(diphenylphosphino)cyclohexane]⁹³, and pyrazole based HC(pz)₃ [= tris(pyrazolyl)methane]⁹⁴. Chart 1 shows the structures of some tridentate-metal complexes featuring these ligands and Table 1 summarizes their catalytic performance for CO₂ hydrogenation to methanol. Figure 4 shows the performance of some representative catalysts over a long reaction time.

Table 1 Monofunctional molecular hydrogenation catalysts for CO₂ to methanol conversion

Entry	Pre-catalyst	solvent	additives	P _{H₂/CO₂} (bar)	T/°C	t/h	TOF ^b / (h mol) ⁻¹	TON ^c	Ref.
1	Ru(triphos)(TMM)	THF/ MeOH	HNTf ₂	60/20	140	24	70	221	62, 63
2	[Co/triphos]	THF/ EtOH	HNTf ₂	70/20	100	96	~1	78	57, 58
3	Ru(tdppcy)(TMM)	EtOH	Al(OTf) ₃	90/30	120	20	458	2148	95
4	[FeCl ₂ {κ ³ -HC(pz) ₃ }]	-	PEHA ^a	56/19	80	36	66	2387	56
5	Ru[P(CH ₂ CH ₂ PPh ₂) ₃](H) ₂ , Sc(OTf) ₃ , Ir-PCP ^{tBu}	EtOH	-	80/10	155	40	10.7	428	96

^a PEHA: pentaethylenhexamine. ^b TOF: turnover frequency (an average TOF was calculated if no initial TOF was reported). ^c TON: turnover number. TMM: trimethylenemethane.

Leitner^{62, 63} and co-workers investigated Ru(triphos)(TMM) as the first monofunctional molecular catalyst for CO₂ hydrogenation to methanol with HNTf₂ as additive in THF (Table 1, entry 1). This catalyst showed high selectivity and good activity, i.e. a TON of 258 and 603 after 16 and 50 h respectively, under optimized conditions, i.e. 60 bar of H₂ and 20 bar of CO₂ at 140 °C (Figure 4). The initial turnover frequency (TOF) of 70 h⁻¹ is in the range of the activity of the state-of-the-art heterogeneous Cu/ZnO-based catalysts^{41, 97}. The catalyst also showed reasonable stability with decarbonylation of

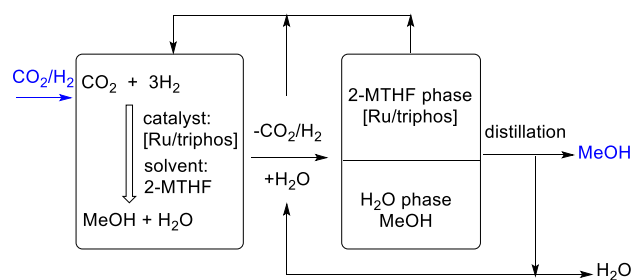


Figure 3 Concept of a biphasic system for CO₂ hydrogenation to methanol with integrated product separation by distillation (2-MTHF: 2-methyltetrahydrofuran). Ref. 63.

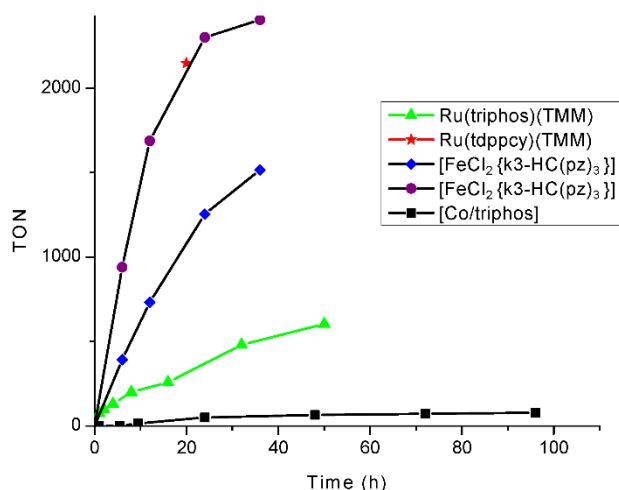


Figure 4 Performance of reported monofunctional molecular catalysts in CO₂ hydrogenation to methanol. Reactions conditions: [Co/triphos], H₂ (70 bar), CO₂ (20 bar), 100 °C; Ru(triphos)(TMM), H₂ (60 bar), CO₂ (20 bar), 140 °C; Ru(tdppcy)(TMM), H₂ (90 bar), CO₂ (30 bar), 120 °C; [FeCl₂{κ³-HC(pz)₃}], H₂ (56 bar), CO₂ (19 bar), 80 °C, pentaethylenehexamine (PEHA) = 3.4 mmol, if applied. Refs: 56, 57, 62, 63, 95.

intermediates and dimerization into [Ru₂(μ-H)₂(triphos)₂] as potential deactivation pathways over a long reaction time. Recycling of the catalyst was also possible in an aqueous biphasic system 2-MTHF/water, indicating the potential for a continuous-flow operation (Figure 3). Though conceptually very interesting, the TON halved over 4 cycles showing further optimization is still required.

Later, Leitner⁶³ and co-workers studied the mechanism of this Ru(triphos)(TMM) catalyzed CO₂ reduction to methanol reaction by *in situ* FT-IR, NMR, X-ray spectroscopy and DFT calculations. Scheme 3 shows the general catalytic cycle involving formation of a molecularly-defined cationic Ru complex from Ru(triphos)(TMM). Three crucial stages can be identified: 1) formic acid stage, 2) aldehyde stage, and 3) methanol stage. In the formic acid stage, CO₂ coordinates to the Ru metal *via* oxygen and a cationic Ru-formate complex [Ru(triphos)(κ²-O₂CH)(s)]⁺ (s = solvent) is then formed through hydride migration to the bound CO₂ molecule. The transition state barrier **I_II-TS** is 21.2 kcal mol⁻¹ with respect to the starting cationic complex **I**. Compared to species further in the catalytic cycle, the cationic Ru-formate complex [Ru(triphos)(κ²-O₂CH)(s)]⁺ (s = solvent) is energetically low lying (-3.2 kcal mol⁻¹ with respect to **I**) and therefore a crucial resting state complex of the catalytic cycle. *In situ* NMR spectroscopic studies revealed

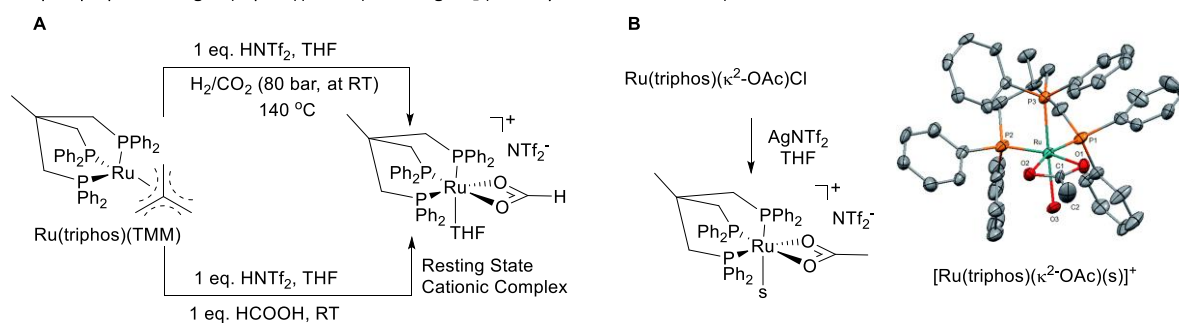
that this cationic resting state Ru-formate complex can be obtained from readily available catalyst precursor Ru(triphos)(TMM) and formic acid. Scheme 1 shows the preparation of the resting state complex using CO₂/H₂ or formic acid as reactants in a reaction with Ru(triphos)(TMM). X-ray and chemical structure of a similar cationic carboxylate complex prepared using Ru(triphos)(κ²-OAc)Cl and AgNTf₂ is also shown in Scheme 1.

At the aldehyde stage, the formate is further hydrogenated through a series of hydride transfer and protonolysis steps into formaldehyde within the coordination sphere of the ruthenium center. The highest barrier **II_III-TS** in this stage is 29.8 kcal mol⁻¹ with respect to the starting complex **I**, which is also the highest transition state barrier of all steps. Scheme 3 also shows the structure of this transition state complex, of which a hydride migrates from the Ru metal to the carbonyl group of the associated formic acid molecule. Importantly, the barrier **III_IV-TS** in the protonolysis steps is 27.1 kcal mol⁻¹ with respect to the starting complex **I** thanks to the assistance of carboxylate acid *via* hydrogen bonding interactions, indicating a similar enhancement for formic acid formed under reaction conditions. This step involves the cleavage of a C-O bond and the generation of formaldehyde from methanediol by protonolysis. The carboxylic acid-assisted protonolysis step shows a significantly lower barrier than the non-assisted protonolysis step in methanediol conversion to formaldehyde.

In the stage of formaldehyde hydrogenation to methanol, i.e. methanol stage, the highest reaction barrier is the hydride transfer step. The barrier **IV_V-TS** is 27.3 kcal mol⁻¹ with respect to the starting complex **I**. Again, protonolysis steps of this stage can lower barriers thanks to the assistance of a carboxylic acid *via* hydrogen bonding interactions.

The facial coordination of the triphos ligand probably imposes a favourable geometrical arrangement for hydride transfer to the carbonyl units in all the three stages next to the increased hydricity of the Ru-hydride originated from the tridentate coordination of the triphos ligand. Furthermore, hydrogen bonding interactions seem to play a crucial role in the hydrogenation of CO₂ beyond the formic acid stage reducing TS energy levels. Note that, inspired by enzyme catalysis, the beneficial effect of hydrogen bonding and carboxylate/carboxylic acid assistance have been demonstrated

Scheme 1 Synthesis of A) the resting state cationic Ru-formate complex from catalyst precursor Ru(triphos)(TMM) in the presence of 1 eq. HNTf₂ under H₂/CO₂ pressure (upper pathway) or by the addition of 1 eq. HNTf₂ and 1 eq. HCO₂H (lower pathway), and B) a similar cationic Ru-carboxylate complex prepared using Ru(triphos)(κ²-OAc)Cl and AgNTf₂ (with crystal structure shown). Ref. 63.

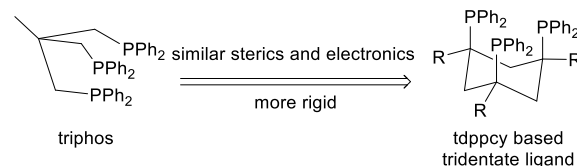


in asymmetric hydrogenation, hydroformylation and C-H bond activations.⁹⁸⁻¹⁰²

Triphos ligand based molecular catalysts were further extended from ruthenium to cobalt metal by Beller⁵⁷ and co-workers. It was initially demonstrated by de Bruin¹⁰³ and co-workers that [Co/triphos] can reduce esters and carboxylic acids to alcohols. As expected, [Co/triphos] displayed interesting results in CO₂ hydrogenation with a methanol selectivity higher than 97%, though a low stability and productivity (TON 78 after 96 h) were observed under mild reaction conditions (70 bar of H₂, 20 bar of CO₂, 100 °C, Table 1, entry 2, Chart 1, and Figure 4). Figure 4 shows severe deactivation of catalyst [Co/triphos] over a longer reaction time, where the catalytic activity completely vanishes after 48 h. Characterization of the formed cobalt complexes by high-resolution electrospray ionization mass spectrometry and *in situ* high pressure (HP) phosphorus NMR spectroscopy suggested that the reaction follows an inner-sphere mechanism

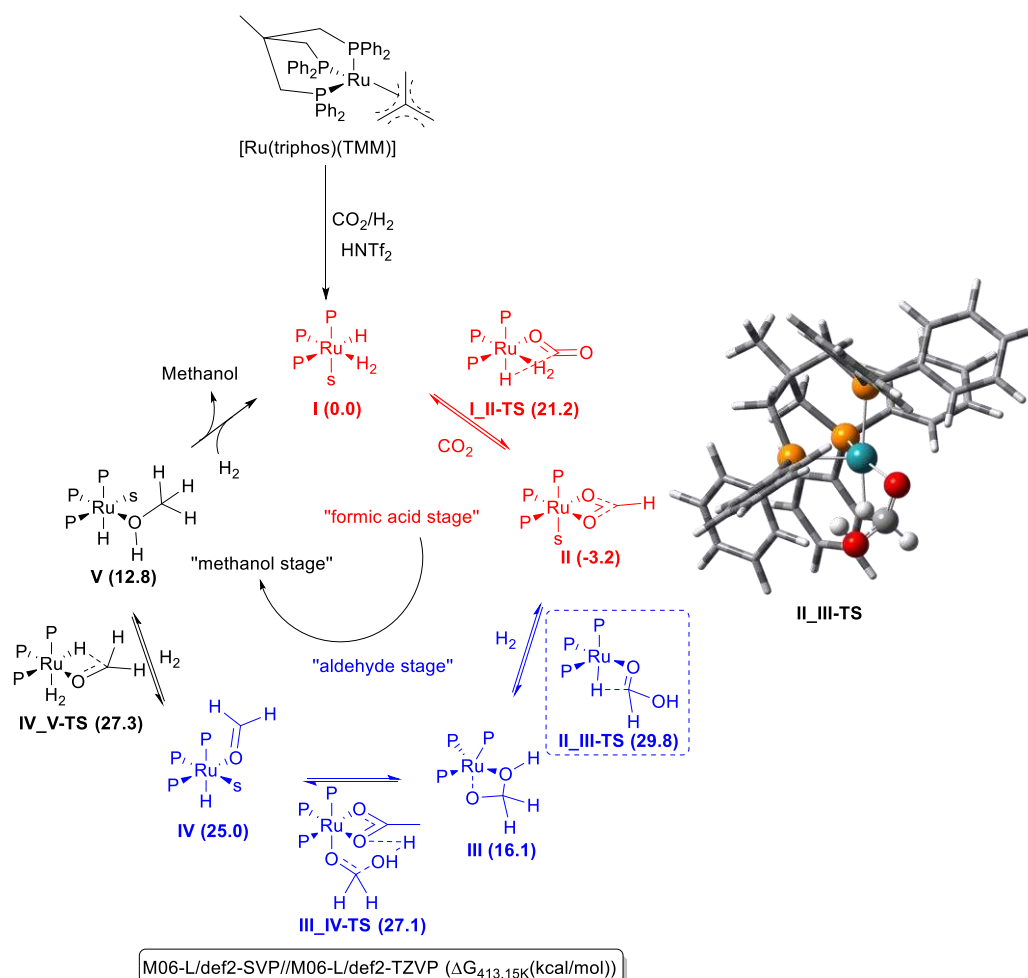
catalyzed by a cationic [Co/triphos] complex, likely similar to Ru(triphos)(TMM).

Scheme 2 Development of tridentate tdppcy ligand for CO₂ hydrogenation to methanol. Ref. 95.



In order to improve the performance of [Co/triphos], Beller⁵⁸ and co-workers synthesized [Co/triphos] derivatives and investigated the influence of metal precursors, acid additives and substituents on the triphos ligand with the variation of electronic and steric properties. However, there was no significant improvement compared to [Co/triphos] complex in terms of productivity and stability. Interestingly, water, methanol product, and CO side-product showed strong

Scheme 3 General mechanism of the Ru(triphos)(TMM) catalyzed CO₂ hydrogenation to methanol via formic acid stage, aldehyde stage and methanol stage.



All the ruthenium complexes involved in the catalytic cycle are cationic species with charge +1. The triphos ligand that coordinates to the ruthenium metal centre is simplified as P in the chemdraw structures. s refers to a solvent molecule. The free energy values are versus complex I. II_III-TS: Ruthenium metal, phosphorus, hydrogen, carbon, and oxygen atoms are shown in green, yellow, white, grey, and red colour balls, respectively. III_IV-TS: acetic acid was used as model for the carboxylate units as proton shuttles. Details see ref. 63.

inhibitory effects to the [Co/triphos] catalytic system under the reaction conditions.

Blankmeyer⁹⁵ recently reported on the use of Ru(tdppcy)(TMM), a rigid version of Ru(triphos)(TMM), with similar electronics and sterics but using a conformationally more restricted cyclohexane backbone (Chart 1 and Scheme 2). This new molecular catalyst showed much higher productivity and activity, i.e. TON > 2000 in 20 h with an average TOF of 458 h⁻¹ (90 bar of H₂, 30 bar of CO₂, 120 °C), compared to Ru(triphos)(TMM) and Co(triphos)(TMM) (Table 1, entries 1-3, Chart 1 and Figure 4). This is one of the most active molecular complexes reported to date for CO₂ reduction to methanol operating under rather mild reaction conditions. Furthermore, Ru(tdppcy)(TMM) can operate with high activity and stability in a biphasic solvent system consisting of water and long-chain alcohols (*vide infra*). These experiments yielded a methanol concentration of roughly 2.5 M in the aqueous phase, showing applicative potential.

Besides phosphorus, also nitrogen based ligands have been studied. The nitrogen based tridentate HC(pz)₃ has been used by Pombeiro and co-workers⁵⁶ to synthesize an iron molecular catalyst [FeCl₂{κ³-HC(pz)₃}. This complex showed high productivity and activity, i.e. 2283 TON with 95 h⁻¹ TOF, for CO₂ hydrogenation to methanol under very mild reaction conditions (80 °C, total pressure of 75 bar of CO₂ and H₂ with 1:3 ratio, 24 h of reaction time, Table 1, entry 4, Chart 1 and Figure 4). The N atoms of its pyrazolyl rings can possibly promote the heterolytic cleavage of H₂, which is one of the key catalytic steps in hydrogenation reactions. Interestingly, this catalyst showed a much higher TON in the presence of pentaethylenhexamine (PEHA), indicating the involvement of other intermediates, i.e. formamides, in the hydrogenation process. In the absence of amines, the methanol yields decreased significant, i.e. from around 45% (24 h reaction time) to 30% (36 h reaction time) and carbon efficiency was halved (max 86% to 41%). Unfortunately, following the reaction over time showed a clear catalyst deactivation after 24 h, at which the conversion dropped below 50%. Regarding the cost of first row transition metal based catalysts, [FeCl₂{κ³-HC(pz)₃}] is an interesting alternative to noble metals such as ruthenium for CO₂ hydrogenation. A full understanding of the reaction mechanism will be of interest to further improve the catalyst stability and efficiency.

Using a cascade catalysis approach by stepwise formation and conversion of formic acid and formate ester intermediates,

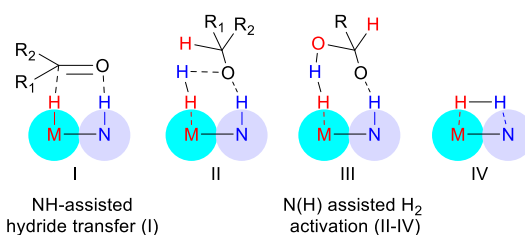


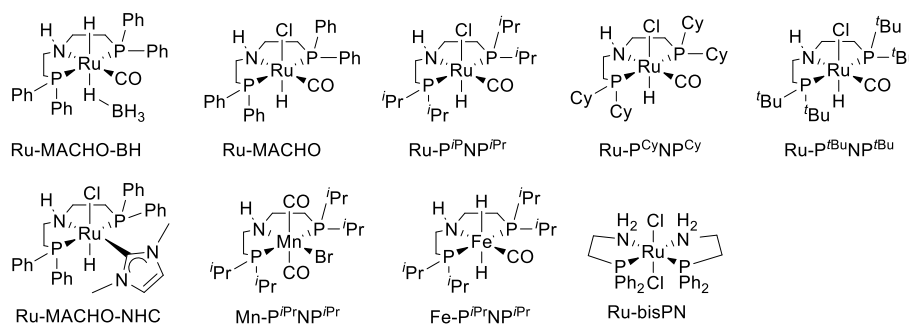
Figure 5 M/NH bifunctional molecular catalysts in crucial hydride/proton transfer and dihydrogen activation steps.

Goldberg⁹⁶ and co-workers reported the combination of Ru[P(CH₂CH₂PPh₂)₃](H)₂, Sc(OTf)₃, and Ir-PCP^{tBu} complexes in a one pot CO₂ to methanol hydrogenation process with a TON of 428 after 40 h at 155 °C (Table 1, entry 5, and Chart 1). Ru[P(CH₂CH₂PPh₂)₃](H)₂ catalyzed the formation of formic acid from hydrogenation of CO₂, followed by formic acid transformation to ethyl formate (with EtOH) catalyzed by Sc(OTf)₃. Finally, formate was reduced to methanol by Ir-PCP^{tBu} catalysis. A side reaction that generates CO inhibits the catalyst activity of Ru[P(CH₂CH₂PPh₂)₃](H)₂, and, to a lesser extent, of Ir-PCP^{tBu}, hereby limiting the overall TON of the catalytic system indicating the challenging nature of this approach.

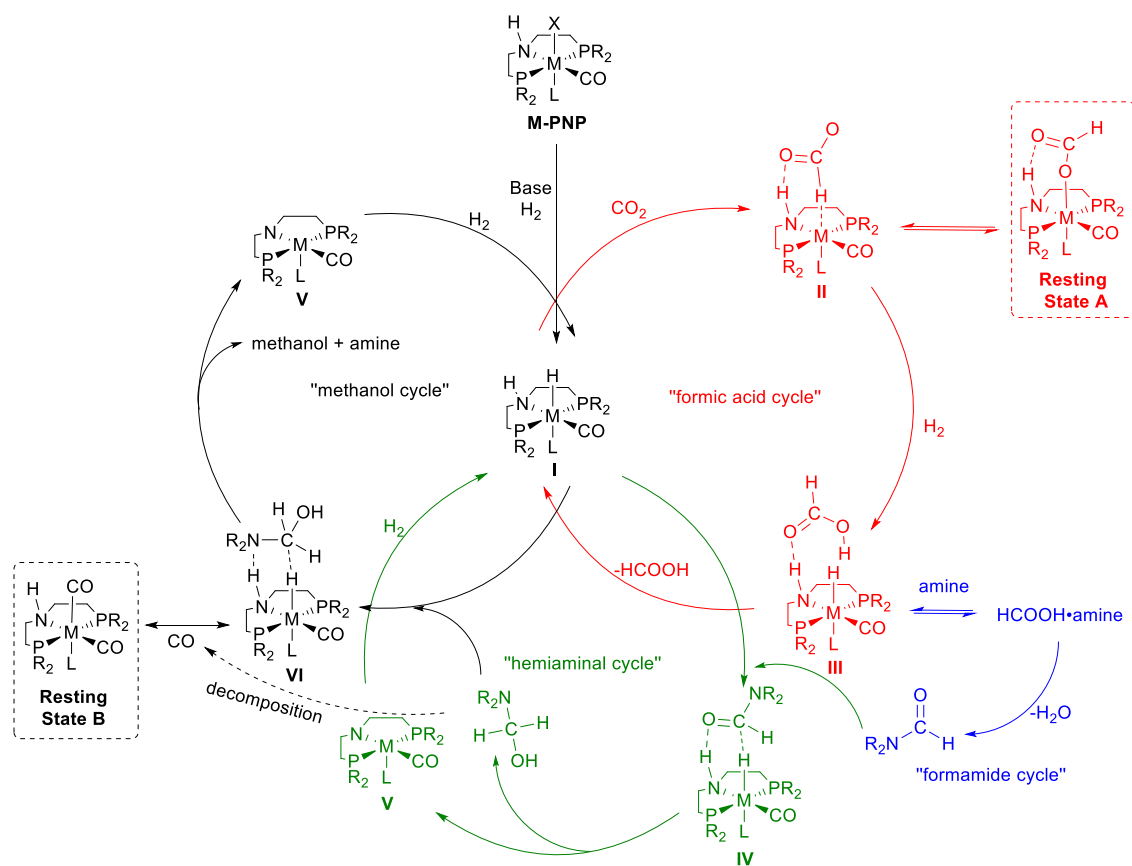
2.2 Metal/NH bifunctional molecular catalysts

In 1995, Noyori and co-workers disclosed an activity enhancement of chiral diamine ligands on the enantioselective hydrogenation of ketones with a Ru-BINAP system (BINAP: 2,2'-bis(diphenylphosphino)-1,1'-binaphthyl) under basic conditions, i.e. in the presence of KOH.^{104, 105} Noyori, Ikariya^{53, 106-109} and co-workers subsequently developed a series of phosphine-free Ru/NH bifunctional catalysts for (asymmetric) (transfer) hydrogenation of ketones, aldehydes, carboxylic and carbonic acid derivatives. These Ru/NH type catalysts showed remarkable activity compared to traditional monofunctional molecular catalysts. Mechanistic studies revealed the bifunctional properties of the catalyst, i.e. cooperation of the NH function of the non-innocent ligand and the Ru metal, thereby rationalizing the unusual high activity in (asymmetric) hydrogenation reactions at ambient temperature.^{53, 104, 106, 110-112} The catalytic cycle involves both an amidoruthenium complex and the coordinatively saturated hydrido(amine)ruthenium complex. Inspired by this pioneering research work, M/NH bifunctional hydrogenation catalysts have been extended to other metals (Mn, Fe). Simplified ligands based on P,N bidentate and P,N,P tridentate ligands¹¹³⁻¹¹⁷, such

Chart 2 Chemical structures of explored molecular M/NH bifunctional catalysts for CO₂ hydrogenation to methanol.



Scheme 4 General mechanism of M/NH bifunctional pincer type molecular complexes catalyzed CO₂ hydrogenation to methanol involving an amine additive via formic acid cycle, formamide cycle, hemiaminal cycle and methanol cycle.



as 2-(diphenylphosphino)ethylamine (PN), bis[2-(diphenylphosphino)ethyl]amine (MACHO), bis[2-(di-*tert*-butylphosphino)ethyl]amine (*P*^{*t*Bu}*NP*^{*t*Bu}), bis[2-(dicyclohexylphosphino)ethyl]amine (*P*^{*CV*}*NP*^{*CV*}) and bis[2-(diisopropylphosphino)ethyl]amine (*P*^{*iPr*}*NP*^{*iPr*}), have been developed (Chart 2). Some of these catalysts have been applied in the CO₂ hydrogenation to methanol processes (Table 2). Note that in many cases additives are used to form more reactive intermediates, which are further reduced to methanol. Typically amines are added delivering formamides, but also other additives have been reported such as epoxides forming carbonates. The NH function cooperates with the metal center in M/NH bifunctional catalysts assisting molecular dihydrogen activation and hydride/proton transfer (Figure 5). Importantly, as amines are generally applied in CO₂ capture processes, M/NH bifunctional catalysts offer great benefits in integrated CO₂ capture and conversion to methanol processes.

The general mechanism of M/NH bifunctional catalysts in CO₂ hydrogenation to methanol with an amine as additive can be divided into four cycles (Scheme 4).^{60, 61, 82, 107, 118-123} Three cycles involve a metal catalyst, i.e. the formic acid, hemiaminal and methanol cycle, and in the fourth cycle amines react with formic acid providing formamides, i.e. the formamide cycle. In the formic acid cycle, the hydride transfer to CO₂ is facilitated by the NH functionality *via* N-H...O hydrogen bonding interactions. The amino group also assists the crucial heterolytic activation of H₂ by placing carboxylate anions close to the metal center. The

formic acid cycle is connected to the formamide cycle through formation of a stable ammonium formate salt, which is the thermodynamic driving force of the formic acid cycle. The formate salts are converted to formamides typically under thermal conditions by an amine assisted condensation reaction.²³ In the hemiaminal cycle, as amide compounds are very stable and less reactive to metal-hydrides than CO₂ and formaldehyde, the barrier of hydrogenation of formamide to hemiaminal is the highest among the four cycles. Importantly, the N-H functionality can assist the hydride/proton transfer steps, hereby lowering energy barriers. In the methanol cycle, the hydrogenation of hemiaminal to methanol is rather straightforward as also shown in the hydrogenation of carbamate and urea derivatives by Ru-MACHO and similar pincer complexes^{53, 124-131}.

Scheme 4 shows two key **resting state complexes A** and **B**. The formation of metal-formate complex **A** *via* metal-hydride transfer to CO₂ followed by rearrangement in **II** with a small energy barrier is thermodynamically favored due to both metal-oxygen bonding and N-H...O hydrogen bonding interactions. In contrast, reaction energy barriers in formamide formation and its further hydrogenation are significantly higher. Therefore, **resting state A** formed in the early stage of the reaction can slow down the production of formic acid and the further hydrogenation *via* formamide into methanol.¹³² **Resting state B** is formed by coordination of CO possibly formed from hemiaminal *via* the known formaldehyde decomposition

route¹³³. **Resting state B** can be reactivated by H₂ and therefore this issue can possibly be solved by using a higher H₂ pressure, and/or avoiding the formation of CO by optimization of the catalytic system and reaction conditions.

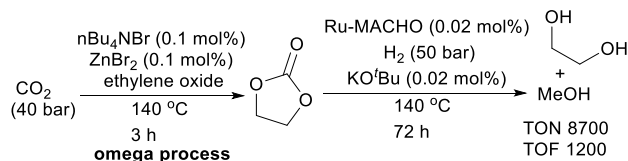
Table 2 M/NH bifunctional molecular catalysts for CO₂ hydrogenation to methanol

Entry	Catalyst	Solvent	Additives	$P_{\text{H}_2/\text{CO}_2}$ (bar)	$T/^\circ\text{C}$	t/h	^c TOF/ (mol h) ⁻¹	^d TON	Ref
^a 1	Ru-MACHO	THF	KOtBu	50/-	140	72	1,200	8,700	134
	(ZnBr ₂)	(-)	(<i>n</i> Bu ₄ NBr)	(-/40)	(140)	(3)			
^b 2	Ru-MACHO	THF	KO ^t Bu	50/-	160	1	3,600	3,600	135
	(Ru-MACHO)	(THF)	(morpholine)	(35/35)	(120)	(40)			
3	Ru-MACHO-BH	THF	NHMe ₂ , K ₃ PO ₄	50/2.5	95 to 155	18+1 8	6	220	136
4	Ru-MACHO-BH	Triglyme, THF, or 1,4-dioxane/water	PEHA, K ₃ PO ₄	67.5/7.5	145	200	70	>2,000	137
^{bc} 5	Ru-MACHO-BH	2-MTHF	K ₃ PO ₄	70/-	145	72	~7	520	138
	(-)	(Water)	(PEHA)	(-/0.07)	(r.t.)	(4)			
6	Ru-MACHO-BH	THF	Pyrrolizidines, K ₃ PO ₄	65/10	155	134	< 1	28	139
7	Ru-MACHO-BH	THF	Poly(ethyleneimine)	60/20	150	100	6	599	67
8	Ru-MACHO-BH	Triglyme	PEHA, K ₃ PO ₄	56/19	145	244	41	9,900	122
9	Ru-MACHO-BH	THF	SSA	60/20	145	40	13	520	65
^b 10	Ru-MACHO-BH	Ethylene glycol	-	70/-	140	20	10	200	140
	(-)	(Ethylene glycol)	(KOH)	(air)	(r.t.)	(3)			
^b 11	Mn-P ⁱ Pr ⁱ NP ⁱ Pr	THF	-	80/-	150	36	1	36	60
	(Mn-P ⁱ Pr ⁱ NP ⁱ Pr)	(THF)	(Amine, KO ^t Bu)	(30/30)	(110)	(36)			
^b 12	Fe-P ⁱ Pr ⁱ NP ⁱ Pr	THF	LiOTf, DBU	80/-	100	16	16	590	132
	(Fe-P ⁱ Pr ⁱ NP ⁱ Pr)	(THF)	(morpholine, 3Å molecular sieves)	(80/17)	(100)	(16)			
13	Ru-bisPN	Toluene	ⁱ Pr ₂ NH, NaOEt	30/10	100	20	4,500	8,900	64

CO₂ conversion to methanol by capturing and subsequent hydrogenation reactions.^a Two steps process. ^b One pot two steps process ^c TOF: turnover frequency (average TOF was calculated if no initial TOF was reported) and for a two steps process, TOF was calculated or reported based on the second step. ^d TON: turnover number (for a two steps process, TON was calculated or reported based on the second step). Reaction parameters in and outside the brackets are the reaction conditions for the first step and the second step, respectively. SSA: solid-supported amine. PEHA: pentaethylenehexamine. 2-MTHF: 2-methyltetrahydrofuran.

Carbonates have been used both as starting materials as well as active intermediates for the hydrogenation of carbon dioxide to methanol. They are also prepared from CO₂ industrially.¹⁴¹ In this respect, Ding¹³⁴ and co-workers investigated a series of Ru-PNP complexes for the hydrogenation of CO₂ via cyclic 5 and 6 ring carbonate derivatives^{142, 143}, which were prepared under 40

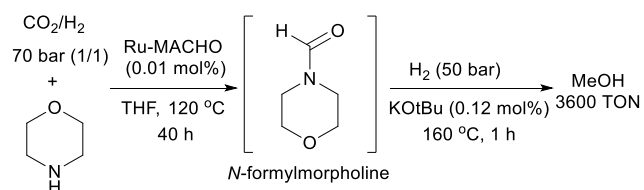
Scheme 5 Ru-PNP complexes catalyzed CO₂ hydrogenation to methanol in a two steps process via carbonates formed from reaction of CO₂ reaction with epoxides in the Omega process. Ref. 134.



bar of CO₂ in the presence of *n*Bu₄NBr and ZnBr₂ in neat epoxide at 140 °C for 3-10 h. Among the investigated complexes, Ru-MACHO (Chart 2) was shown to be highly efficient under relatively mild conditions. For instance, with ethylene carbonate, a TON up to 8,700 and a TOF up to 1,200 h⁻¹ (Table 2, entry 1 and Scheme 5) were obtained. The cyclic carbonates are produced industrially *via* the Omega process¹⁴⁴ mainly for ethylene glycol production by subsequent hydrolysis reaction, concomitantly yielding CO₂ which can be recycled. Hydrogenation of ethylene carbonate results in the production of methanol, hereby indirectly converting ethylene oxide and CO₂ into methanol and ethylene glycol in two steps. This catalytic system also provides a potential process for the utilization of waste poly(propylene carbonate)^{145, 146} as a resource to make propylene glycol and methanol, as well as a convenient method for the preparation of deuterated methanol from CO₂ and D₂. The hydrogenation of carbonates to methanol by base metal catalyst Mn-P^{*i*}NP^{*r*} with TONs up to 400 reported by Leitner¹²⁶ and co-workers is also an interesting alternative in CO₂ to methanol transformation *via* a similar two steps process.

Later, Ding¹³⁵ and co-workers extended their initial method with Ru-MACHO to the hydrogenation of CO₂ in a one-pot two steps procedure without intermediate isolation involving morpholine as additive, though the choice of this amine was not clear (Table 2, entry 2, and Scheme 6). CO₂ was first converted to *N*-formylmorpholine under 70 bar CO₂ and H₂ (1:1 ratio) at 120 °C, followed by hydrogenation of the formamide intermediate to

Scheme 6 One-pot two-step Ru-MACHO catalyzed CO₂ hydrogenation to methanol via *N*-formylmorpholine. Ref. 135.

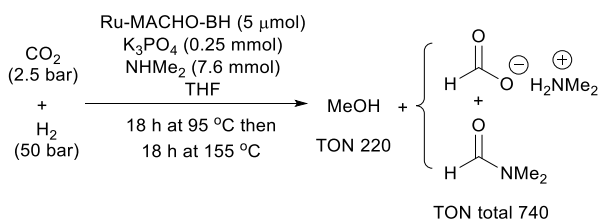


methanol under 50 bar H₂ at 160 °C. Methanol was obtained in 36% yield, corresponding to a TON of 3,600. Noteworthy, *N*-formylmorpholine was not converted to methanol under CO₂/H₂ atmosphere, therefore requiring venting and re-pressurization of the reactor.

Sanford¹³⁶ and co-workers simultaneously reported a one-pot approach using Ru-MACHO-BH precatalyst, featuring a borohydride counter anion, for CO₂ hydrogenation to methanol using dimethylamine as additive (Table 2, entry 3, and Scheme 7). Since catalyst decomposition was observed at high temperatures over time, a “temperature ramp” strategy was applied. A TON of 220 for methanol and 740 for formamide and formate in total was obtained using 0.1 mol% catalyst under 2.5 bar CO₂ and 50 bar H₂ after 18 h of reaction at 95 °C, followed by 18 h of reaction at 155 °C. This approach avoids de-pressurization and re-pressurization steps and immediately reduces formamide further. However, the productivity in 36 h is very low.

Prakash^{137, 147} and co-workers used the same catalyst in combination with polyamines as additives for integrated CO₂ capture and conversion to methanol. This provided the first, efficient homogeneous Ru-based catalyst for the production of CH₃OH from CO₂ with H₂ at 125-165 °C. Best results were obtained in solvents such as THF, triglyme or 1,4-dioxane. The polyethyleneamine showed surprising benefits over dimethylamine and morpholine used by Sanford¹³⁶ and Ding¹³⁵, likely due to more efficient CO₂ capture, as well as trapping formic acid as a formate salt and thus promoting its conversion to formamide for further hydrogenation reactions (Figure 6A).¹⁴⁸ This catalyst system gave an initial 70 h⁻¹ TOF at 145 °C, which is similar to Ru(triphos)(TMM) (Table 1, entry 1 and Table 2, entry 4). Given the large differences in boiling points between product and high boiling solvent, e.g. triglyme, on the one hand and PEHA on the other hand, methanol can be easily separated by distillation from the reaction mixture. However, recycling of the catalyst over five runs under optimized conditions showed a 25% loss of activity as evidenced by the decrease in methanol formation, indicating long term stability issues like many other related catalysts (Figure 6B). At best, a total TON > 2,000 over 200 h in the recycling experiments in triglyme performed under 75 bar CO₂/H₂ (1:9) at 145 °C was obtained. Furthermore, CO₂ firstly captured from synthetic air (400 ppm of CO₂ in N₂/O₂

Scheme 7 One-pot Ru-MACHO-BH catalyzed CO₂ hydrogenation to methanol using a temperature ramp approach via *N,N*-dimethylformamide. Ref. 136.



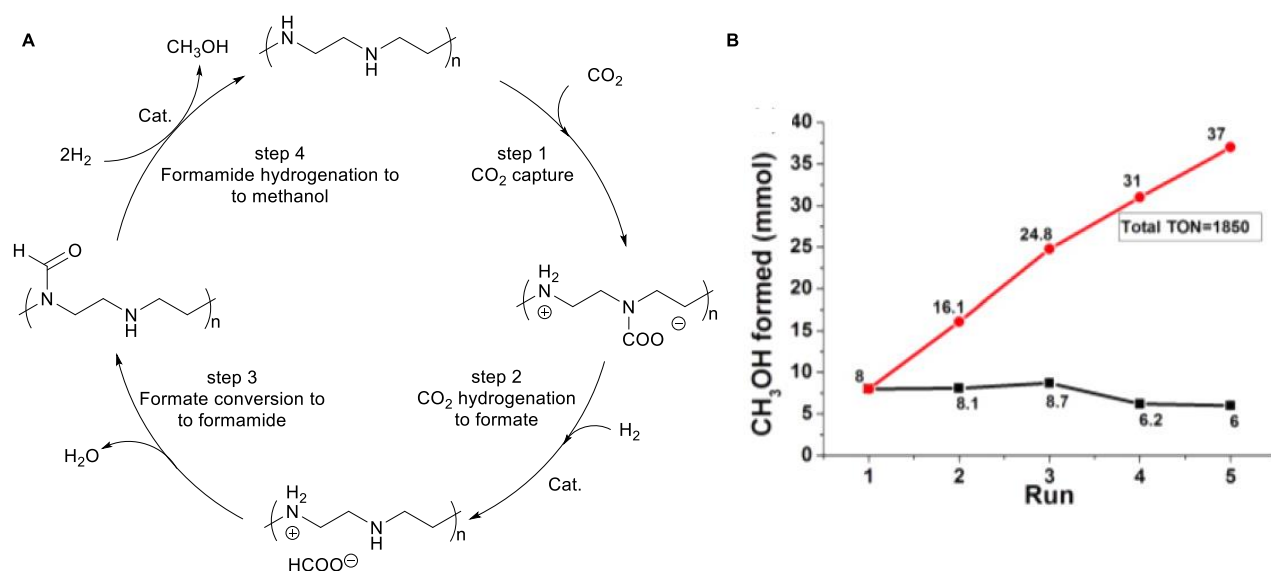


Figure 6 A) Ru-MACHO-BH catalyzed direct CO₂ hydrogenation to methanol using pentaethylenehexamine (PEHA) as additive. B) Recycling study of the catalyst ($t = 40$ h for each run), reaction conditions: PEHA = 3.4 mmol, Ru-MACHO-BH = 20 μ mol, CO₂/H₂ (1:3) = 75 bar, $T = 155$ °C, and THF = 10 mL. Black line, CH₃OH formed in each run; red line, total amount of CH₃OH formed. Partially reproduced with permission from ref. 137. Copyright (2016) American Chemical Society.

80/20) and its subsequent hydrogenation to methanol was also shown featuring methanol yields up to 79%.

Prakash¹³⁸ and co-workers extended their initial work with an efficient and recyclable system for integrative CO₂ capture and hydrogenation to methanol at low CO₂ concentrations (Figure 7, and Table 2, entry 5). Various aqueous amine solutions, including industrially applied ethanolamine and polyamines, were initially tested for CO₂ capture at a constant pressure of 0.07 bar CO₂. The aqueous pentaethylenehexamine (PEHA) solution captured 11.0 mmol of CO₂ per gram of PEHA after 4 h, corresponding to 0.43 mol CO₂ per mol of amino group (CO₂/N) or 48 wt%. Interestingly, monoethanolamine (MEA), an industrially applied CO₂ absorbent, was better for CO₂ capture (11.7 mmol, 0.71 CO₂/N) and is also cheaper compared to PEHA (\$35/kg = \$2.1/mol for MEA, \$105/kg = \$24.4/mol for PEHA). However, subsequent hydrogenation of MEA-CO₂ did not produce methanol but only formate and formamide. Characterization of CO₂ rich PEHA solution by ¹³C NMR spectroscopy revealed the presence of carbamate and carbonate/bicarbonate species, in accordance with various CO₂-

amine systems^{8, 149-151}. 2-MTHF and Ru-MACHO-BH or its derivatives were added and then the biphasic solution was pressurized with 70 bar of H₂ at room temperature and heated to 145 °C. High yield (>90%) was obtained with a catalyst TON up to 520 in this biphasic 2-MTHF/water system. This biphasic system allows for easy separation of methanol through phase separation followed by distillation under reduced pressure, as well as for recycling of the amine and catalyst (Figure 7B). Employing this strategy, Ru-MACHO-BH and/or PEHA were recycled three times with 87% of the methanol production of the first cycle retained, along with 95% of the catalyst activity maintained after three cycles. As shown previously, CO₂ from dilute sources, such as air and combustion sources, could also be converted to CH₃OH using this setup.

Following the same approach, Gademann, Kayaki and co-workers^{67, 139} investigated pyrrolizidine-based diamines and poly(ethyleneimine)s, respectively, in integrated CO₂ capture and subsequent hydrogenation to methanol (Table 2, entries 6-7, Scheme 8). Pyrrolizidine-based diamines showed fast CO₂-uptake at room temperature, i.e. a remarkable $t_{90\%}$ value of only

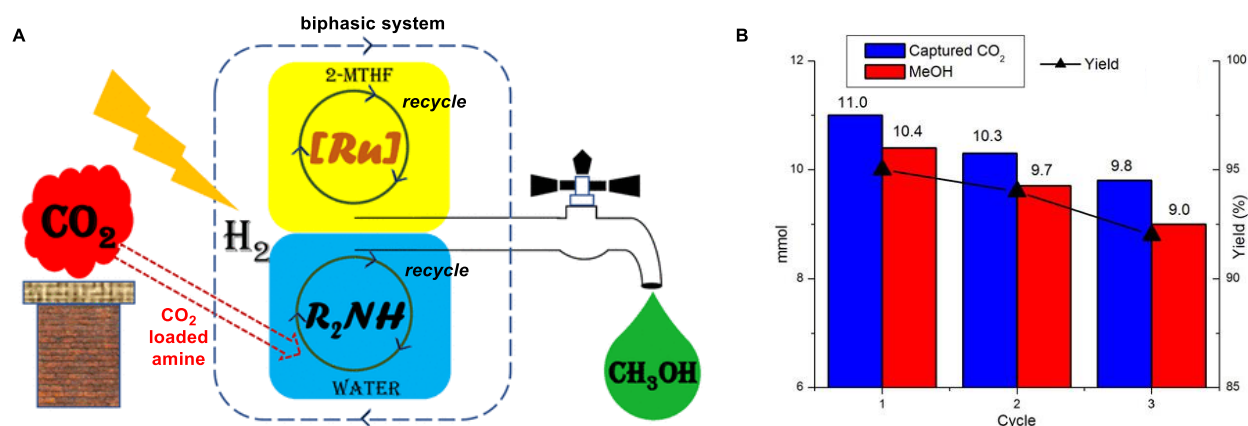


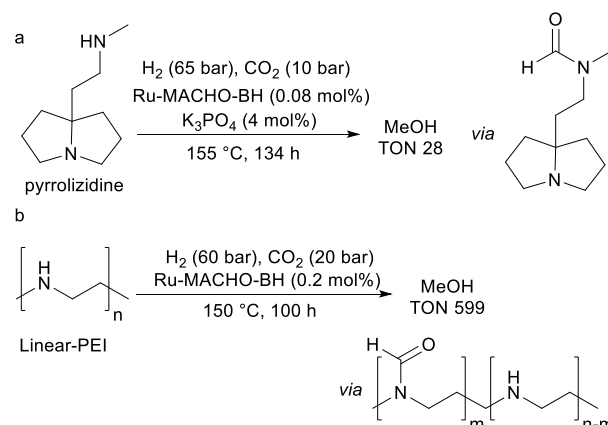
Figure 7 A) One-pot two-step CO₂ capture and hydrogenation to methanol by Ru-MACHO-BH catalysis using a biphasic setup. B) Methanol formation with catalyst and amine recycling. Reaction conditions: CO₂ capture with 1 g PEHA in 3 mL water stirred in CO₂ atmosphere at a constant pressure of 1 psi, H₂ (80 bar), Ru-MACHO-BH (50 μ mol), 2-MTHF (10 mL), 145 °C, 72 h. Reproduced with permission from ref. 138. Copyright (2018) American Chemical Society.

28 minutes, compared to conventional hydroxyalkanamines, and remained active over multiple absorption-desorption cycles. Besides CO₂ capture from pure CO₂ and flue gas, uptake from compressed air (400 ppm CO₂) was shown but rather slow, requiring multiple days. Unfortunately, one pot pyrrolizidine-based diamine assisted CO₂ capture and reduction to methanol using Ru-MACHO-BH catalyst resulted in a low TON of 28. The corresponding formamide was the main product, contrary to the use of polyamines such as PEHA. Poly(ethyleneimine)s on the other hand required a high temperature (100 °C) for CO₂-uptake. However, Ru-MACHO-BH efficiently catalyzed the reduction of *N*-formylated poly(ethyleneimine)s with methanol yields up to 94%. Combination of CO₂-uptake and reduction in a one pot process was also reported with a TON up to 599.

Recently, Prakash¹²² and co-workers performed detailed mechanistic studies on amine-assisted Ru-catalyzed hydrogenation of CO₂ to methanol. Various ruthenium pincer type catalysts and amines, varying in electronic and steric properties, were investigated. Catalytic species were characterized by *in situ* ¹³C, ³¹P and ¹H NMR, X-ray and ATR-IR spectroscopy.

First, catalysts were compared using the same amine, namely PEHA (Table 3). As expected, Ru-MACHO-BH and Ru-MACHO performed equally in the formation of methanol with a TON of 1050 and 1040, respectively (Table 3, entries 1 and 2). However, Ru-MACHO required the addition of K₃PO₄ for its initial activation. Changing of the P substituents resulted in a severe decrease in methanol formation, indicating the importance of P^{Ph}NP^{Ph} as the pincer ligand (Table 3, entries 2-5). However, TON for formate and formamide were significantly increased with aliphatic substituents ^{*i*}Pr (P^{*i*Pr}NP^{*i*Pr}), Cy (P^{Cy}NP^{Cy}) and ^{*t*}Bu (P^{*t*Bu}NP^{*t*Bu}) rather than Ph groups on phosphor (Table 3, entries 3-5). These results suggest that electron donating ligands are helpful for CO₂ hydrogenation up to the formate stage. However, an electron-rich metal center can also lead to the formation of a rather stable metal-formate resting state

Scheme 8 One-pot Ru-MACHO-BH catalyzed integrated CO₂ capture and hydrogenation to methanol in the presence of a) 7a-methylaminoethylpyrrolizidine or b) linear polyethyleneimine. Ref. 67, 139.



complex *via* a metal-oxygen bond, thus inhibiting the hydrogenation process (*vide supra*). As such, replacing the CO in Ru-MACHO by a strong electron donating NHC ligand, i.e. Ru-MACHO-NHC, showed substantially lower TON for methanol corresponding to a lower activity (Table 3, entries 2, 6). Milstein's pyridine PNN pincer complex Ru-P^{*t*Bu}N^{P^{*v*}}N^{Et} (Chart 3, Table 3, entry 7) and PNP acridine pincer complex Ru-P^{*i*Pr}N^{acrP^{*i*Pr}} (Chart 3, Table 3, entry 8) only showed intermediate formamide products with no observable methanol formation. Analysis of the catalyst structures suggest that while these molecular catalysts have rather similar electronic and steric properties on the metal center (Table 3, entries 3, 7-8), their cooperative mode of action is different as they do not contain an N-H moiety and are covered in the next section (*vide infra*). Clearly, these results indicate that the activity of molecular catalysts with M/NH bifunctionality is higher than those with aromatization-dearomatization bifunctionality for CO₂ hydrogenation to methanol.

Table 3 Comparison of several M/NH bifunctional pincer type catalysts in CO₂ hydrogenation to CH₃OH with PEHA additive under the same reaction conditions ^a

Entry	Catalyst	formate ^b (mmol)	formamide ^b (mmol)	methanol ^b (mmol)	CO ^c (%)	TON _{formate+formamide}	TON _{MeOH}
1 ^d	Ru-MACHO-BH	1.2	8.0	10.5	0.21	920	1,050
2	Ru-MACHO	1.6	8.1	10.4	0.22	970	1,040
3	Ru-P ^{<i>i</i>Pr} NP ^{<i>i</i>Pr}	1.1	22.6	3.2	0	2,370	320
4	Ru-P ^{Cy} NP ^{Cy}	1.0	14.7	0.5	0	1,570	50
5	Ru-P ^{<i>t</i>Bu} NP ^{<i>t</i>Bu}	1.6	17.5	0	0	1,910	0
6	Ru-MACHO-NHC	1.3	7.0	6.8	0.1	830	680
7	Ru-P ^{<i>t</i>Bu} N ^{P^{<i>v</i>}} N ^{Et}	0.4	18.4	0	0	1,880	0
8	Ru-P ^{<i>i</i>Pr} N ^{acrP^{<i>i</i>Pr}}	0.7	11.0	0	0	1,170	0

^aRefer to Chart 2 and 3 for the structures of the tested pincer complexes. Reaction conditions: PEHA (5.1 mmol), cat. (10 μmol), K₃PO₄ (1 mmol), triglyme (10 mL), CO₂/3H₂ (75 bar), 145 °C, 40 h. ^bYields were determined from ¹H NMR spectra with 1,3,5-trimethoxybenzene (TMB) as an internal standard. ^cCO detection limit -0.099%. ^dIn the absence of K₃PO₄. TON_{formate+formamide} = mol of formate+formamide formed per mol of cat. TON_{CH₃OH} = mol of CH₃OH formed per mol of cat. For details see ref. ¹²².

Figure 8 shows the effect of amine additives on the CO₂ reduction process. While monoamines such as piperidine **8** gave almost exclusively formamide and formate products, (di/poly)amines featuring primary amines and/or secondary amines were effective in assisting Ru-MACHO-BH catalyzed

integrated CO₂ capture and hydrogenation to methanol. Particularly, polyamine **10** showed superior performance among the different amines tested. In contrast, diamines **4** and **5** containing both a tertiary amine and primary or secondary amine displayed low activity. However, diamines featuring one

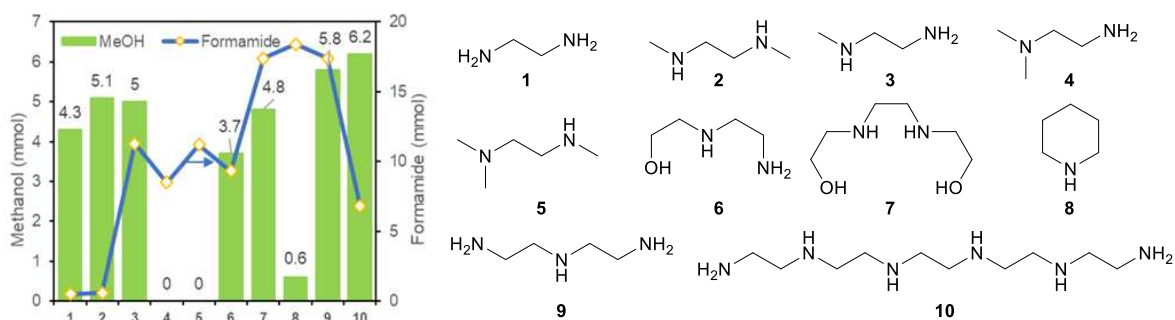


Figure 8 Methanol and formamide yields with different amines as additives in a one pot reaction with Ru-MACHO-BH. Reaction conditions: Ru-MACHO-BH (10 μ mol), Amine NH group equivalents (30.6 mmol) [PEHA (**10**) 5.1 mmol, DETA (**9**) 10.2 mmol, all diamines 15.3 mmol], triglyme (10 mL), CO₂/3H₂ (75 bar), 145 °C, 20 h. Partially reproduced with permission from ref. 122. Copyright (2019) American Chemical Society.

tertiary amine have been reported for their high CO₂ scavenging properties.¹⁵² Tertiary amines¹⁵³ were unsuitable, indicating formamide instead of formate and carbamate instead of bicarbonate as crucial intermediates in integrated CO₂ capture and hydrogenation to methanol. An amine traps the formic acid as an ammonium formate salt and then promotes the formation of stable formamide for further hydrogenation reactions. However, detailed experimental and *in situ* spectroscopic investigation of these species in CO₂ hydrogenation to methanol are rarely reported.

In situ ¹³C NMR spectroscopic study of the Ru-MACHO-BH catalyzed reaction revealed the formation of cationic resting state ruthenium biscarbonyl bis[2-(diphenylphosphino)ethyl]amine monohydride complexes, which were also identified by ³¹P and ¹H NMR, and X-ray crystal

structure determination (Figure 9A-B). Importantly, under the reaction conditions (dihydrogen pressure), this biscarbonyl species can return to the active species, and thereby catalyzes the hydrogenation of formamide to methanol (Figure 9C). As the electron-donating ability of the R group on the P^RNP^R ligand rises (R = ^tBu > ⁱPr > Ph), the electron density at the metal center increases. As a result, there will be more metal-carbonyl back-bonding. Indeed, Figure 9D showed higher frequencies of the characteristic CO bond stretch for Ru P^{Ph}NP^{Ph} derived biscarbonyl pincer complex. However, when a 5 bar CO pressure was introduced in the system, the formation of hydride species was completely inhibited and no methanol formation was observed. These results reveal that the lability of the axial CO group is crucial for CO₂ hydrogenation. Considering some CO can form *in situ* under the reaction conditions *via* formaldehyde

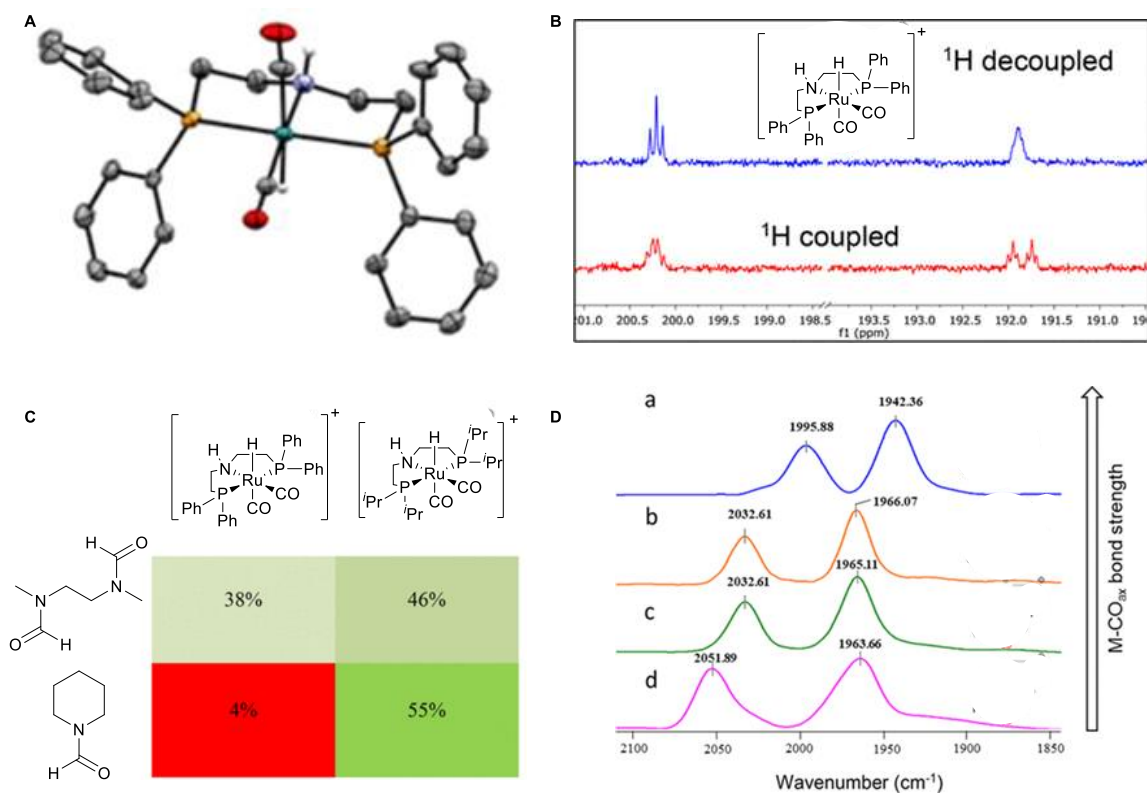


Figure 9 Observation of cationic ruthenium biscarbonyl bis[2-(diphenylphosphino)ethyl]amine monohydride complex. A) Single-crystal X-ray structure. B) ¹³C NMR spectra (top, ¹H decoupled; bottom, ¹H coupled). C) Hydrogenation of formamides using Ru-MACHO-BH and Ru-P^RNP^R derived biscarbonyl complexes. Reaction conditions: formamide (10 mmol), cat. (10 μ mol), triglyme (10 mL), H₂ (60 bar), 145 °C, 20 h. D) ATR-IR spectra: CO stretching frequencies of Ru-P^RNP^R pincer derived biscarbonyl complexes (R = ^tBu, Cy, ⁱPr, Ph for a, b, c and d, respectively). Modified with permission from ref. 122. Copyright (2019) American Chemical Society.

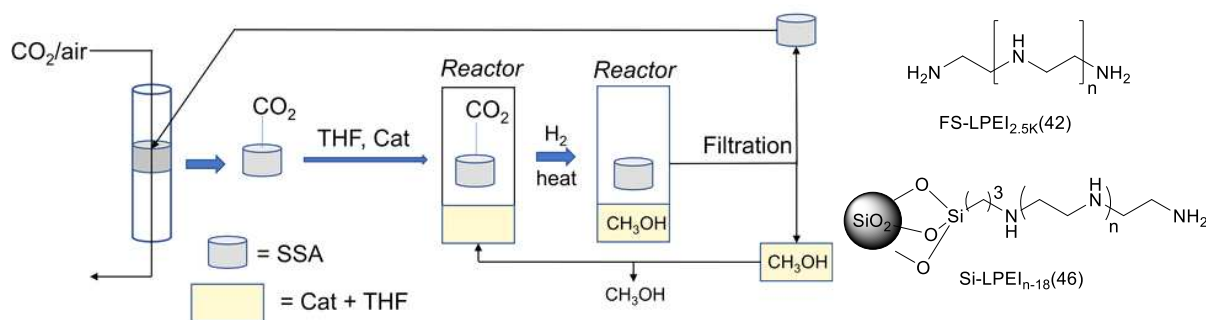


Figure 10 Schematic for integrated CO₂ capture and conversion to methanol with solid-supported amines (SSA). The numbers in parenthesis represents the percentage of organic content. Partially reproduced with permission from ref. 65. Copyright (2019) Wiley-VCH Verlag GmbH & Co. KGaA, Weinheim.

decomposition, this is not self-evident to control. This also rationalizes the high activity of pincer complex Ru-MACHO-BH, given Ru pincer complexes with increasing electron-donating PNP ligands form more stable bis-carbonyl complexes, such as those derived from Ru-P^{iPr}NP^{iPr}, Ru-P^{Cy}NP^{Cy}, and Ru-P^{tBu}NP^{tBu}. Similarly, Ru-formate¹⁵⁴ species with a stronger Ru-O bond can also lead to more stable resting state species in case of more electron-donating ligands (*vide supra*).

Further optimization of the reaction conditions demonstrated Ru-MACHO-BH to be effective for CO₂ hydrogenation to methanol in the presence of PEHA (5.1 mmol) under 75 bar of CO₂/H₂ (1/3) at 145 °C.¹²² In this case, the catalytic system remained active even after 10 days of continuous reaction using a catalytic concentration as low as 11 ppm wrt CO₂ (1 μmol, 0.6 mg), achieving a maximum TON of 9,900 (Table 2, entry 8). Remarkably, a dilute reaction mixture had a positive impact on the methanol turnovers, likely due to the limited solubility of the formamide intermediates in triglyme solvent.

Prakash⁶⁵ and co-workers also explored solid supported amines (SSAs) for integrated CO₂ capture and its subsequent hydrogenation to methanol in the presence of Ru-MACHO-BH (Figure 10, Table 2, entry 9). Eight solid-supported amines were prepared by using three different preparation methods, including physical impregnation on fumed silica, covalently binding to a solid support, and cross-linking with glyoxal or glycerol diglycidyl ether on fumed silica. All SSAs were able to facilitate CO₂ capture and its subsequent hydrogenation to methanol as well as to be easily recovered by filtration. The highest TON (TON = 520) was obtained within 40 h in the presence of physically-impregnated silica-supported amine FS-

LPEI2.5K (42) and Ru-MACHO-BH (Figure 10). However, for this type of SSA, leaching of amines up to 18% in the solution was detected by ¹H NMR spectroscopy. Pleasingly, covalently-attached solid amine Si-LPEIn-18(46) showed promise owing to its high leaching resistance and amine loading, i.e. number of nitrogen atoms per unit weight (~10 mmol g⁻¹), which might be beneficial for CO₂ capture and its conversion. During recycling experiments, similar methanol yields were observed but the CO₂ capture efficiency of the optimized SSA halved from 87 to 46 mg CO₂ g⁻¹ SSA in the third cycle.

Prakash¹⁴⁰ and co-workers recently reported the first example of an alkali hydroxide-based system for integrated CO₂ capture and conversion to methanol in ethylene glycol (Figure 11, Table 2, entry 10). The alkali hydroxide deprotonates ethylene glycol and the corresponding alcoholate salt captures CO₂ quantitatively forming the corresponding alkyl carbonate salts. The resulting carbonate salts were then efficiently hydrogenated to methanol at relatively mild temperatures (100–140 °C) using Ru-MACHO-BH catalyst with a TON up to 200 and a quantitative methanol yield after 20 h. Involvement of alkali carbonates *via* reaction of hydroxide with CO₂ is also possible. CO₂ captured from ambient air followed by hydrogenation to methanol was also successfully demonstrated using this amine free system, delivering methanol in quantitative yield after 72 h. Methanol can be easily separated by distillation, in line with previous work (*vide supra*). However, the low TON suggests that CO₂ capture and direct

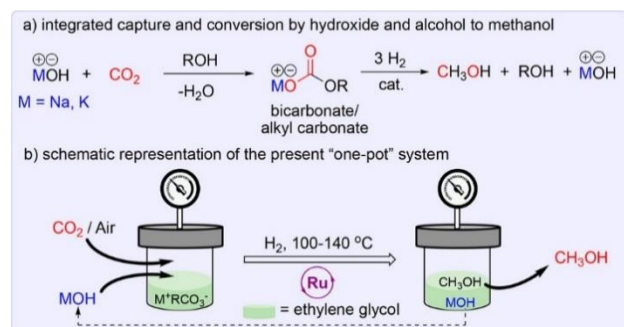
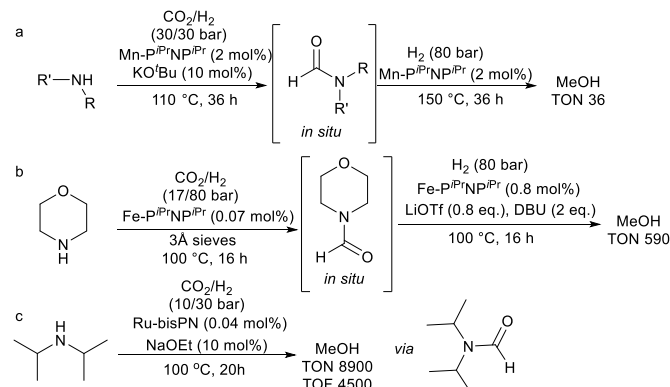


Figure 11 Integrated one-pot two-step CO₂ scavenging using alkali hydroxide with ethylene glycol and subsequent Ru catalyzed conversion to methanol. Reproduced with permission from ref. 140. Copyright (2020) American Chemical Society.

Scheme 9 Mn-P^{iPr}NP^{iPr}, Fe-P^{iPr}NP^{iPr} and Ru-bisPN catalyzed CO₂ hydrogenation to methanol in the presence of amines via a one-pot two steps (a and b) and one-step (c) process. Ref. 60, 64, 132.



hydrogenation using alkali hydroxide is more challenging than with amines, which is worth further fundamental research. Unfortunately, only partial recycling was possible in this one pot two steps protocol due to dehydrogenation of ethylene glycol to carboxylates under the reaction conditions.

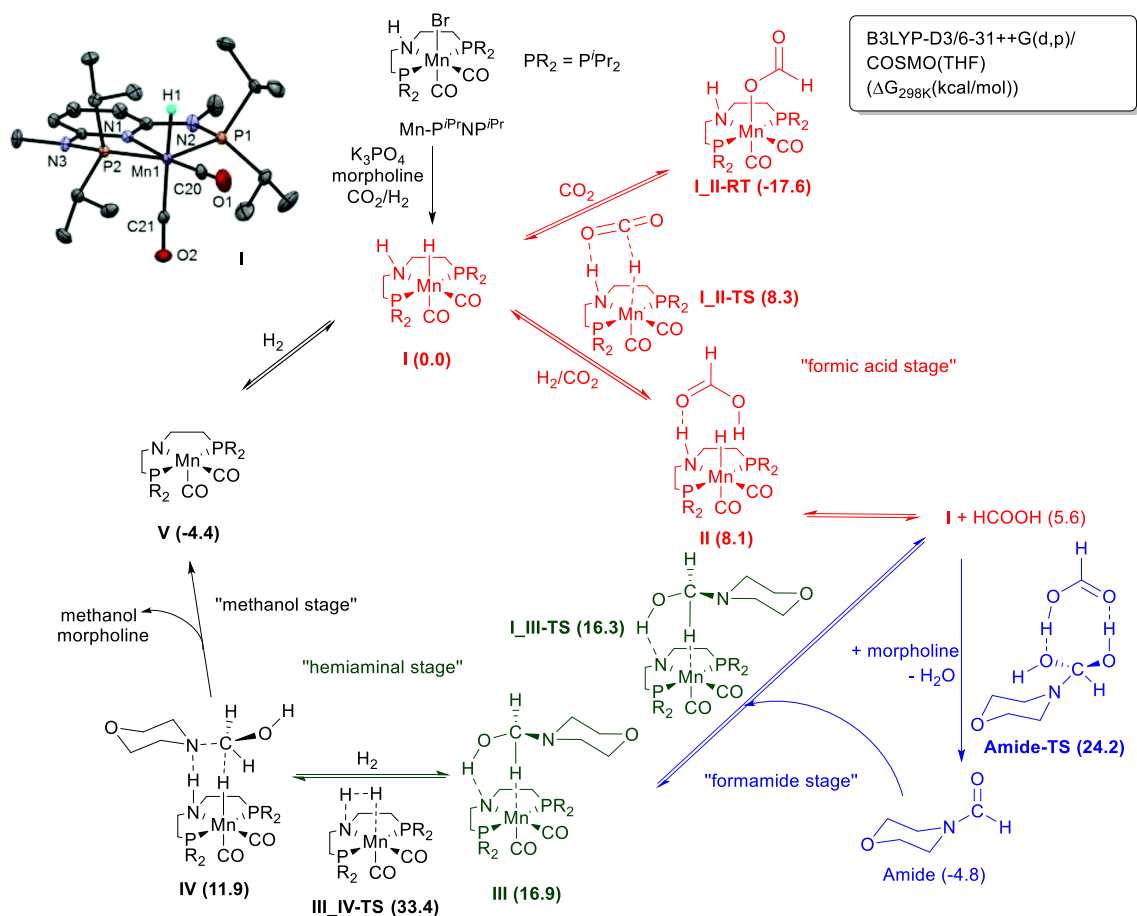
Prakash⁶⁰ and co-workers also explored cheaper non-noble metal complexes for CO₂ hydrogenation to methanol (Table 2, entry 11, Scheme 9a and Chart 2). Here, they applied a one-pot two steps process for CO₂ hydrogenation to methanol *via* a formamide intermediate with a Mn-P^{iPr}NP^{iPr} pincer complex. As reported by Ding¹³⁵ et al., the hydrogenation reaction consists of two steps: *N*-formylation of an amine utilizing CO₂ and H₂, and subsequent formamide hydrogenation to methanol under H₂ pressure. High methanol molar yields (w.r.t amine) were obtained when benzylamine (84%) and morpholine (71%) were used, with TON up to 36. A similar attempt has been made by Bernskoetter¹³² and co-workers (Table 2, entry 12, Scheme 9b and Chart 2) using a Fe-P^{iPr}NP^{iPr} pincer complex. The addition of molecular sieves led to an enhanced TON up to 590 with 84% methanol yield. It is expected that molecular sieves can trap water and/or capture CO₂ and formic acid, and hereby assist the formation of formamide due to its basic nature, but the details are not clear. Noteworthy to mention is that the sieves have to

be removed before the formamide hydrogenation step as it scavenges methanol.

Wass⁶⁴ and co-workers reported one case of a non-pincer type M/NH bifunctional Ru-bisPN catalyst for CO₂ hydrogenation to methanol in a tandem process (Table 2, entry 13, Scheme 9c and Chart 2). Ru-bisPN displayed a TON of 8,900 and a TOF of 4,500 h⁻¹ using low catalyst loadings (50 nmol) in the presence of diisopropylamine at low temperature of 100 °C. Unlike Ru-MACHO pincer type catalysts, follow-up investigations on this interesting M/NH bifunctional catalyst type remain scarce.

Pathak⁶¹ and co-workers performed detailed DFT calculations to understand the mechanisms of Mn-P^{iPr}NP^{iPr}, Ru-P^{iPr}NP^{iPr}, and Fe-P^{iPr}NP^{iPr} catalyzed CO₂ hydrogenation to methanol *via* a formamide intermediate derived from morpholine. In line with the generally accepted mechanism (Scheme 4), Scheme 10 shows the calculated revised Noyori type mechanism in the presence of Mn-P^{iPr}NP^{iPr} catalyst with crucial catalytic intermediates and their free energies relative to the starting complex I. The X-ray crystal structure of the starting active complex formed from precomplex added under catalytic conditions is displayed in the top left corner of Scheme 10. Again, the catalytic process is divided into four stages: formic acid stage, formamide stage, hemiaminal stage and methanol stage.

Scheme 10 DFT calculated M/NH bifunctional mechanism of Mn-P^{iPr}NP^{iPr} catalyzed CO₂ hydrogenation to methanol via formic acid stage, formamide stage, hemiaminal stage and methanol stage.



All the manganese complexes involved in the catalytic cycle are neutral species. Only key species are displayed here; for more details, see ref. 61.

stage. In the formic acid cycle, the reaction barrier of complex **I_II-TS** is 8.3 kcal mol⁻¹ with respect to the starting complex **I**. NH hydrogen bonding to the carbonyl-O of CO₂ is shown to stabilize the transition state complex of the hydride transfer step. Importantly, the resting state complex **I-II-RT** with an anionic formate coordinated to the Mn center *via* a Mn-O bond can easily form after one hydride transfer to CO₂ *via* rearrangement with small barriers. This resting state complex is -17.6 kcal mol⁻¹ more stable than the starting active manganese hydride complex **I**. The Mn-formate complex has the lowest free energy in the catalytic cycle and as such makes the overall catalytic process rather challenging.⁶⁰

The second stage represents the formamide formation with morpholine. In solution morpholine will form a salt with formic acid, followed by conversion to the thermodynamically stable *N*-formylmorpholine at high temperatures. Due to hydrogen bonding interactions, the transition state complex of the formamide formation (**Amide-TS**) is also easy to overcome under the reaction conditions. This occurs *via* a transition state, featuring stabilization *via* a second molecule of formic acid. The *N*-formylmorpholine is more stable compared to formic acid. The overall reaction free energy for CO₂ to amide is exergonic (-4.8 kcal mol⁻¹), while transformation to formic acid from CO₂ is endergonic (5.6 kcal mol⁻¹) with respect to the starting complex **I**. Morpholine also captures CO₂ *via* carbamate salt formation,¹³⁶ indicating the multiple roles of amines under catalytic conditions.

For the remaining stages, two different pathways for *N*-formylmorpholine hydrogenation have computationally been explored, i.e. C=O followed by C-N vs. C-N followed by C=O bond hydrogenations. The pathway of C=O hydrogenation followed by C-N bond cleavage is slightly more favorable and shown.^{61, 118-120} In the hemiaminal stage, the C=O bond is hydrogenated *via* simultaneous proton and hydride transfer through N-H and Mn-H bifunctionality. The transition barrier **II_III-TS** is 16.3 kcal mol⁻¹ with respect to the starting manganese hydride complex **I**. The second crucial step concerns decomplexation of hemiaminal and H₂ activation of amido-Ru-complex *via* the N/M bifunctionality and its barrier **III_IV-TS** is 33.4 kcal mol⁻¹ with respect to the starting hydride complex **I** in the reaction potential energy surface. This transition state complex is the most unstable complex in the catalytic cycle. Given the participation of solvents and product molecules are known to act beneficially for H₂ activation through hydrogen bonding interactions,¹⁵⁵⁻¹⁵⁷ its transition state barrier might be overestimated. Hemiaminal, which is released in **III** and rebounds in **IV** obviously can also play an active role. However, further detailed computational investigations on this mechanism were not reported. The methanol formation stage is rather straightforward with small energy barriers as generally observed in the hydrogenation of ketones and aldehydes. The energy barrier of this step **IV** is 11.9 kcal mol⁻¹ with respect to the starting manganese hydride complex **I**.

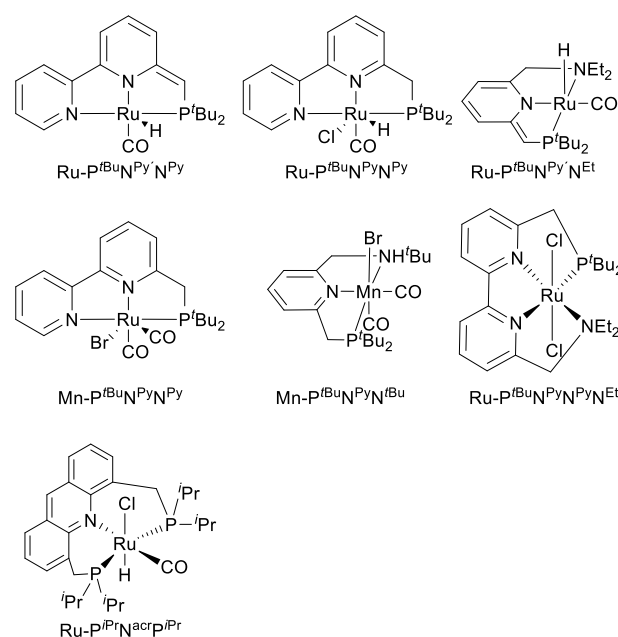
Similar barriers and intermediate complexes were also found for Ru-P^{*i*Pr}NP^{*i*Pr} and Fe-P^{*i*Pr}NP^{*i*Pr} based catalytic cycles. Note that the highest reaction barriers with respect to their respective metal-hydride complexes are very similar, i.e. 33.4, 32.8 and

34.0 kcal mol⁻¹ for Mn-P^{*i*Pr}NP^{*i*Pr}, Fe-P^{*i*Pr}NP^{*i*Pr} and Ru-P^{*i*Pr}NP^{*i*Pr}, respectively. However, due to relatively larger stability difference among the metal-formate resting state complexes, the energy span between the resting state complexes and the highest energy transition state complexes for Mn-P^{*i*Pr}NP^{*i*Pr} and Fe-P^{*i*Pr}NP^{*i*Pr} is larger than that for Ru-P^{*i*Pr}NP^{*i*Pr}, i.e. the reaction potential energy surface span is 51.0, 49.5 and 48.4 kcal mol⁻¹ for Mn-P^{*i*Pr}NP^{*i*Pr}, Fe-P^{*i*Pr}NP^{*i*Pr} and Ru-P^{*i*Pr}NP^{*i*Pr} respectively. This predicts that Ru-PNP^{*i*Pr} should be more promising for CO₂ hydrogenation to methanol primarily due to the formation of a less stable resting state complex, when compared to catalysts such as Mn-P^{*i*Pr}NP^{*i*Pr} and Fe-P^{*i*Pr}NP^{*i*Pr}, agreeing with experimental findings (*vide supra*). When comparing Ru-P^{*i*Pr}NP^{*i*Pr} with Ru-MACHO, the former showed a lower activity likely for the same reason. These complexes feature the same metal but just differ in the substitution patterns of the PNP ligand, *i*Pr versus Ph as substituent on phosphorus as already shown in Table 3.¹²² Combination of metal and pincer ligand in a cooperative catalytic manner is clearly determining the overall efficiency. Comparative detailed computational studies on Ru-MACHO in CO₂ hydrogenation to methanol would be interesting to directly compare energy levels of Ru-MACHO with Ru-P^{*i*Pr}NP^{*i*Pr}.

2.3. Aromatization-dearomatization bifunctional molecular catalysts

Milstein¹⁵⁸⁻¹⁶⁰ and co-workers were the first to introduce a mode of metal-ligand cooperation involving aromatization-dearomatization of pyridine-derived pincer ligands. These systems are just as the M/NH based systems also able to absorb and release hydrogen. While the M/NH bifunctional catalysts of the previous section contain a secondary amine in the pincer ligand, which is transformed into an amide during catalysis, the aromatization-dearomatization is based on the nitrogen of an

Chart 3 Chemical structures of aromatization-dearomatization bifunctional molecular catalysts for CO₂ hydrogenation to methanol. Py = aromatic form of the ligand, Py' = non-aromatic form of the ligand.



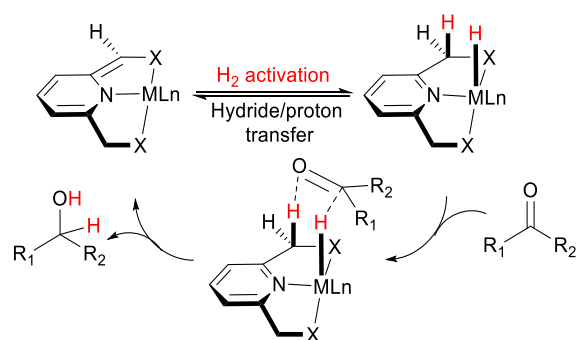


Figure 12 Aromatization-dearomatization bifunctional molecular catalysts in H_2 activation and hydride/proton transfer to a carbonyl group.

azine-based pincer ligand cycling between an imine and enamide through removal of a proton from the benzylic position rather than from nitrogen. Figure 12 shows the general

aromatization-dearomatization bifunctional mechanism in H_2 activation and hydride/proton transfer steps in the hydrogenation of carbonyl groups.¹⁶¹

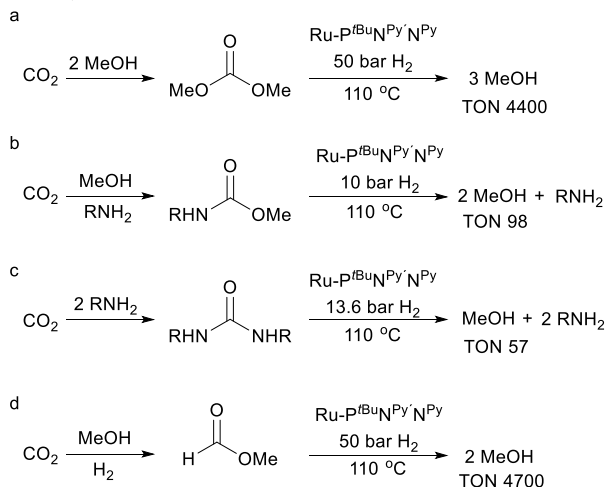
Various CO_2 -derived compounds such as carbonates, carbamates, ureas, formates, and polycarbonates can be hydrogenated to the corresponding alcohols and amines employing this type of catalyst.^{53, 54} Considering those can essentially be produced from CO_2 ,¹⁶² hydrogenation of such CO_2 derivatives is an interesting approach to solve the thermodynamic, kinetic, and incompatibility challenges in the direct transformation of CO_2 to methanol. When such derivatives were used in a two steps process, the authors did not discuss the exact conditions for their production from CO_2 . Table 4 displays the performance of aromatization-dearomatization bifunctional molecular catalysts, of which the chemical structures are shown in Chart 3.

Table 4 Aromatization-dearomatization bifunctional molecular catalysts for hydrogenation of CO_2 to methanol

Entry	Catalyst	Solvent	Additives	P_{H_2/CO_2} (bar)	$T/^\circ C$	t (h)	TOF ($mol\ h^{-1}$)	TON	Ref
°1	Ru- $P^{tBu}N^{Py}N^{Py}$ / Ru- $P^{tBu}N^{Py}N^{tBu}$	THF	-	10-50/-	110	14-72	~1-2,500	57- 4,700	163, 164
		(n.r.)	-	(n.r.)	(n.r.)	(n.r.)			
°2	Mn- $P^{tBu}N^{Py}N^{Py}$ / Mn- $P^{tBu}N^{Py}N^{tBu}$	Toluene	KH/ KO^tBu	20-50/-	130-150	50	~1	~50	165, 166
		(n.r.)	-	(n.r.)	(n.r.)	(n.r.)			
°3	Ru- $P^{tBu}N^{Py}N^{Py}$ (Cs_2CO_3)	DMSO	KO^tBu	60/-	135	72	< 1	30	167
		(DMSO)	(-)	(-/3)	(150)	(24)			
4	Ru(PMe_3) ₄ (OAc)Cl, Sc(OTf) ₃ , Ru- $P^{tBu}N^{Py}N^{Py}$	MeOH, 1,4- dioxane	-	30/10	75-135	16	~1	21	168
5	Ru- $P^{tBu}N^{Py}N^{Py}N^{Et}$	<i>i</i> PrOH	$tBuOK$, NHMe ₂	50/2.5	90->170	48+72	17.5	2,100	66

CO_2 conversion to methanol by capturing as intermediates [i.e. carbonates, ureas, formates and carbamates (entries 1-2) and oxazolidinones (entry 3)], and subsequent hydrogenation reactions. ° A two steps process. Reaction parameters in and outside the brackets are the reaction conditions for the first step and the second hydrogenation step, respectively. TOF: turnover frequency (an average TOF was calculated if no initial TOF was reported) and for a two steps process, TOF was calculated or reported based on the second step. TON: turnover number (the highest TON was calculated based on the yield if no TON was reported). n.r. not reported.

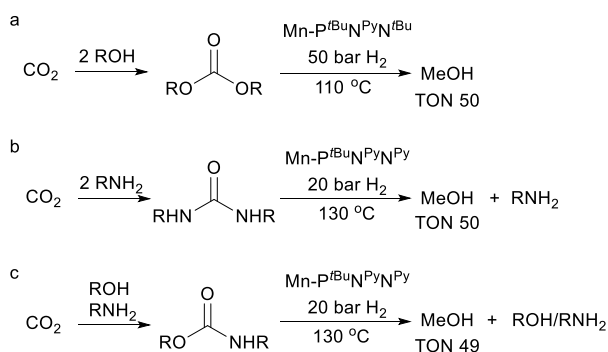
Scheme 11 Ru-^tBuN^{Py}N^{Py} catalyzed CO₂ hydrogenation to methanol via a) carbonate, b) carbamates, c) ureas, and d) formate ester using two steps. Ref. 163, 164.



Milstein^{163, 164} and co-workers reported the catalytic hydrogenation of CO₂-derived organic carbonates, carbamates and urea derivatives to methanol (Scheme 11, and Table 4, entry 1) for the first time. Ru-^tBuN^{Py}N^{Py} and Ru-^tBuN^{Py}N^{Et} pincer complexes derived from 6-[(di-*tert*-butylphosphino)methyl]-2,2'-bipyridine and 2,6-bis(diethylphosphinomethyl)pyridine tridentate pincer ligands, respectively, were investigated in these hydrogenation reactions. While hydrogenation of dimethyl carbonate resulted in high methanol yield (88%) and high TON (4,400), methyl carbamates and ureas were considerable more challenging with yields higher than 90% and 46-94%, respectively, corresponding to TONs up to 98 and 57, respectively. The hydrogenation of methyl formate that can be obtained from CO₂ hydrogenation to formic acid followed by esterification showed high yield and a TON of 94% and 4,700, respectively.

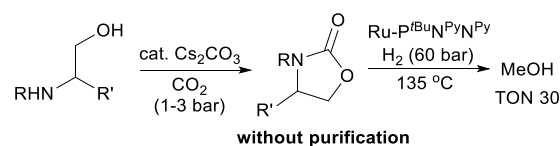
As noble metals are generally expensive, resulting in cost issues

Scheme 12 Mn-^tBuN^{Py}N^{Py} and Mn-^tBuN^{Py}N^tBu catalyzed CO₂ hydrogenation to methanol via a) carbonates, b) ureas, and c) carbamates. Ref. 165, 166.



in terms of industrial applications,^{165, 166} cheaper alternatives have also been reported for the hydrogenation of carbonates, carbamates, and ureas. Mn derivatives of Mn-^tBuN^{Py}N^{Py} and Mn-^tBuN^{Py}N^tBu complexes gave a TON up to 33 and 50, respectively, under mild conditions (Scheme 12, and Table 4, entry 2). Although much lower activity was observed, these

Scheme 13 Ru-^tBuN^{Py}N^{Py} catalyzed CO₂ hydrogenation to methanol via oxazolidinones using a one-pot two-step approach. Ref. 167.

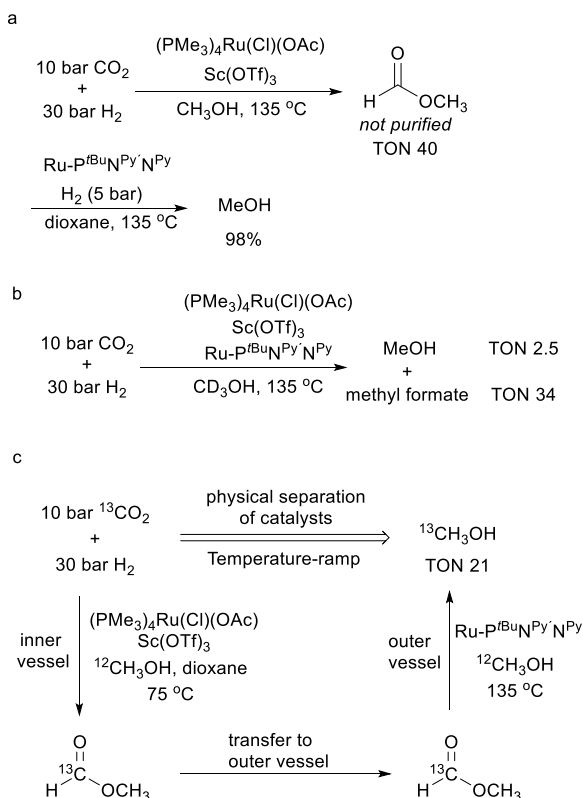


complexes are the first non-noble metal based aromatization-dearomatization bifunctional catalysts reported for the hydrogenation of CO₂ derivatives. However, at this point it should be made clear that for most of these complexes not the central metal, but instead the ligand is the cost determining factor. This is also true for most of the sophisticated aliphatic PNP pincer ligands.

Ru-^tBuN^{Py}N^{Py}, the aromatic form of Ru-^tBuN^{Py}N^{Py}, was later applied in a one-pot two steps procedure involving oxazolidinones (Scheme 13, Table 4, entry 3).¹⁶⁷ These were obtained *via* CO₂ capturing by aminoethanol at low pressures (1-3 bar of CO₂) in the presence of catalytic amounts of Cs₂CO₃ providing a high yield (>90%). The cyclic nature of these compounds makes CO₂ capture easier. The CO₂ captured product without isolation was then subjected to hydrogenation with Ru-^tBuN^{Py}N^{Py} in the presence of KO^tBu for *in situ* activation under 60 bar of H₂ pressure yielding methanol with yields up to 74% and a TON of 30 in the hydrogenation step.

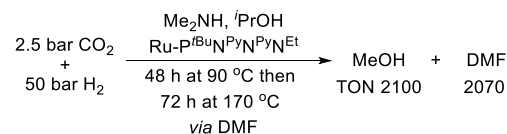
Sanford and co-workers¹⁶⁸ disclosed an approach for CO₂ hydrogenation to methanol by combining three homogeneous catalysts, i.e. (PMe₃)₄Ru(Cl)(OAc), Sc(OTf)₃, and Ru-^tBuN^{Py}N^{Py} (Table 4, entry 4, and Scheme 14). First, a one-pot two steps protocol was explored. Conversion of CO₂ to methyl formate using (PMe₃)₄Ru(Cl)(OAc) as catalyst was established. While the reaction was slow, addition of Sc(OTf)₃ acting as a Lewis acid enhanced the Ru catalyst TON (40 vs. 3). In the second step, hydrogenation of methyl formate with Ru-^tBuN^{Py}N^{Py} proceeded with high methanol yield (98%). A proof-of-principle reaction combining all three catalysts in a one-pot process (i.e. tandem catalysis) resulted in a disappointingly low TON of 2.5 for methanol, which was attributed to the deactivation of Ru-^tBuN^{Py}N^{Py} by Sc(OTf)₃. Interestingly, physically separating Ru-^tBuN^{Py}N^{Py} from (PMe₃)₄Ru(Cl)(OAc) and Sc(OTf)₃ in a two-chamber reactor setup resolved this issue, increasing the TON for methanol to 21 although still very low.

Scheme 14 Ru- $P^{tBu}N^{Py}N^{Py}$ catalyzed CO₂ hydrogenation to methanol *via* methyl formate using: a) a one-pot two steps, b) one-pot, or c) physically separated one-pot approach. Ref. 168.



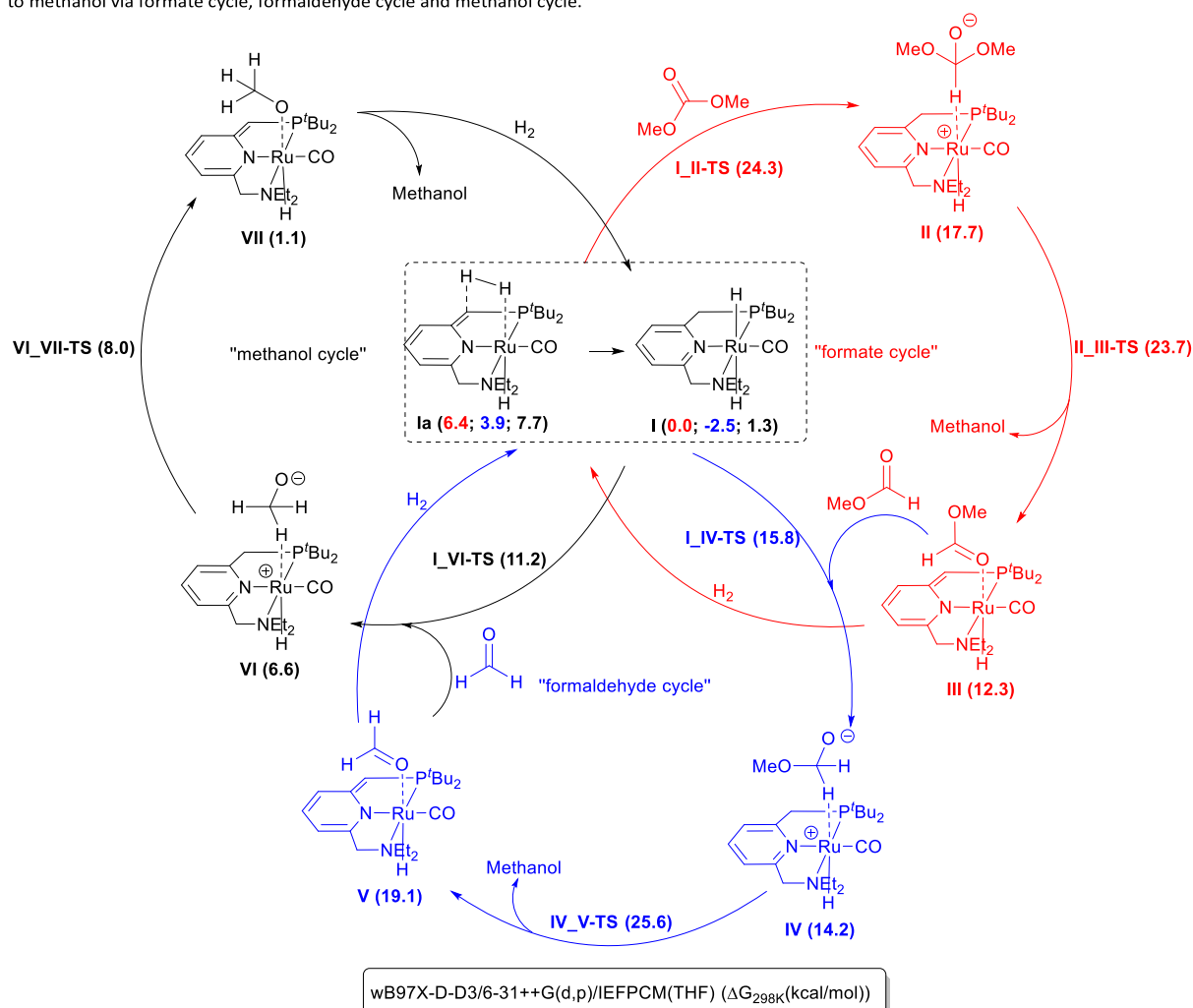
Zhou⁶⁶ and co-workers reported the use of Milstein type pincer complex $\text{Ru-P}^{t\text{Bu}}\text{N}^{\text{Py}}\text{N}^{\text{Py}}\text{N}^{\text{Et}}$ derived from *N*-({6'-[(di-*tert*-butylphosphanyl)methyl][2,2'-bipyridin]-6-yl)methyl)-*N*-ethylethanamine ligand for one-pot CO₂ hydrogenation to methanol (Scheme 15, Table 4, entry 5). This specific catalyst showed high activity and selectivity for the hydrogenation of lactones and esters¹⁶⁹ at room temperature, though no data on amides was disclosed. A tandem transformation approach was used in which dimethylamine captured CO₂ in the presence of H₂ and the resulting DMF was directly hydrogenated to methanol. A high TON of 2,100 was achieved at low CO₂ pressure (2.5 bar) and 50 bar of H₂ pressure. Based on the known benefits of polyamines in assisting CO₂ capture and subsequent hydrogenation to methanol, higher catalytic performance is expected upon fine tuning the amines (*vide supra*) but not shown. Unfortunately, higher CO₂ pressure (5 bar) showed strong inhibition of the catalyst and only limited amounts of methanol were observed. In this case, one possible deactivation route might be CO₂ addition to the nitrogen arm of the pincer ligand, as was proposed by Sanford and Milstein^{170, 171}. However, the exact deactivation mechanism of this catalyst under the given reaction conditions was not studied in detail. Yang^{172, 173} and co-workers investigated the mechanism of $\text{Ru-P}^{t\text{Bu}}\text{N}^{\text{Py}}\text{N}^{\text{Et}}$ catalyzed hydrogenation of dimethyl carbonate (DMC), as a representative CO₂ derivative, to methanol *via* DFT calculations. Scheme 16 shows the calculated metal-hydride, ligand-proton transfer and C-O bond cleavage mechanisms for sequential tandem hydrogenation of DMC, methyl formate, and

Scheme 15 Ru- $\text{PN}^{\text{Py}}\text{N}^{\text{Py}}\text{N}^{\text{Et}}$ catalyzed CO₂ hydrogenation to methanol in a one-pot process *via* DMF (dimethyl formamide) intermediate. Ref. 66.



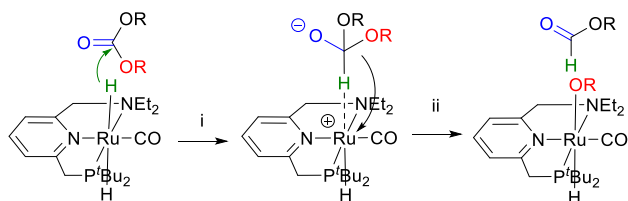
formaldehyde to methanol. The resting state in the catalytic reaction is the *trans* dihydride complex *trans*- $\text{Ru}(\text{P}^{t\text{Bu}}\text{N}^{\text{Py}}\text{N}^{\text{Et}})(\text{H})_2(\text{CO})$ **I**, which is the central point of each catalytic cycle. This complex is formed after H₂ addition to complex **Ia** through formal addition of a proton at the methylenic carbon on the phosphorous side-arm and a hydride at the Ru metal center. The rate-determining step in the overall catalytic cycle is the formation of the target methanol molecule through simultaneous breaking of a C-OCH₃ bond and transferring a ligand methylene proton to form formaldehyde in the formaldehyde cycle, explaining the slow conversion rate for the hydrogenation of methyl formate. A common feature of all three cycles is the transfer of a hydride to a carbonyl group (i.e. dimethyl carbonate, methyl formate, formaldehyde) forming an anionic complex *via* a direct hydride insertion mechanism. DFT calculations reveal the essential role of the non-innocent $\text{P}^{t\text{Bu}}\text{N}^{\text{Py}}\text{N}^{\text{Et}}$ pincer ligand, which participates in H₂ cleavage in its non-aromatic form and assists in methanol formation through the dearomatization of the pyridine ring. However, compared to the M/NH bifunctional mechanism, in which the NH functionality can stabilize the transition state through hydrogen bonding interactions, the amide functionality (deprotonated NH) can as well facilitate heterolytic H₂ activation in cooperation with metal center (Scheme 10). Direct hydride insertion leading to the formation of unstable anionic species might be another reason for the moderate efficiency of aromatization-dearomatization bifunctional catalysts in integrated CO₂ capture and hydrogenation to methanol. Computational studies by Baroudi^{174, 175} and co-workers confirmed the possibility of a direct ion-pair mediated metathesis pathway for the transformation of **I** into **III** (Scheme 16) in the C-OCH₃ bond cleavage step in DMC hydrogenation with $\text{Ru-P}^{t\text{Bu}}\text{N}^{\text{Py}}\text{N}^{\text{Et}}$ as catalyst (Scheme 17). This reaction pathway can proceed *via* three steps: (i) an outer-sphere hydride transfer from $[\text{Ru}(\text{H})_2(\text{P}^{t\text{Bu}}\text{N}^{\text{Py}}\text{N}^{\text{Et}})(\text{CO})]$ to the carbonyl group of DMC to give an ion pair of the cationic metal fragment and the $[\text{OCH}(\text{OMe})_2]^-$ anion in which the C-H bond is facing the metal center, followed by (ii) reorientation of the $[\text{OCH}(\text{OMe})_2]^-$ anion within the intact ion pair to coordinate a methoxy group to the metal, and (iii) C-OMe bond cleavage (methoxide abstraction by the cationic ruthenium center) to yield methyl formate and *trans*- $[\text{Ru}(\text{H})(\text{OMe})(\text{P}^{t\text{Bu}}\text{N}^{\text{Py}}\text{N}^{\text{Et}})(\text{CO})]$.

Scheme 16 DFT calculated aromatization-dearomatization bifunctional mechanism of Ru- $P^tBu_2N^iPyNEt$ catalyzed hydrogenation of dimethyl carbonate to methanol via formate cycle, formaldehyde cycle and methanol cycle.



All ruthenium complexes involved in the catalytic cycle are neutral species. For details see ref. 172.

Scheme 17 Ru- $P^tBu_2N^iPyNEt$ catalyzed DMC hydrogenation to methanol in a H/OR metathesis pathway via ion-pair formation and rearrangement. Ref. 174, 175.



3. Development of heterogeneous catalysts

Compared to molecular catalysts, heterogeneous catalysts can offer several benefits, such as improved catalyst stability, easier recycling and/or lower manufacturing costs important for industrial applications. For these reasons, heterogeneous catalytic systems have been extensively explored in the context of CO_2 hydrogenation to methanol. In this section, design of heterogeneous materials for CO_2 reduction to methanol at low

temperature is summarized. Based on their composition and mechanism, these catalytic systems can be organized into three sections: 1) metal/metal or metal/support bifunctional heterogeneous catalysts, 2) active-site/N or active-site/OH bifunctional heterogeneous catalysts, and 3) cooperation of catalysts and additives in a tandem process *via* crucial intermediates.

3.1 Metal/metal and metal/support bifunctional heterogeneous catalysts

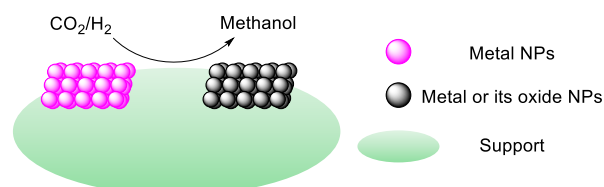


Figure 13 General concept of metal/metal and metal/support bifunctional heterogeneous catalysts in CO_2 hydrogenation to methanol. NPs: nanoparticles.

Figure 13 shows the general concept of metal/metal and metal/support bifunctional heterogeneous catalysts in CO₂ hydrogenation to methanol. Metal/metal and metal/support bifunctionality is generally achieved by the optimization of supports, (co-)loaded metal nanoparticles (NPs) and/or second metal or its oxide nanoparticles (NPs). Spatial organization of support or a second metal in proximity to the genuine active sites has also been investigated with novel materials such as MOF (metal-organic framework). The second metal or support can possibly provide co-catalytic or Lewis acid/base sites that are required for the formation of intermediates, and ultimately the hydrogenation of these intermediates to methanol.

Shimizu¹⁷⁶ and co-workers reported a Re(1)/TiO₂ (Re 1 wt%) catalyst for hydrogenation of CO₂ to methanol at 150 °C, 10 bar CO₂, and 50 bar H₂ (Figure 14). Both in terms of activity and methanol selectivity, i.e. 44 total TON based on Re and 82% methanol selectivity, respectively, the performance of TiO₂ (anatase) supported Re is superior to that of TiO₂ (anatase) supported other metals and also to Re catalysts supported on

other materials, as well as industrial Cu-based catalyst Cu/Zn/Al₂O₃. Notably, the benchmark Cu-catalyst Cu/Zn/Al₂O₃ gave less than 1 TON under identical operational conditions. This low activity is in line with the large amount of Cu (34wt%, Cu/Re ratio of 100) that typically exhibits low catalytic activity at low temperature. Even with the promotion of alcohol additives, low 1.4, 2.1 and 7.6 TONs over 16 h at 120, 150 and 170 °C, respectively, were reported for this reference Cu catalyst (*vide infra*)¹⁷⁷⁻¹⁸⁰. The results suggest a bifunctional role of TiO₂ and Re-nanoparticles in CO₂ hydrogenation to methanol. The hydrogenation of CO₂ carried out using Re(x)/TiO₂ (with x = 0.2, 1.0, 5.0, 10, and 20 wt %) revealed that the formation of methanol is favored with x = 1 wt % given the subnanometer size of the Re species. In fact, the larger clusters of Re nanoparticles favored the formation of CH₄, while isolated atoms (single atoms) of Re favored the formation of CO. Reduction of CO₂ in the presence of Re(1)/TiO₂ pretreated with H₂ at different temperatures ranging from 200 to 900 °C showed that the best performance is observed for catalyst pretreated at

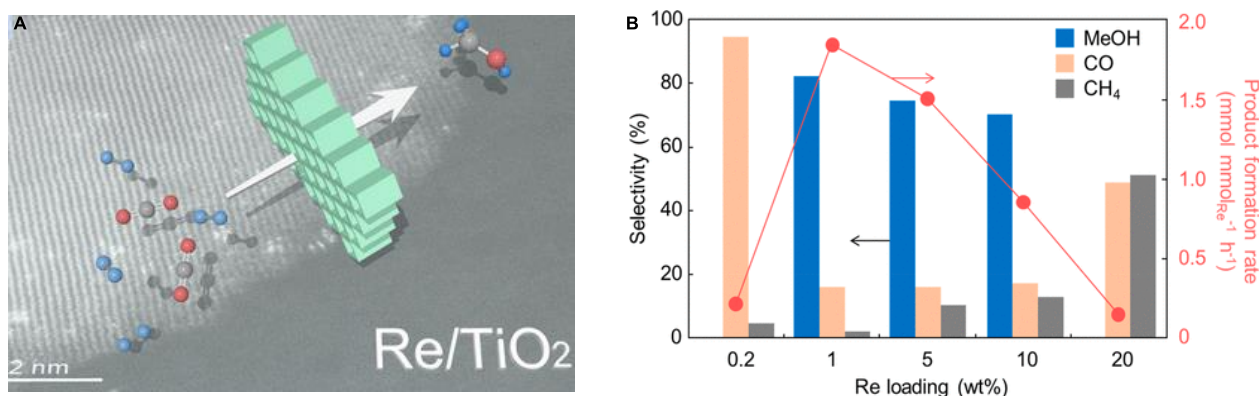


Figure 14 Low-temperature hydrogenation of CO₂ to methanol over heterogeneous TiO₂-supported Re nanoparticle catalysts A) Re-Ti bifunctional catalyst. B) Effect of the Re loading on the hydrogenation of CO₂ catalyzed by Re(x)/TiO₂ (x = 0.2, 1, 5, 10, and 20 wt %). Pretreatment: H₂ (30 mL min⁻¹), 500 °C, 0.5 h. Reaction conditions: 0.0054 mmol of Re, 1,4-dioxane (1 mL), CO₂ (10 bar), H₂ (50 bar), 150 °C, 24h. Modified with permission from ref. 176. Copyright (2019) American Chemical Society.

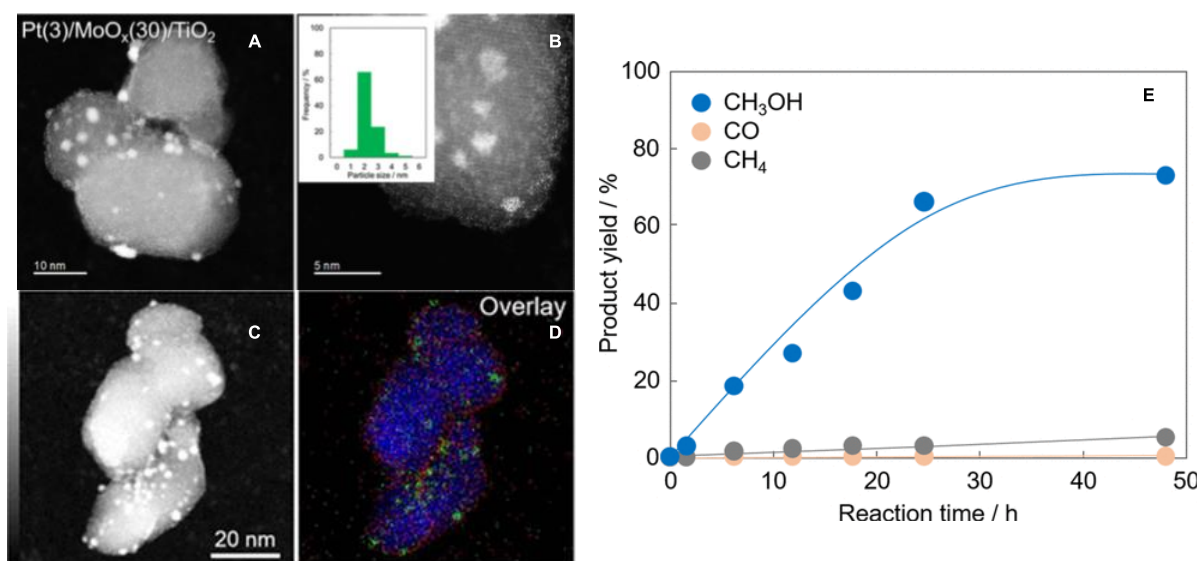


Figure 15 Pt and MoOx co-loaded TiO₂ catalysts Pt(3)/MoOx(30)/TiO₂ (Pt 3 wt %, MoO₃ 30 wt %) for low-temperature CO₂ hydrogenation to methanol. A-B) High-angle annular dark-field scanning transmission electron microscopy (HAADF-STEM) images for Pt(3)/MoOx(30)/TiO₂ together with the particle size distribution of Pt. C) HAADF-STEM image and D) EDX mapping of Pt(3)/MoOx(30)/TiO₂. E) Time course for the hydrogenation reaction of CO₂ over Pt(3)/MoOx(30)/TiO₂. Pretreatment: H₂ (20 cm³ min⁻¹), 300 °C, 0.5 h. Reaction conditions: catalyst (300 mg), CO₂ (10 bar), H₂ (50 bar), 1,4-dioxane (1 mL), 150 °C, 24 h. Partially adapted with permission from ref. 181. Copyright (2019) American Chemical Society.

500 °C. Characterization by X-ray absorption near edge structure (XANES) measurements showed a reduction in valence of the Re species with increasing reduction temperature. This means that the average oxidation state of Re responsible for the catalytic formation of methanol should be higher than 0 and below +4. Catalytic experiments using CO and formic acid as feedstock in control experiments showed that the hydrogenation of CO₂ to methanol goes through formic acid instead of CO. The crucial formate intermediates were identified by *in situ* FT-IR (Fourier-Transform Infrared) spectroscopy at 1,360 and 1,560 cm⁻¹. How exactly the formate species were formed and its further conversion into methanol on the interface of Re and TiO₂ was not investigated. Further studies are required to uncover the complete mechanistic picture.

Shimizu¹⁸¹ and co-workers reported co-loaded Pt nanoparticles and MoOx on similar TiO₂ for CO₂ hydrogenation to methanol (Figure 15). Pt(3)/MoOx(30)/TiO₂ (3 wt% Pt, 30 wt% MoO₃) was prepared by sequential impregnation using Pt(NH₃)₂(NO₃)₂, (NH₄)₆Mo₇O₂₄·4H₂O, and TiO₂, followed by H₂ reduction at 300 °C. Pt nanoparticles and Mo species are highly dispersed over the TiO₂ particles, as evidenced by HAADF-STEM image and EDX mapping. Catalytic CO₂ hydrogenation reactions using 300 mg Pt(3)/MoOx(30)/TiO₂ catalyst in a 10 mL stainless steel autoclave showed a 66% methanol yield along with CH₄ as a minor product under rather mild reaction conditions (T = 150 °C, P_{CO₂} = 10 bar, P_{H₂} = 50 bar, t = 24 h). In contrast, no significant amount of methanol was formed in the presence of other metal catalysts supported on MoOx(30)/TiO₂. Also, MoO₃(30)/TiO₂ or

Pt supported on other materials was unable to form methanol, while Pt(3)/MoO₃ yielded a small amount of methanol along with CO and CH₄ as major products. A combination of Pt and Mo species on other supports resulted in efficient production of methanol, although in lower yield than with Pt(3)/MoOx(30)/TiO₂. The authors tested the industrially used Cu-based catalyst Cu/Zn/Al₂O₃ as benchmark, but this catalyst was ineffective (20% yield) under the applied reaction conditions. These results clearly reveal the importance of a combination of Pt and Mo as active components, and the crucial role of TiO₂ as catalyst support in promoting CO₂ hydrogenation. Time on stream experiments using Pt(3)/MoOx(30)/TiO₂ showed a methanol yield of 73% after 48 h, which approaches the theoretical equilibrium yield under the applied reaction conditions. A total methanol TON of 3,588 was estimated on the basis of CO adsorption amount performed at 30 °C for a fresh sample. Pt(3)/MoOx(30)/TiO₂ that was separated from the reaction solution, washed with 1,4-dioxane and dried in an oven (110 °C) in an air atmosphere, can be reused, albeit with gradual decrease of the methanol yield and selectivity. Mechanistic studies by *in situ* X-ray absorption fine structure (XAFS) measurements of Pt(3)/MoOx(30)/TiO₂ suggested that presence of reduced MoOx species are important for the hydrogenation reaction. CO used as starting material also led to methanol thus indicating that CO is a possible intermediate, but direct hydrogenation of CO₂ to form methanol is preferred. The rate of formic acid hydrogenation to methanol was found considerably higher than that of CO₂, implying that formic acid and its derivatives such as formate adsorbed on the surface of

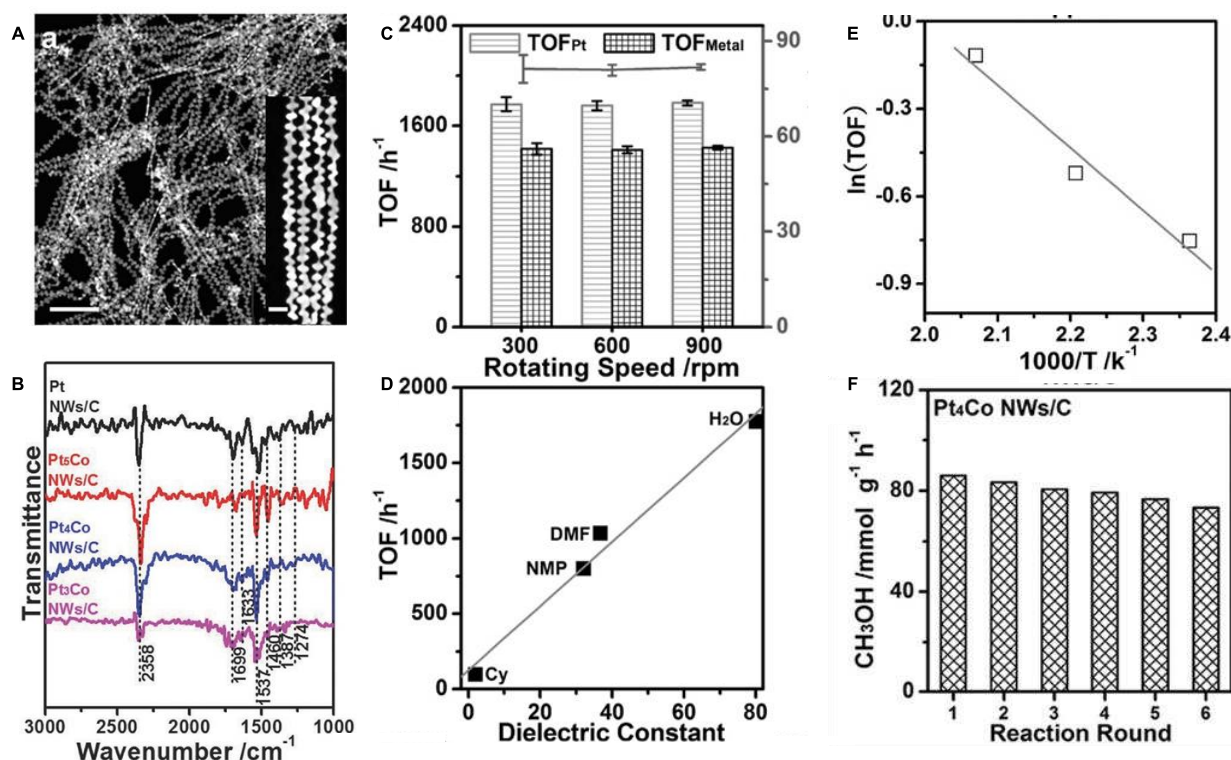


Figure 16 CO₂ hydrogenation to methanol catalyzed by zigzag platinum-cobalt nanowires. A) HAADF-STEM image of Pt₄Co NWs. B) CO₂ adsorption spectra of Pt NWs/C, Pt₅Co NWs/C, Pt₄Co NWs/C, and Pt₃Co NWs/C after CO₂ treatment (1 bar) at 150 °C. C) The achieved product yields and the comparisons of the TOF_{Metal} and TOF_{Pt} values of 1 wt% Pt₄Co NWs/C catalysts at 150 °C for 3 h at different rotating speeds. D) The correlation of TOF_{Pt} to the dielectric constant of various solvents over 1 wt% Pt₄Co NWs/C at 150 °C. E) The Arrhenius plot for the methanol production of 1 wt% Pt₄Co NWs/C. F) Product yields achieved with 1 wt% Pt₄Co NWs/C over six rounds of successive reactions. Partially adapted with permission from ref. 183. Copyright (2017) Wiley-VCH Verlag GmbH & Co. KGaA, Weinheim.

the catalyst may be the crucial intermediates towards methanol formation. *In situ* IR analysis of a reaction carried out using Pt(3)/MoOx(30)/TiO₂ at ambient pressure and 150 °C under continuous gas flow containing CO₂ (10 cm³ min⁻¹), H₂ (30 cm³ min⁻¹), and He (50 cm³ min⁻¹) showed several features in the range of 1,300-1,600 cm⁻¹ wavenumber, associated with the presence of carbonate and formate species (typically at 1,370 and 1,555 cm⁻¹). In contrast, these bands were not observed in the reaction mixture in the presence of MoOx(30)/TiO₂, demonstrating the importance of Pt for H₂ activation and thus providing hydride in the formation of the formate species. *In situ* Mo K-edge XANES analysis showed a positively shifted edge position in the spectrum of Pt(3)/MoOx(30)/TiO₂ upon introducing CO₂. This observation reveals the role of CO₂ as an oxidant. This redox reaction of the Mo species taking place during CO₂ hydrogenation is consistent with an oxygen-vacancy-driven mechanism (or the reverse Mars-Van Krevelen mechanism¹⁸²). However, the detailed mechanism regarding the cooperation of these three components has not been clarified and requires further investigation.

Huang¹⁸³ and co-workers reported zigzag Pt-Co nanowires (NWs) with Pt-rich surfaces containing abundant steps/edges for active and stable CO₂ hydrogenation to methanol (Figure 16). These Pt-Co NWs were prepared by a combination of platinum(II) acetylacetonate [Pt(acac)₂], cobalt(III) acetylacetonate [Co(acac)₃], cetyltrimethylammonium chloride (CTAC), and glucose dissolved in oleylamine by ultrasonication, followed by subsequent reaction at 160 °C for 5 h. HAADF-STEM showed that the Pt-Co NWs zigzagged along the whole NWs, exhibiting a crenel-like nanostructure several micrometers (μm) in length and an average aspect ratio of 50 (Figure 16A). The well-defined structure was also proven by X-ray diffraction (XRD) and STEM energy-dispersive X-ray spectroscopy (EDS) elemental mappings. The catalytic performance of Pt₄Co NWs/C at different rpms, viz. 300, 600 and 900 rpm, were identical under 8 bar CO₂ and 24 bar H₂ at 150 °C in a 60 mL stainless steel autoclave, indicating the experiments are carried out in a kinetic control without film mass transfer issues under these conditions (Figure 16C). Through tuning of the Pt/Co ratio and the support, Pt₄Co NWs/C showed the best performance for CO₂ hydrogenation to methanol in water, showing a highest turnover frequency (TOF_{Pt}) of 1,773 h⁻¹. The beneficial effect of the C support was explained by the presence of unpaired electrons from abundant defects and dislocations at the disordered structures and edge areas, which played a significant

role in chemisorption/activation of reactants on Pt₄Co NWs/C. Non-polar solvents, such as cyclohexane, exhibited the worst catalytic behaviour. In contrast, polar solvents such as NMP and DMF, and in particularly H₂O, significantly improved the CO₂ hydrogenation to methanol under otherwise identical reaction conditions (Figure 16D). Likely, water with its high dielectrical constant impacts the free energy of the product thus stabilizing the transition state leading to lower reaction barriers. Water may also participate in the catalytic reaction as source of hydrogen assisting the formation of crucial intermediates, such as carboxyl species. Arrhenius plot analysis of the optimal catalyst system showed a low apparent activation energy (E_a) of 6.0 kcal mol⁻¹ (Figure 16E). This value is low, but not due to film mass transfer issues as shown in Figure 16C. Such low value may be due to highly enthalpic chemisorption of intermediates on the catalyst surface in the rate determining step, but this hypothesis needs evaluation. The catalyst stability study showed clear activity decays after six catalytic cycles with 86% preservation of its activity. The authors explained this deactivation to be due to loss of catalyst during the catalyst collection process (Figure 16F). The Diffuse Reflectance Infrared Fourier Transform Spectroscopy (DRIFTS) study of CO₂ adsorption on Pt₄Co NWs/C showed peaks at around 2,358 cm⁻¹, corresponding to the asymmetric stretching vibration modes of CO₂. A series of bands at 1,200-1,700 cm⁻¹, belonging to the products at the active sites and the chemical adsorptions of CO₂. Particularly the strong adsorption of bidentate carbonates observed at 1,537 and 1,699 cm⁻¹ were observed (Figure 16B). These results indicate the formation of appropriate carboxylate intermediates upon interaction likely at the basis of the enhanced methanol production.

Thompson¹⁸⁴ and co-workers investigated CO₂ hydrogenation to methanol over a nanostructured metal catalysts supported on Mo₂C (Figure 17). Mo₂C and various M/Mo₂C catalysts gave methanol as the major product with up to 0.7 h⁻¹ TOF and a selectivity higher than 79%, along with CO and CH₄ in small quantities at 135 °C in 1,4-dioxane. Compared to Mo₂C, the deposited metals moderately enhanced the CO₂ conversion to methanol with selectivity and activity decreasing in the following order: Pd/Mo₂C ≈ Cu/Mo₂C > Fe/Mo₂C > Co/Mo₂C > Mo₂C. Notably, Pd/Mo₂C and Cu/Mo₂C yielded mainly methanol, whereas Co/Mo₂C and Fe/Mo₂C catalysts yielded significant amounts of C₂₊ hydrocarbons and ethanol. The latter yields further increased at higher reaction temperature. Activation energies for hydrocarbon formation are much higher

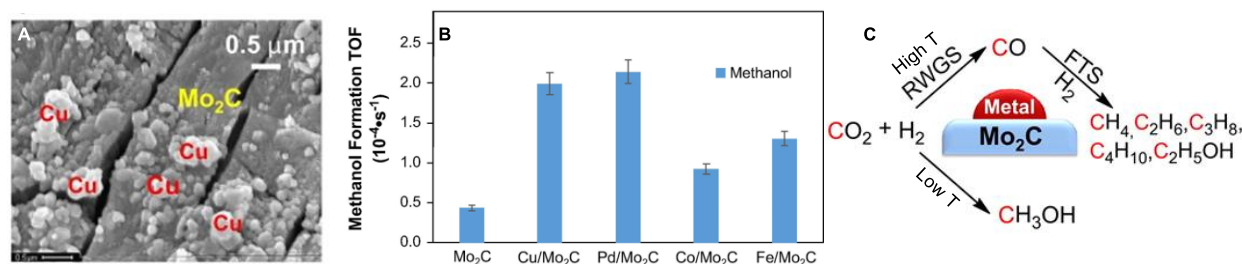


Figure 17 Mo₂C supported metal catalysts for CO₂ hydrogenation to methanol. A) SEM (Scanning electron micrographs) for Cu/Mo₂C. B) TOF of methanol at 135 °C on M/Mo₂C catalysts. Experiments were performed at 10 bar CO₂ and 30 bar H₂ in 37.5 mL 1,4-dioxane, at 135 °C. C) Plausible reaction mechanism in the production of methanol and hydrocarbons from CO₂ and H₂ at high temperature or lower temperature conditions. FTS = Fischer-Tropsch synthesis. Partially adapted with permission from ref. 184. Copyright (2016) Elsevier Inc.

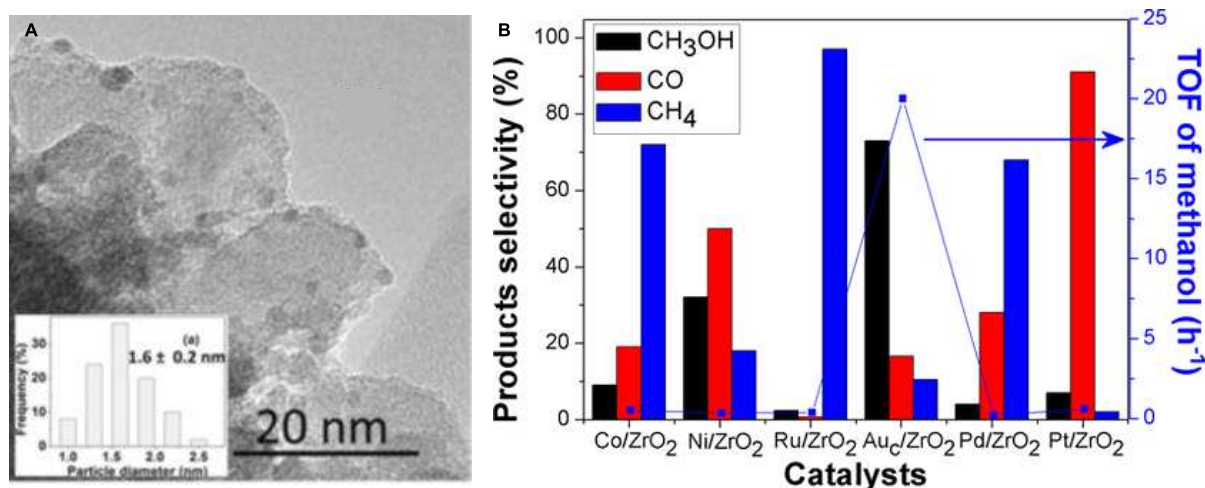


Figure 18 Hydrogenation of CO₂ to methanol over supported subnanometric gold catalysts at low temperature. A) TEM (transmission electron microscopy) image of the Au_c/ZrO₂ catalyst and B) its catalytic performance in comparison with other metals supported on ZrO₂. Reaction conditions: 0.1 g reduced catalyst, P_{H₂} = 30 bar, P_{CO₂} = 10 bar, with 5 bar N₂ as internal standard (initial pressure at room temperature), T = 180 °C, 8 h. TOF represents moles of methanol formed per mole gold per hour and the selectivity to products is based on CO₂ converted. Partially adapted with permission from ref. 185. Copyright (2017) Wiley-VCH Verlag GmbH & Co. KGaA, Weinheim.

than those for methanol formation, reflecting the involvement of different intermediates and perhaps different active sites in the rate determining steps of the two processes. At 200 °C, the methanol produced during CO hydrogenation was only 7.7% and 3.2% of that produced during CO₂ hydrogenation over Cu/Mo₂C and Fe/Mo₂C catalysts, respectively. These results suggest that methanol is predominantly produced *via* a direct CO₂ hydrogenation process instead of *via* CO from RWGSR. In contrast, the hydrocarbon formation TOFs from CO were 3-4 times higher than those from CO₂ hydrogenation, suggesting that the hydrocarbons are primarily produced *via* CO hydrogenation, which is indeed more favourable at the higher

temperatures *via* the RWGSR process, followed by the Fischer-Tropsch reactions.

In addition, Han¹⁸⁵ and co-workers investigated the use of subnanometric gold nanoparticles supported on ZrO₂ for the efficient hydrogenation of CO₂ to methanol at low temperature (Figure 18). The supported gold catalyst Au_c/ZrO₂ (*c* represents 1.6 nm Au nanoclusters) was prepared by a deposition-precipitation method and characterized by TEM showing 1.6 nm Au nanoclusters well-dispersed over ZrO₂ support. The TOF (to methanol) reached 20 mol of methanol per mol Au per hour with 73 % methanol selectivity for Au_c/ZrO₂ at 180 °C (P_{H₂} = 30 bar, P_{CO₂} = 10 bar). In contrast, the M/ZrO₂ catalysts featuring

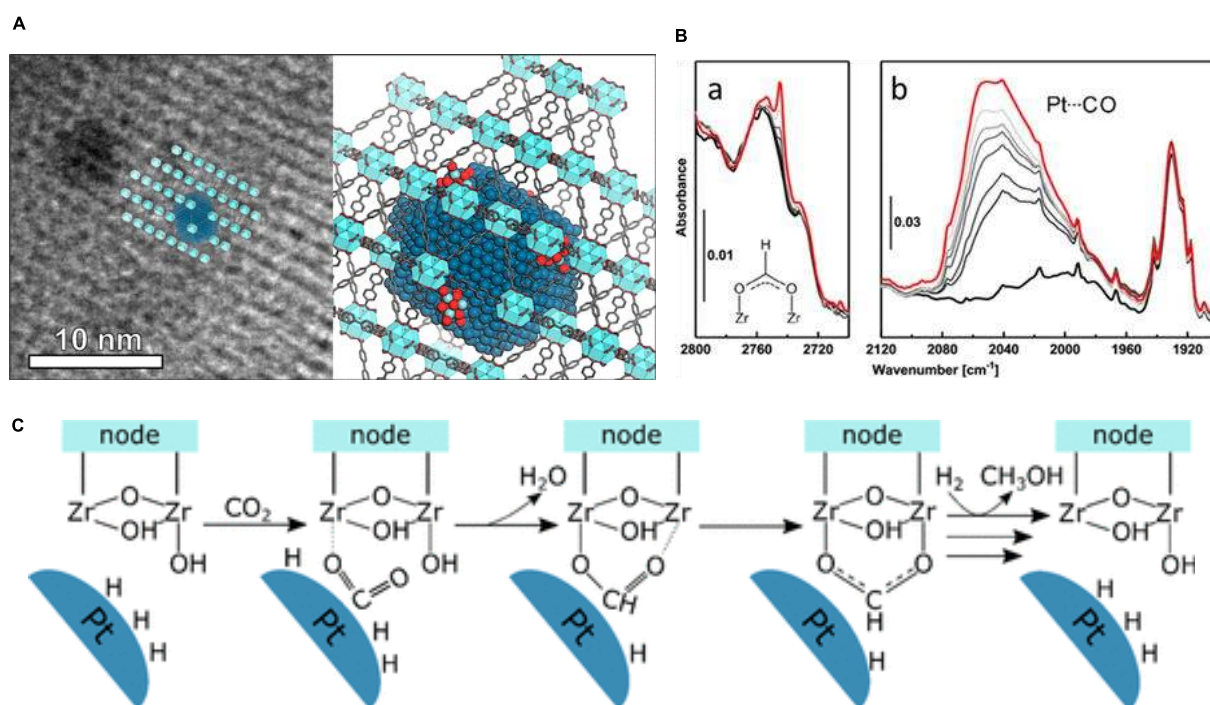


Figure 19 CO₂ hydrogenation to methanol with A) Pt Nanoparticles encapsulated in UiO-67 synthesized using an impregnation approach. B) FT-IR spectra of UiO-67-Pt collected during CO₂ hydrogenation (CO₂/H₂ = 1/6, 10 mL min⁻¹, 170 °C, 1 bar) at different times: (a) spectral region of the ν(C-H) for formate groups, and (b) spectral interval typical for CO linearly adsorbed on metal nanoparticles. C) Proposed reduction mechanism. Modified with permission from ref. 188. Copyright (2020) American Chemical Society. Further permissions related to the material excerpted should be directed to the ACS.

metals which are frequently used for hydrogenation (with M = Co, Ni, Ru, Pd, and Pt) showed surprisingly low activity and selectivity to methanol, confirming the unique property of supported gold nanoclusters in promoting the reaction. Unfortunately, the activity of the catalyst decreased considerably already after reuse, likely due to aggregation of the active Au nanoparticles. Investigation of the cluster size revealed that both the activity and selectivity of nanoparticles below 2 nm were much higher than larger Au particles. The selectivity to CO decreased with the increase of temperature while an opposite trend was observed for CH₄. This implies that the formation of methane requires higher temperature and the formation of CO from RWGS was inhibited at the higher temperatures. AP-XPS (Ambient-Pressure X-ray Photoelectron Spectroscopy) studies suggested that the supported gold catalyst holds a similar reaction mechanism as with copper based catalysts^{186, 187} such as Cu-Zn-Zr catalyst and CeOx/Cu(111) catalyst and HCOO*, HCOOH*, H₂COOH*, H₂CO*, and H₃CO* are the main surface intermediates.

Olsbye¹⁸⁸⁻¹⁹⁰ and co-workers reported Pt nanoparticles encapsulated in MOF UiO-67 for the hydrogenation of CO₂ to methanol at ambient pressure (Figure 19). More specifically, MOF UiO-67 was impregnated with K₂PtCl₄ in DMF at 100 °C overnight with stirring to obtain UiO-67-Pt. Given the confinement effects in the structure, the Zr metal node of MOF in proximity to Pt active sites partakes in catalysis by formation, orientation, and stabilization of the crucial intermediates. The encapsulated catalyst UiO-67-Pt showed higher activity and selectivity towards methanol than Pt nanoparticles on other supports such as Pt/Al₂O₃ and Pt/SiO₂ (36 vs. 0-0.36 h⁻¹ TOF and 20-40% vs. 0-10% selectivity) at 170 °C in a fixed-bed flow setup. FT-IR experiments showed surface formate intermediates, which are formed by metal-hydride transfer to CO₂ from

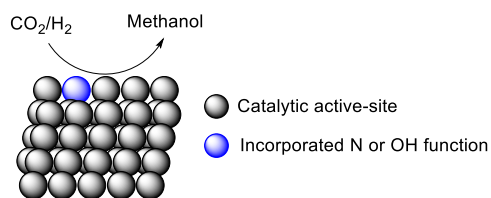


Figure 20 Active-site/N or active-site/OH bifunctional heterogeneous catalysts in CO₂ hydrogenation to methanol.

adjacent Pt NPs, binding to two Zr nodes in a bidentate configuration (Figure 19A). The Zr-formate species appears as a key intermediate in the methanol formation path, as ascertained by kinetic experiments, detailed modelling studies, and ¹³C/¹²C and (CO₂+H₂)/(CO₂+D₂) isotope transient experiments. The formate species formed are further hydrogenated according to a hydrogen spill-over mechanism from the adjacent Pt NPs in a cooperation with the Zr nodes. Despite all this insight, it is still an open question how the enhancement of CO₂ hydrogenation selectivity and activity *via* the formate intermediate stabilization and hydrogenation can be explained precisely. More research efforts are necessary to uncover the fundamental aspects behind this elegant encapsulation approach.

3.2 Active-site/N or Active-site/OH bifunctional heterogeneous catalysts

Figure 20 shows the general concept of active-site/N and active-site/OH bifunctional heterogeneous catalysis. Here, N or OH functionalities incorporated on the surface cooperate with the active (metal) sites for H₂ activation, CO₂ adsorption, hydride/proton transfer and intermediate stabilization. Originally developed in M/NH bifunctional molecular catalysts, this approach receives significant general interest in the design

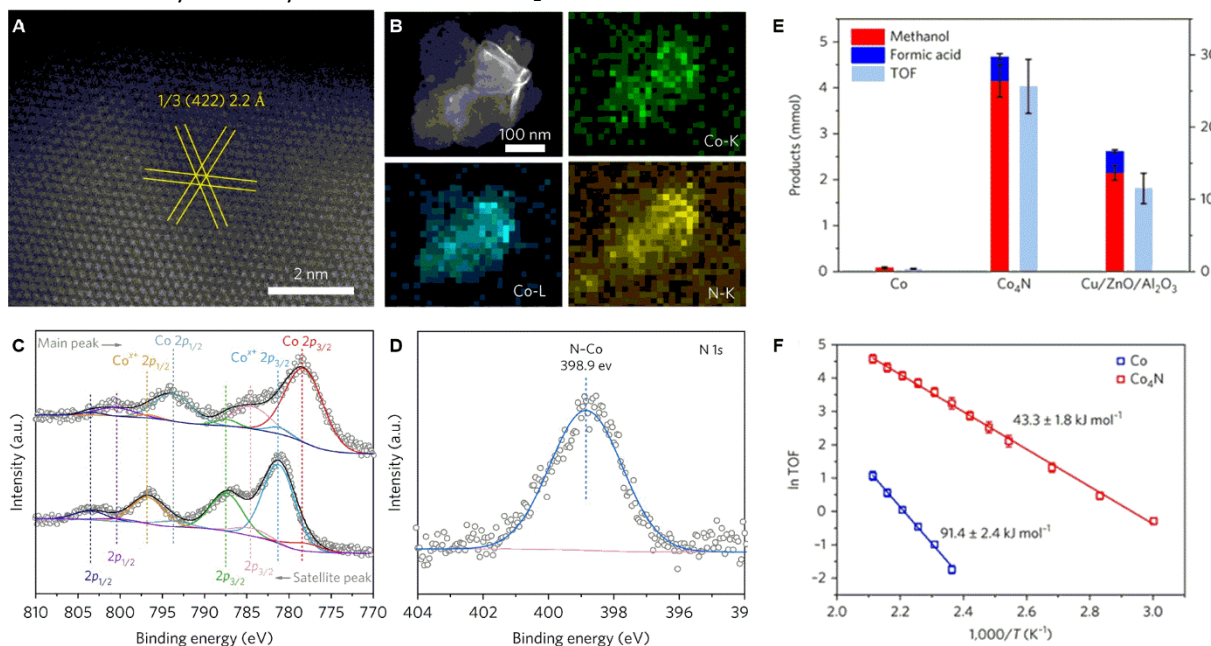


Figure 21 Structural characterization of Co₄N nanosheets: A) HAADF-STEM image of Co₄N nanosheets. The lattice parameter indicated by the parallel yellow lines was determined as 2.2 Å, corresponding to the 1/3(422) fringes. B) STEM image and STEM-EDX elemental mapping of the Co-K, Co-L and N-K edges of Co₄N nanosheets. C) Co 2p XPS spectra for Co and Co₄N nanosheets. D) N 1s XPS spectrum for Co₄N nanosheets. The peak at 398.9 eV was assigned to N species in Co nitrides. E) Catalytic performance of Co₄N in the hydrogenation of CO₂: comparison of products and TOFs of Co nanosheets, Co₄N nanosheets, and Cu/ZnO/Al₂O₃ under 32 bar of CO₂/H₂ mixed gas (CO₂/H₂ = 1:3) at 150 °C after 3 h. F) The Arrhenius plots of Co and Co₄N nanosheets. Modified with permission from ref. 191. Copyright (2017) Macmillan Publishers Limited, part of Springer Nature.

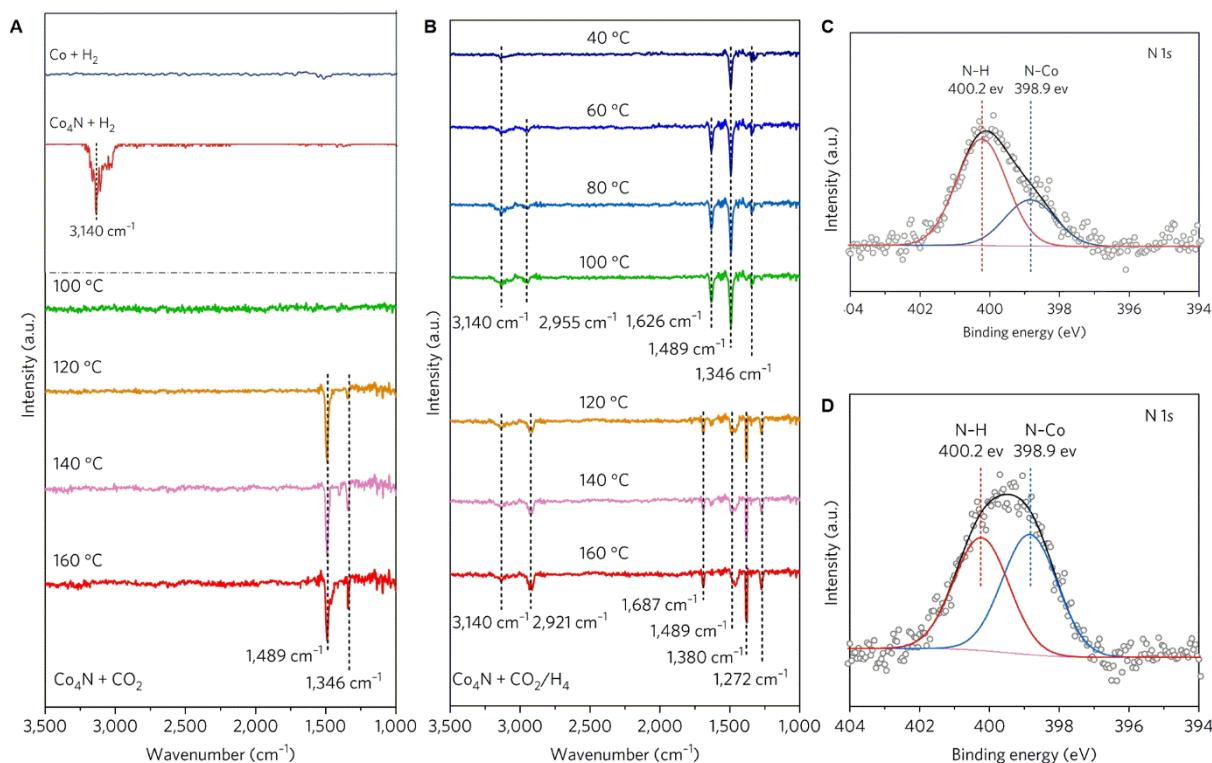


Figure 22 Mechanistic study of Co_4N nanosheets in CO_2 hydrogenation. A) *In situ* DRIFT spectra of Co_4N nanosheets after the exposure to H_2 or CO_2 . B) *In situ* DRIFT spectra of Co_4N nanosheets after the exposure to CO_2/H_2 mixed gas ($\text{CO}_2/\text{H}_2 = 1:3$, 1 bar). Quasi *in situ* XPS spectra of N 1s for Co_4N nanosheets after the treatment with C) H_2 and D) H_2/CO_2 . The peaks at 400.2 and 398.9 eV were assigned to N atoms coordinated with H and Co atoms, respectively. Modified with permission from ref. 191. Copyright (2017) Macmillan Publishers Limited, part of Springer Nature.

of heterogeneous catalysts for various applications including the CO_2 conversion to methanol.

As an example, Zeng¹⁹¹ and co-workers reported a Co_4N nanosheet catalyst with nitrogen atoms incorporated to achieve high activity for CO_2 hydrogenation to methanol (Figure 21). The Co_4N nanosheets were prepared by placing Co nanosheets in a quartz tube and heated to 400 °C at a rate of 10 °C min^{-1} under NH_3 flow, followed by reaction at 400 °C for 2 h. Characterization of the Co_4N nanosheet catalyst by TEM, HAADF-STEM, STEM-EDX, XRD and Co 2p XPS spectroscopy revealed a homogeneous distribution of both Co and N with both characteristic Co-Co and Co-N bonding interactions, indicating N atoms incorporation on the Co metal surface (Figure 21A-D). In CO_2 hydrogenation experiments, Co_4N displayed a 25.6 h^{-1} TOF (calculated based on surface metal atoms) with high selectivity in a slurry reactor under 32 bar of CO_2/H_2 (1:3) at 150 °C (Figure 21E), which was substantially higher than the 11.5 h^{-1} TOF of the reference commercial catalyst Cu/ZnO/ Al_2O_3 . In contrast, the corresponding Co nanosheets catalyst without nitrogen doping showed 0.4 h^{-1} TOF under otherwise identical conditions. Arrhenius plots analysis showed that the activation energy of Co_4N nanosheets was 10.3 kcal mol^{-1} , about half (21.8 kcal mol^{-1}) that of Co nanosheets (Figure 21F). Clearly, the presence of nitrogen in the Co_4N nanosheets enhanced the catalytic activity by lowering the apparent activation energy. This catalyst also showed a relatively stable performance in production of methanol with an accumulated total TON up to 2,742 after 16 cycles.

The same group¹⁹¹ further conducted *in situ* spectroscopy to study the CO_2 hydrogenation mechanism of the nanosheet catalyst Co_4N (Figure 22). *In situ* DRIFTS experiments in the presence of H_2 showed the formation of Co_4NH_x with characteristic vibration at 3,140 cm^{-1} , corresponding to the stretching vibration of N-H. The formation of Co_4NH_x was also evidenced by solid-state D-NMR (deuterium nuclear magnetic resonance), XRD, XPS spectroscopy, and H_2 -TPD (temperature-programmed desorption) experiments. Solid-state D-NMR showed peaks at 0.4 and 4.5 ppm assigned to D on the surface and inside the lattice of the Co nanosheets, respectively. XRD showed slightly lower angles shifts of the characteristic peaks of the Co_4N nanosheets after H_2 treatment due to lattice expansion by permeation of dissociated H atoms into the lattice relative to those without gas treatment. XPS spectroscopy showed a new peak at 400.2 eV corresponding to the N atoms in the amido groups. *In situ* DRIFTS measurements after exposing Co_4N nanosheets to CO_2 or mixtures of CO_2 and H_2 showed two new features at 1,489 and 1,346 cm^{-1} , corresponding to the stretching vibration of $\text{CO}_2^{\delta-}$,¹⁹²⁻¹⁹⁴ indicative of CO_2 activation on the surface of the Co_4N nanosheets. This was corroborated by CO_2 -TPD profile of Co_4N . Absorption signals at 2,921, 1,687, 1,380, and 1,272 cm^{-1} , corresponding to the stretching vibration of C-H and C=O, the deformation vibration of C-H, and the out-of-plane wagging vibration of C-H in CH_2O^* species, respectively, were observed. Spectroscopic features at 955 and 1,626 cm^{-1} , which were assigned to the stretching vibrations of C-H and bidentate O-C-O in HCOO^* species, appeared at lower temperatures, i.e. 60 °C.

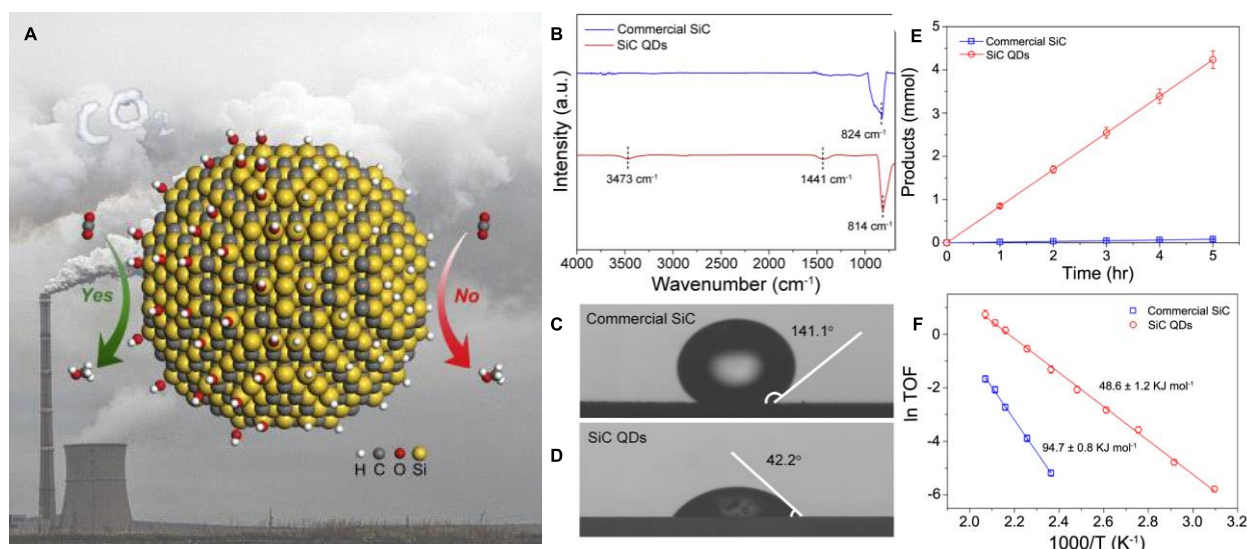


Figure 23 A) General concept of hydroxylation of the surfaces of SiC quantum dots for boosted CO₂ hydrogenation to methanol. B) FT-IR spectra of commercial SiC and SiC QDs (hydroxyl functionalized SiC quantum dots). Contact angles of water droplets on C) commercial SiC and D) SiC QDs deposited on glass. E) Time courses of the products for commercial SiC and SiC QDs under 32 bar of CO₂/H₂ mixed gas (CO₂:H₂ = 1:3) at 150°C. F) The Arrhenius plots of commercial SiC and SiC QDs. The amounts of commercial SiC and SiC QDs were kept at 226.1 and 5.0 mg, respectively, for a catalytic test to ensure that the total surface areas for each catalytic test were the same. Partially adapted with permission from ref. 195. Copyright (2018) Elsevier Inc.

This indicates that Co₄NH_x facilitates the activation and transformation of CO₂ to HCOO* intermediates at low temperature. The N 1s spectra of XPS measurements after the exposure of Co₄NH_x to CO₂ showed that the ratio of peak intensity of N-H to N-Co decreased relative to that of Co₄NH_x, suggesting the participation of N-H in the CO₂ transformation. The kinetic isotope effect (KIE) value for Co₄N nanosheets was also much higher than that for Co nanosheets, i.e. 4.9 vs. 1.9, and therefore bond cleavage of N-D rather than Co-D is likely involved in the reaction over Co₄N nanosheets. However, the genuine CO₂ hydrogenation mechanism behind the Co₄N bifunctional catalysis is still not well understood.

Following a similar concept, Zeng¹⁹⁵ and co-workers reported on surface hydroxyl groups installed on hydrophilic SiC quantum dots (QDs) (Figure 23). Their presence significantly boosted CO₂ hydrogenation to methanol compared to the original commercial SiC, from which it is made. SiC QDs were prepared by etching commercial SiC powders larger than 100 nm with nitric acid and hydrofluoric acid, leading to highly dispersed QDs with an average diameter of 3.2 nm. FT-IR measurements of SiC QDs showed a peak at 814 cm⁻¹ for the stretching vibration of Si-C, and peaks at 3,473 and 1,441 cm⁻¹, corresponding to the stretching vibrations of O-H and Si-O, respectively, compared to the Si-C stretching vibration at 824 cm⁻¹ of commercial SiC (Figure 23B). The contact angle of water droplets on the commercial SiC and SiC QDs deposited glass were 141.1° and 42.2°, respectively, and thus showed the distinct hydrophilicity difference between commercial SiC and SiC QDs, attributed to the presence of surface hydroxyl functionalities on the quantum dots (Figure 23C-D). For CO₂ hydrogenation to methanol, commercial SiC yielded 0.08 mmol of methanol under 32 bar of CO₂/H₂ mixed gas (CO₂:H₂ = 1:3) at 150 °C after 5 h in 30 mL of H₂O in a 100 mL slurry reactor (Figure 23E). In contrast, SiC QDs gave 4.24 mmol methanol under otherwise identical conditions (Figure 23E). The exhibited mass activity of 169.5 mmol g⁻¹ h⁻¹ of hydrophilic SiC QDs was more than three orders of magnitude

higher than that of the hydrophobic commercial SiC. The TOF numbers of the commercial SiC based catalyst and the SiC QDs based material were 0.01 and 0.27 mmol m⁻² h⁻¹ at 150°C, respectively. Arrhenius plots analysis revealed that the activation energy for SiC QDs was 11.6 kcal mol⁻¹, about half of that for commercial SiC (22.6 kcal mol⁻¹) (Figure 23F). Mechanistic studies *via in situ* DRIFT, XPS and XANES measurements and DFT calculations revealed that the surface hydroxyl species on SiC QDs were directly involved in CO₂ hydrogenation through the addition of H atoms from -OH groups into CO₂ to form HCOO* as the intermediate with decreased reaction barriers. Presence of surface hydroxyl seems thus important. Using the same principle, the mass activities of Ni(OH)₂, CoMn LDHs (layered double hydroxides), NiTi LDHs, and NiCo LDHs with hydroxyl functionalities, reached 141.4, 176.1, 282.6, and 335.7 mmol g⁻¹ h⁻¹, respectively, which are 18.4, 16.6, 15.6, and 14.4 times higher than that of NiO, MnCo₂O₄, NiO·TiO₂, and NiCo₂O₄, respectively.

3.3 Tandem processes involving cooperation of catalysts and additives

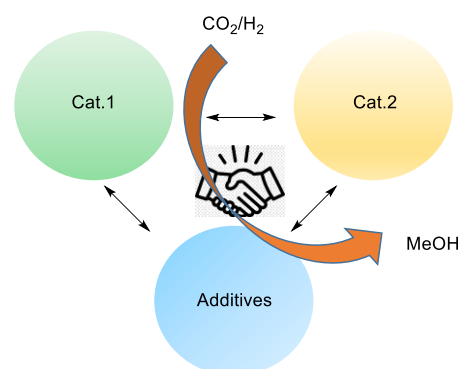


Figure 24 General concept of cooperation of catalysts and additives via a tandem process in CO₂ hydrogenation to methanol.

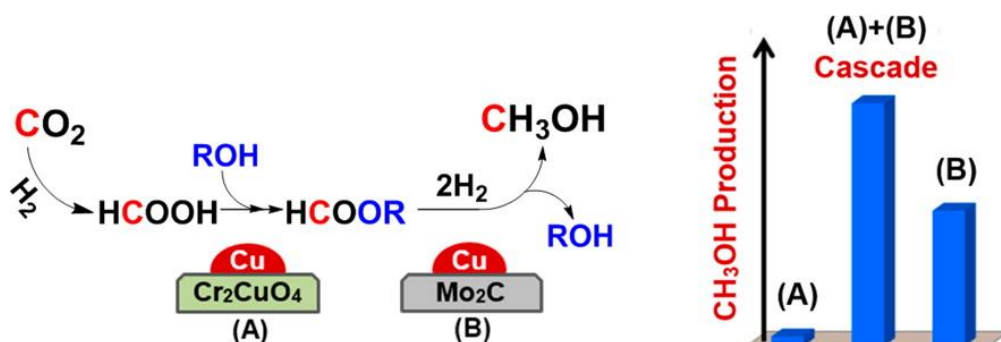


Figure 25 CO₂ hydrogenation to methanol via orthogonal tandem catalysis with Cu/Cr₂CuO₄ and Cu/Mo₂C as heterogeneous catalysts *via* formic acid and/or formate intermediates involving alcohol additives. Reproduced with permission from ref. 197. Copyright (2015) American Chemical Society.

Figure 24 shows the general concept of cooperation of catalysts and additives in a tandem process, thus realizing CO₂ conversion to methanol under mild conditions. The tandem reaction process can either be auto¹⁹⁶ (one catalyst) or orthogonal (two or more catalysts) depending on the number of catalysts required for the different catalytic cycles that are involved. Obviously, as already shown in the above sections, additives play a crucial role here. The potential advantages of combined catalysts and alcohol additives for CO₂ conversion to methanol *via* formate ester have been demonstrated both with homogeneous (*vide supra*), heterogeneous catalysts and combinations thereof. While homogeneous catalysts typically suffer from incompatibility issues, heterogeneous catalysts can intrinsically solve these issues thanks to the natural isolation of their catalytic sites on surfaces or even better in pore confinements, thereby offering the potential to substantially improve CO₂ to methanol hydrogenation catalytic performances.

Inspired by the homogeneous tandem catalysis system reported by Sanford¹⁶⁸ (Scheme 14), Thompson¹⁹⁷ and co-workers explored a heterogeneous cascade catalytic system for the hydrogenation of CO₂ to methanol *via* formic acid and/or formate intermediates (Figure 25). A Cu/Cr₂CuO₄ catalyst was investigated for CO₂ hydrogenation to formate intermediates, and a Cu/Mo₂C catalyst was used to convert the formates to methanol. The Cu/Cr₂CuO₄ catalyst showed high activity and selectivity for CO₂ hydrogenation to ethyl formate in the presence of ethanol at 135 °C, 10 bar of CO₂ and 30 bar of H₂ in 1,4-dioxane. For the second step, Cu/Mo₂C¹⁸⁴ was selected to catalyze the formate hydrogenation to methanol, which yielded methanol as the major product (~74% selectivity), along with a small amount of ethyl formate (~20%). As similar rates for the hydrogenation of CO₂ to ethyl formate and ethyl formate to methanol in presence of Cu/Cr₂CuO₄ and Cu/Mo₂C, respectively, were observed, equal masses of the two catalysts were used in the cascade system. The Cu/Mo₂C and Cu/Cr₂CuO₄ cascade system showed an enhancement in methanol production by ~60%, compared to the catalytic experiments only using Cu/Mo₂C. Moreover, a decrease in the formation of ethyl formate by a similar amount was observed when compared to the combined amounts for the individual catalysts. These results confirmed the orthogonal tandem feature of the Cu/Mo₂C and Cu/Cr₂CuO₄ catalysts for the hydrogenation of

CO₂ to methanol *via* formic acid and/or ethyl formate intermediates. The heterogeneous cascade system displayed a CO₂ conversion rate of 416 μmol g_{cat}⁻¹ h⁻¹ with 77% methanol and 20% ethyl formate selectivity after 24 h of reaction. A nice 1.7 h⁻¹ TOF calculated after 2 h was reported for this cooperation tandem catalysis system at 135 °C.

Interestingly, inspired by biological systems where catalytic reactions are performed in well-confined compartments^{198, 199} with excellent control of activity and selectivity, Tsung²⁰⁰ and co-workers reported a combination of an immobilized PNP pincer molecular catalyst **Cat.1**@UiO-66, by its encapsulation inside a metal-organic framework (MOF), and a homogeneous PNN pincer molecular catalyst **Cat.3** for converting CO₂ into methanol in the presence of catalytic amounts of alcohol additives (Figure 26). **Cat.1**²⁰¹ is one of the most active molecular catalysts for CO₂ hydrogenation to formic acid, showing 110,000 h⁻¹ TOF, while **Cat.3**²⁰² is an efficient molecular catalyst for ester hydrogenation to alcohols. The immobilized **Cat.1**@UiO-66 was prepared by diffusion of the complex **Cat.1** into the pores of MOF UiO-66²⁰³ *via* linker dissociation. Linker dissociation occurs readily in protic solvents, but is very slow in polar aprotic or nonpolar solvents. Consequently, such immobilized constructs can be used as catalysts in polar aprotic or nonpolar solvents without complications from catalyst leaching. The isolation of catalyst **Cat.1** achieved by the encapsulation inside the pores of UiO-66 avoids possible bimolecular decomposition pathways between **Cat.1** and **Cat.3**, as well as incompatibility issues between the three catalysts, as observed by Sanford¹³⁶ et al (Scheme 14). Besides, by separating these two molecular catalysts in space, the Lewis acidic zirconium oxide nodes of UiO-66 can additionally catalyze esterification reactions, such as formic acid with alcohol to form formate ester. In fact it is another active site present in the same heterogeneous **Cat. 1**. Thus, in the presence of 3 bar of CO₂, 37 bar of H₂, and ethanol as a superstoichiometric additive (10 mmol), the combination of immobilized catalyst **Cat.1**@UiO-66 and molecular catalyst **Cat.3** yielded methanol as the only product with 4,710 TON in *N,N*-dimethylformamide (DMF) at 70 °C after 16 h. The TON with respect to **Cat.1**@UiO-66 improved to 6,600, an averaged 412 h⁻¹ TOF, when 2,2,2-trifluoroethanol (TFE, 10 mmol) was used as an alcohol additive. In contrast, a combination of **Cat.1**, UiO-66 (**Cat.2**), and **Cat.3** did not show any methanol formation. The following emerges from

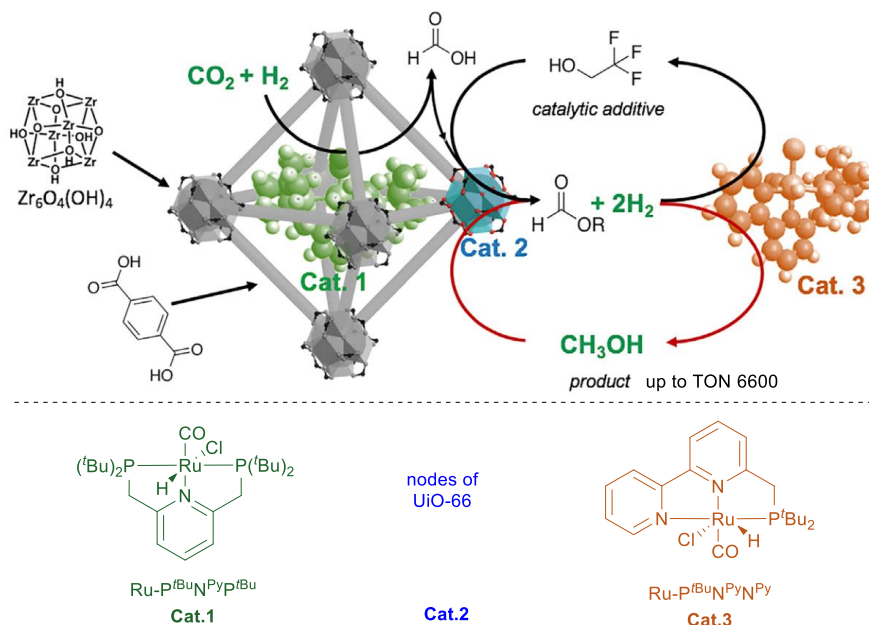


Figure 26. Orthogonal tandem CO₂ hydrogenation to methanol using a immobilized molecular catalyst and a molecular catalyst *via* a formate ester intermediate involving 2,2,2-trifluoroethanol additive. Reproduced with permission from ref. 200. Copyright (2020) Elsevier Inc.

evaluation of the alcohol additives: 1) slower reaction rates were observed with increasing alcohol size and branching possibly due to mass transport limitation for the steps involving the alcohol additive, and 2) faster reaction rates were observed for more acidic alcohols in consistency with a mechanism involving an ester intermediate because of the formation of a more reactive electrophilic formate ester for further reduction. In order to recycle the catalyst, a fully heterogeneous system, i.e. **Cat.1@UiO-66** plus **Cat.3@UiO-66**, was explored and demonstrated to be highly active. No appreciable loss in activity was observed over five cycles, leading to a total 17,500 TONS. Conversion of CO₂ to methanol at various concentrations of the TFE additive also revealed a catalytic feature in additive that enables the catalysis system to be carried out without superstoichiometric amount of alcohol.

Mertens¹⁷⁸ and co-worker investigated the usage of *N,N*-diethylethanolamine (DEEA) as additive for the chemical fixation of CO₂ and its direct hydrogenation to methanol in the presence of a commercially available catalyst Cu/ZnO/Al₂O₃ (Figure 27). In the presence of DEEA, Cu/ZnO/Al₂O₃ yielded methanol at 100 and 170 °C with intermediate formation of 2-diethylaminoethyl formate, as evidenced by NMR and GC analysis. Given the involvement of only one catalyst for all reductive steps, it is an interesting example of auto tandem catalysis. The activity for methanol production at 100 °C was 0.542 mmol (kg-cat-h)⁻¹, and significantly increased at 170 °C to 1,640 mmol (kg-cat-h)⁻¹, corresponding to 0.06 and 0.20 h⁻¹ TOF, respectively. The energetics of the process was seen as a partial heat integration process, of which the exothermic heat of the hydrogenation reaction is partially used by the endothermic CO₂ release from pre-CO₂ loaded DEEA. Operando NMR

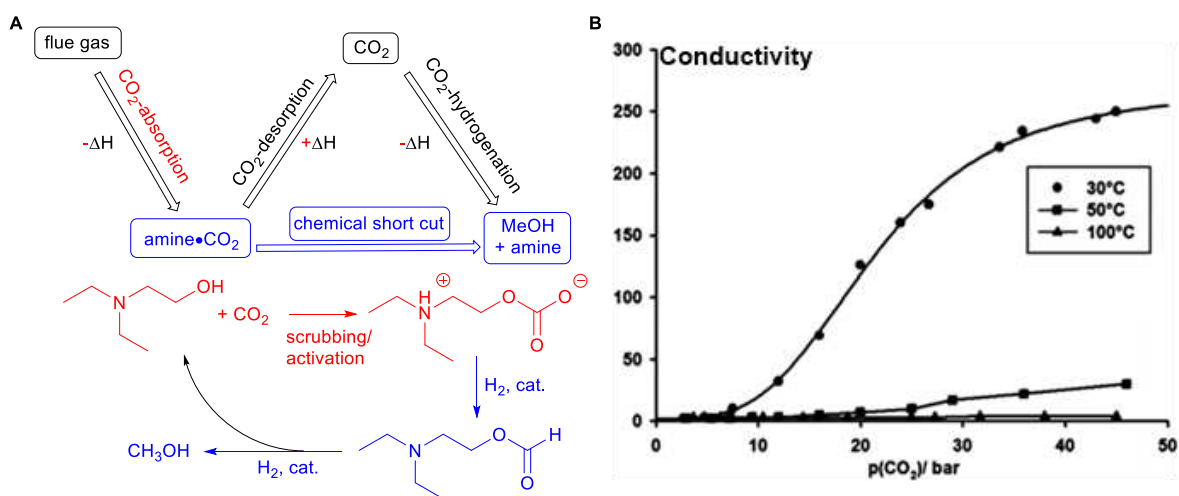


Figure 27 A) Auto tandem Cu/ZnO/Al₂O₃ catalyzed CO₂ hydrogenation to methanol employing *N,N*-diethylethanolamine (DEEA) as additive. B) Conductivity measurements of pure DEEA exposed to a CO₂ atmosphere (T = 30, 50, and 100 °C) indicating the formation of the zwitterionic species. Partially modified with permission from ref. 178. Copyright (2014) American Chemical Society.

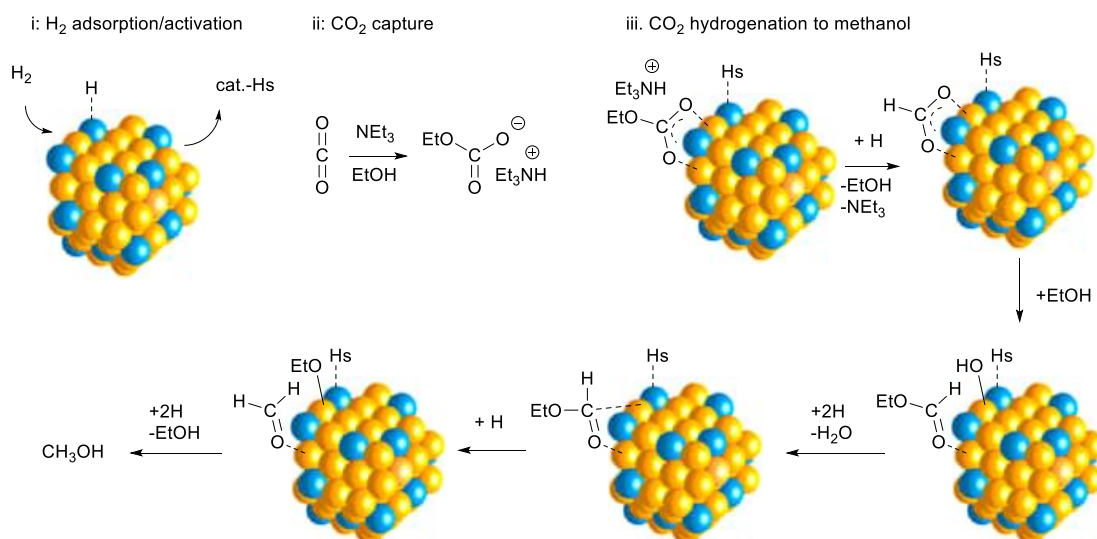


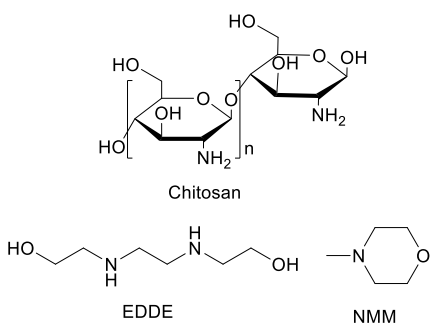
Figure 28 Proposed reaction mechanism for the one-pot CO₂ capture and conversion into methanol by auto tandem catalysis with Cu/ZnO/Al₂O₃ with use of alcohol-amine additives. Ref. 179.

spectroscopy and electric conductivity measurements showed the formation of zwitterion species predominately at temperatures below 100 °C (Figure 27B), indicating the activation mechanism based on zwitterionic species is more relevant at low than high temperatures.

Heldebrant¹⁷⁹ and co-workers further investigated the commercial catalyst Cu/ZnO/Al₂O₃ for CO₂ hydrogenation to methanol in the presence of primary, secondary and tertiary amines and alcohols as additives at lower temperatures, i.e. 120 to 170 °C range. Using an optimized alcohol-amine combination, i.e. EtOH (200 mmol) and Et₃N (20 mmol), Cu/ZnO/Al₂O₃ showed high selectivity (>95%) to methanol (up to 100% yield with respect to amine and 7.6 TON over 16 h) with only trace amounts of CO and CH₄ at 50 bar pressure of CO₂/H₂ (1/2 ratio) and 170 °C. These results at such low temperature are very promising. Note that heterogeneously Cu/ZnO/Al₂O₃ catalyzed CO₂ to CH₃OH reaction under traditional conditions is applied at much higher temperatures, typically above 250 °C. Operando ¹³C NMR spectroscopy of the catalyst in the presence of NEt₃ and EtOH at 20 bar of CO₂ at 120 °C showed a 2.2 times higher ethyl carbonate (158.9 ppm) concentration, compared to that of the active sites on the catalyst. Both mechanistic and catalytic experiments are in accordance with a reaction pathway proceeding *via* alkyl carbonate, formate, and formate ester intermediates. Figure 28 shows the mechanistic proposal for the combination of alcohol-amine and catalyst Cu/ZnO/Al₂O₃. Studies on the amines basicity suggested an optimal pK_a value of the conjugate acid above 11 (in H₂O). Evaluation of different alcohols revealed that steric demands impact the reaction yield, disfavoring alcohols with increased steric hindrance. This result indicates an active participation of alcohols and amines in integrated CO₂ capture and hydrogenation to methanol over the heterogeneous catalysts. However, mechanistic details or hypotheses of the precise alcohol-amine involvement are not reported.

In the same context, Heldebrant²⁰⁴ and co-workers examined various amines, biodegradable aminoalcohol chitosan, alcohols, and polyols such as polyethylene glycol as additives in cooperation with heterogeneous metal catalysts in CO₂ to methanol hydrogenation. Pd supported on various supports was firstly investigated for CO₂ hydrogenation in the presence of monoethanolamine (MEA). Among all the tested catalysts, Pd on ZnO gave a TON of 1,543 in converting CO₂ to *N*-formylated MEA at 150 °C under 55 bar CO₂/H₂ (1/1.5 ratio). However, no methanol was observed. It was shown that the Pd/ZnO catalyst was unable to hydrogenate the isolated formamide. In contrast, the commercial catalyst Cu/ZnO/Al₂O₃ showed the formation of methanol under identical conditions. The effect of post- and pre-combustion CO₂ capture solvents comprised of various amines and alcohols were further explored in the presence of Cu/ZnO/Al₂O₃ for the one-pot CO₂ capture and subsequent auto tandem conversion to methanol (Table 5).²⁰⁴ An environmentally benign system of bio-derived and biodegradable chitosan and polyethylene glycol (PEG₂₀₀) formed a moderate concentration of methanol, i.e. 139.5 mmol L⁻¹. The highest methanol production (methanol concentration 472 mM or ~2.16 TON over 16 h) was reported for the chitosan/diethyleneglycol system. Thanks to the high boiling properties of the solvent system, a facile separation of volatile products (such as water and methanol) was demonstrated by distillation. The chitosan/PEG₂₀₀ system was recycled three times, albeit with slightly reduced activity, which is likely due to metal sintering. However, unlike homogenous systems, wherein both formate and formamide intermediates are frequently reported in further hydrogenation to methanol, heterogeneous catalysis for the hydrogenation of CO₂ to methanol *via* formamide intermediates is rarely reported.

Table 5 Auto tandem hydrogenation of CO₂ with Cu/ZnO/Al₂O₃ in the presence of high boiling alcohol-amine as CO₂ capturing solvents



Entry	Capture solvent	HCOO ⁻ (mmol L ⁻¹)	HCOOR (mmol L ⁻¹)	CH ₃ OH (mmol L ⁻¹)
1	NMM-ethanol	-	43.2	446
2	N(Hex) ₃ -ethanol	32.4	54	373
3	EDDE-ethanol	-	299.3 ^a	0
4	Chitosan-ethanol	-	181.8	227.3
5	Chitosan-1,2-propyleneglycol	-	22.7	250
6	Chitosan-diethyleneglycol	trace	30	472.7
7	Chitosan-PEG ₂₀₀	-	7	139.5

Reaction conditions: Cu/ZnO/Al₂O₃ = 300 mg, amine 20 mmol or chitosan 1.5 g, alcohol 100 or 200 mmol or PEG₂₀₀ 20 g, 12 h, 60 bar (CO₂/2H₂), 170 °C. ^a Mixture of ester and formamide. HCOO⁻, HCOOR and CH₃OH concentrations were calculated based on ¹H NMR using 1,3,5-trimethoxybenzene as an internal standard. For details see ref. 204.

4. Conclusions and Outlook

Global warming is among the top climate change issues that we will face in the next decades. Given the high concentration of CO₂ is a major cause, its emissions in the atmosphere should be limited to a minimum, both by reducing its formation and by stimulating its use. In view of this, catalytic CO₂ hydrogenation to methanol, which can mitigate CO₂ emissions and replace fossil resources (in part), is an interesting carbon neutral solution. In this review, we summarized and analyzed the state-of-the-art catalysts for selective hydrogenation of CO₂ to methanol at mild temperatures, whereby high theoretical yield can be guaranteed for applications, as well as low capital investment can be expected. Compared to traditional, high-temperature processes that are based on reverse water gas shift reaction (RWGSR) and CO hydrogenation to methanol, several new concepts and guidelines have been developed in recent years. In this context, several catalyst types are identified here as highly promising among the reported literature:

1. Monofunctional molecular catalysts, which take advantage of high hydricity and rigidity enabled by tridentate ligands proved interesting. For example, Ru(tdppcy)(TMM) with a ligand based on a cyclohexane backbone is the most active catalyst (an average TOF up to 458 h⁻¹ and a TON up to 2,148) among these reported catalysts. Experimental and theoretical studies on Ru(triphos)(TMM) suggest that the rate determining step is the hydride transfer from the metal center to the carbonyl group of formic acid. However, catalyst deactivation over a long reaction time for yet unclear reasons is a general problem, particularly, for catalyst [Co/triphos]. Further research work is required to better understand how supramolecular interactions, such as hydrogen bonding, can affect the catalyst performance and on which parameters researchers should focus for a further rational design of the next generation catalysts.

2. M/NH bifunctional molecular catalysts, first introduced by Noyori, Ikariya and co-workers for asymmetric hydrogenation of carbonyl groups, were recently explored in CO₂ reduction to methanol. These catalysts heterolytically activate H₂ and transfer the formed metal-hydride to the carbonyl group with stabilized transition states, involving O...H-N hydrogen bonding interactions. The NH functionality provides the proton for the protonolysis steps and is regenerated concomitantly with the metal-hydride *via* a bifunctional H₂ activation. Applying such catalysts in combination with amine additives to capture CO₂ have been used as well, allowing to convert the *in situ* generated formic acid to formamide intermediates in a one-pot (two steps) or tandem process. Among the various pincer type catalysts, Ru-MACHO (or Ru-MACHO-BH) seems to be the most active and studied system, giving a TON of 9,900, upon recycling both the catalyst and pentaethylenhexamine. Notably, Ru-MACHO can also hydrogenate CO₂, captured directly from air, to methanol in the presence of alkali base, albeit with limited TONs. Detailed mechanistic studies by a combination of catalytic experiments, *in situ* spectroscopy, X-ray structure determination and DFT calculations suggest that the metal-formate and metal-carbonyl species are the resting state complexes. The transition state of H₂ activation step in the hemiaminal stage is the highest barrier of the four reaction cycles. The energy span between the metal-formate complex and transition state in the potential energy surface predicts the activity of a metal complex. Unfortunately, large amounts of amines are generally required, which is not economically beneficial for scale up applications unless integrated with an industrial CO₂ scrubbing process.

3. Aromatization-dearomatization bifunctional molecular catalysts are well known for their activity in hydrogenation of amides and esters and thus also used in a (one-pot) two steps process for CO₂ hydrogenation. Indeed, these catalysts facilitate H₂ activation, hydride/proton transfer to a carbonyl group, and the C-O bond cleavage steps by the participation of a pyridine function and its benzylic methylene protons. Moderate to high activities were observed in the hydrogenation of CO₂ derivatives, including carbonates, carbamates, ureas, and formate esters. So far, Zhou and co-workers reported the only case of direct CO₂ hydrogenation to methanol with a TON up to 2,100 using

aromatization-dearomatization bifunctional catalyst Ru-P^{tBu}N^{Pv}N^{Pv}N^{Et}, although methanol was only formed under a low CO₂ pressure. Therefore developing Milstein type bifunctional catalysts that can operate under high CO₂ pressure will be one of the important future directions.

4. Metal/metal or metal/support bifunctional heterogeneous catalysts, well-known for many transformations,²⁰⁵⁻²⁰⁹ show reasonable performance in CO₂ hydrogenation to methanol under mild conditions. The right choice of metal/metal and its oxide or metal/support combinations is crucial to obtain suitable bifunctional properties. TiO₂ showed good performance as a support in cooperation with Re, Pt and co-loaded Pt/MnO_x catalysts. Attributed to the unpaired electrons from abundant defects and dislocations at the disordered structures and edge areas, carbon was optimized as a beneficial support in Pt-Co NWs (nanowires). In line with Cu based catalysts, ZrO₂ is a promising support in cooperation with nanosized Au catalysts. The size and/or the dispersion properties of the metal and/or co-loaded metal (oxides) nanoparticles have significant effects on the catalytic properties, as demonstrated in detail for the Au nanoparticles supported on ZrO₂. Furthermore, the metal loadings and reduction conditions influence the metal redox state, and as such also the catalytic performance. As one example, the average oxidation state of the Re species responsible for the catalytic formation of methanol should be higher than 0 and below +4 for Re/TiO₂. In contrast to widely applied impregnation methods to prepare bifunctional catalysts, utilizing an encapsulation approach for instance by a MOF material may lead to unique catalysis. The idea of spatial control of support in the proximity of the active metal sites enabling intermediates stabilization along the reaction pathway, e.g. by Lewis acidic or hydrogen bonding coordination, may provide new avenues to the design of novel well-defined heterogeneous catalysts. However, despite the *in situ* observation of formate species on the catalyst surface, the stepwise mechanism of these bifunctional catalysts in CO₂ reduction to methanol is not yet clarified unambiguously.

5. Active-site/N or active-site/OH bifunctional heterogeneous catalysts were recently elaborated in a few examples with exceptional catalytic performance under mild conditions. These catalysts take advantage of N or OH functionalities that are located on the surface of the nanocatalyst and able to assist the H₂ activation, CO₂ adsorption, intermediate stabilization, and hydride/proton transfer reactions. The nanosheet structured catalyst Co₄N for instance displayed significantly higher activity than the parent nanosheet Co catalyst and benchmark Cu based catalysts for CO₂ hydrogenation to methanol due to the presence of N-H. Similarly, surface hydroxyl groups present on hydrophilic SiC quantum dots (QDs) led to a significant boost in CO₂ hydrogenation to methanol, as compared to the commercial SiC due to the direct addition of H atoms of the hydroxyl groups into CO₂ to form HCOO* as the intermediate with decreased energy barrier. This knowledge opens ways to unique approaches with high promise for the design of better heterogeneous catalysts.

6. Compared to tandem homogeneous catalysis, the cooperation of heterogeneous catalysts or homogeneous and

heterogeneous catalysts, and additives provides some benefits in the CO₂ reduction to methanol *via* formate intermediates, including solving mutual catalysts incompatibility issues thereby allowing to take full potential of the catalyst in each reduction step. For example, the combination of Cu/Mo₂C and Cu/Cr₂CuO₄ showed an enhanced production of methanol compared to the catalytic experiment only using Cu/Mo₂C *via* formate ester or formic acid intermediates. An extreme example is the cooperation of immobilized molecular catalyst Ru-P^{tBu}N^{Pv}P^{tBu}@UiO-66 and the soluble molecular catalyst Ru-P^{tBu}N^{Pv}N^{Pv} in the presence of catalytic fluorinated alcohol additives, yielding high 6,600 TON through the corresponding formate ester intermediate. In fact, the formic acid obtained by Ru-P^{tBu}N^{Pv}P^{tBu}@UiO-66 catalysis is esterified with the alcohol, catalyzed by the zirconium oxide nodes of UiO-66. The known bimolecular decomposition of both Ru molecular catalysts is nicely avoided by compartmentalization of one of the catalysts. Heterogenization of both homogeneous catalysts is an even better option. The commercial catalyst Cu/ZnO/Al₂O₃ for instance provided a moderate concentration of methanol in the presence of Chitosan-diethyleneglycol as CO₂ capturing solvent and cooperation additives. However, unlike well-defined molecular catalysts, there are many unknowns, which makes the rational optimization of such heterogeneous catalysts and additives rather challenging at this moment. Furthermore, integrated CO₂ capture and conversion to methanol route has not been disclosed yet although can be interesting considering the applied amine based CO₂ capture process.

Importantly, beyond the highlights and insights concluded in each section across homogeneous and heterogeneous catalysts that can fuel these individual areas further, one can envision to take the advantages of both homogeneous and heterogeneous catalysts as new solutions to drive CO₂ to methanol conversion under mild reaction conditions for industrial applications. Homogeneous catalysts generally show high selectivity and activity, likely thanks to the singular active metal sites that are well modulated by the steric and electronic environment provided by the ligands. Inspired by enzymes, utilizing supramolecular interactions as new tools, powerful homogeneous catalysts showing improved performances in hydrogenation, hydroformylation, C-H bond activation reactions and others are now available.²¹⁰⁻²¹⁷ However, despite these advantages and suitability to apply these catalysts to prepare challenging organic structures in fine and speciality chemicals, incorporation in continuous manufacturing and efficient recyclability are major challenges, though heterogenized²¹⁸ homogeneous catalysts have been successfully developed. Thus, homogeneous catalysts may offer less promise for large scale commodity chemicals synthesis such as methanol mainly due to the poor stability of these catalysts over long time. Additionally, there might be higher operation costs originated from (air, impurities, and moisture) sensitive ligands and poor durability of the catalysts developed up to now. In this regard, heterogeneous catalysts that are generally easy to make, easy to recycle, air compatible and typically stable over a long time offer significant benefits in the production of methanol, as also evidenced by the wide-spread application of

heterogeneous catalysts in industrial production of bulk chemicals and materials in comparison to homogeneous catalysts. However, classic heterogeneous catalysts are supported nanometal particles or clusters and only the heterogenized surface atoms catalyze the reactions with varying catalytic properties, and thus resulting in much lower activity, productivity, selectivity. Furthermore, there remains a great challenge to control the catalytic properties of such materials under mild reaction conditions. For these reasons, it is really appealing to merge homogeneous and heterogeneous catalytic benefits. Single atom catalysis concept introduced by Zhang group among others²¹⁹⁻²²⁴ may provide one applicable tool in this direction. However, despite many advances in this direction, the synthesis and advanced characterization of single atom catalysts with well-defined metal site environment are other great challenges to tackle in the near future. Furthermore, utilizing a catalytic system that combines both homogeneous and heterogeneous catalysis via a 'cooperative strategy' may be another valuable option, as illustrated by one example in this review (Figure 26). Search for such synergistic effects looks an interesting research strategy to further advance the CO₂ to methanol conversion under mild conditions. In particular, this should be of great benefit for a catalytic methanol synthesis process, of which several steps are required and as such heterogeneous and homogeneous catalysts in principle can work cooperatively, provided no incompatibility issues, that are often observed in liquid phase catalysis using homogeneous catalysts, appear or can be solved.

Furthermore, clearly, the CO₂ to methanol economy is still in its infancy despite the many notable and elegant academic concepts, which have been disclosed by scientists all over the world. Nevertheless, the reader should be aware that none of the above described works can be immediately implemented on commercial scale. Hereto, significant improvements still have to be made. Realistically for a product such as methanol, we are seeking for catalyst productivities with TONs >10⁶ and activities with TOFs >10³ h⁻¹. At the same time, no expensive additives or synthesis/purification steps are allowed, unless practically integrated for instance with an industrially applied amines based CO₂ capture process. Nevertheless, the concept of transforming renewable energy to "green" hydrogen and subsequently to methanol *via* reduction of greenhouse gas CO₂ is very attractive and, in principle, can be more energy efficient than natural photosynthesis. Thus, this transformation offers plenty of opportunities for decentralized energy storage and as alternative bulk chemical industry feedstock (methanol economy²²⁵).

We hope that the elaboration and discussion of the catalytic concepts illustrated by specific examples from literature will stimulate the design/optimization of more active, selective, and stable catalysts that can work under mild conditions for next generation CO₂ to methanol hydrogenation technologies using renewable H₂ and see these technologies brought into practical industrial applications.

Conflicts of interest

There are no conflicts to declare.

Acknowledgements

B.F.S., M.B. and B.U.W.M. acknowledge financial support from the Federal Excellence of Science (EoS) call of FWO/FNRS (BIOFACT, No. 30902231). In addition, M. B. thanks European Research Council (ERC; project NoNaCat 670986) for financial support. B. F. S. and S.-T. B. thank the CO₂ project of KU Leuven, named Biorefineries Featuring Carbon Dioxide Capturing and Utilization, for financial support. B.U.W.M. thanks the Francqui Foundation for an appointment as Collen-Francqui professor and the special research fund BOF UAntwerpen for financial support.

Notes and references

1. P. Friedlingstein, M. W. Jones, amp, apos, M. Sullivan, R. M. Andrew, J. Hauck, G. P. Peters, W. Peters, J. Pongratz, S. Sitch, C. Le Quéré, D. C. E. Bakker, J. G. Canadell, P. Ciais, R. B. Jackson, P. Anthoni, L. Barbero, A. Bastos, V. Bastrikov, M. Becker, L. Bopp, E. Buitenhuis, N. Chandra, F. Chevallier, L. P. Chini, K. I. Currie, R. A. Feely, M. Gehlen, D. Gilfillan, T. Gkritzalis, D. S. Goll, N. Gruber, S. Gutekunst, I. Harris, V. Haverd, R. A. Houghton, G. Hurtt, T. Ilyina, A. K. Jain, E. Joetzer, J. O. Kaplan, E. Kato, K. Klein Goldewijk, J. I. Korsbakken, P. Landschützer, S. K. Lauvset, N. Lefèvre, A. Lenton, S. Lienert, D. Lombardozi, G. Marland, P. C. McGuire, J. R. Melton, N. Metzl, D. R. Munro, J. E. M. S. Nabel, S.-I. Nakaoka, C. Neill, A. M. Omar, T. Ono, A. Peregón, D. Pierrot, B. Poulter, G. Rehder, L. Resplandy, E. Robertson, C. Rödenbeck, R. Séférian, J. Schwinger, N. Smith, P. P. Tans, H. Tian, B. Tilbrook, F. N. Tubiello, G. R. van der Werf, A. J. Wiltshire and S. Zaehle, *Earth Syst. Sci. Data*, 2019, **11**, 1783-1838.
2. N. von der Assen, J. Jung and A. Bardow, *Energy Environ. Sci.*, 2013, **6**, 2721.
3. R. B. Jackson, P. Friedlingstein, R. M. Andrew, J. G. Canadell, C. Le Quéré and G. P. Peters, *Environ. Res. Let.*, 2019, **14**, 121001.
4. G. P. Peters, R. M. Andrew, J. G. Canadell, P. Friedlingstein, R. B. Jackson, J. I. Korsbakken, C. Le Quéré and A. Peregón, *Nat. Clim. Change*, 2019, **10**, 3-6.
5. N. S. Diffenbaugh, D. Singh, J. S. Mankin, D. E. Horton, D. L. Swain, D. Touma, A. Charland, Y. Liu, M. Haugen, M. Tsiang and B. Rajaratnam, *Proc. Natl. Acad. Sci. U. S. A.*, 2017, **114**, 4881-4886.
6. K. Hausteijn, M. R. Allen, P. M. Forster, F. E. L. Otto, D. M. Mitchell, H. D. Matthews and D. J. Frame, *Sci. Rep.*, 2017, **7**, 15417.
7. IEA (2016), "20 years of carbon capture and storage", IEA, Paris <https://www.iea.org/reports/20-years-of-carbon-capture-and-storage>.
8. E. S. Sanz-Perez, C. R. Murdock, S. A. Didas and C. W. Jones, *Chem. Rev.*, 2016, **116**, 11840-11876.
9. A. Goepfert, M. Czaun, G. K. Surya Prakash and G. A. Olah, *Energy Environ. Sci.*, 2012, **5**, 7833.

10. R. M. Cuéllar-Franca and A. Azapagic, *J. CO₂ Util.*, 2015, **9**, 82-102.
11. IEA (2019), "Tracking Power", IEA, Paris <https://www.iea.org/reports/tracking-power-2019>.
12. https://ec.europa.eu/info/sites/info/files/iogp_-_report_-_ccs_ccu.pdf.
13. Carbon Capture: A Technology Assessment <https://fas.org/sqp/crs/misc/R41325.pdf>.
14. http://english.cas.cn/newsroom/research_news/chem/202001/t20200113_229335.shtml.
15. <https://northccuhub.eu/north-c-methanol/>.
16. J. Chen, M. McGraw and E. Y. Chen, *ChemSusChem.*, 2019, **12**, 4543-4569.
17. S. N. Riduan, Y. Zhang and J. Y. Ying, *Angew Chem. Int. Ed. Engl.*, 2009, **48**, 3322-3325.
18. S. Chakraborty, J. Zhang, J. A. Krause and H. Guan, *J. Am. Chem. Soc.*, 2010, **132**, 8872-8873.
19. M. R. Espinosa, D. J. Charboneau, A. Garcia de Oliveira and N. Hazari, *ACS Cat.*, 2018, **9**, 301-314.
20. Z. Lu and T. J. Williams, *ACS Cat.*, 2016, **6**, 6670-6673.
21. D. Yang, Q. Zhu, C. Chen, H. Liu, Z. Liu, Z. Zhao, X. Zhang, S. Liu and B. Han, *Nat. Commun.*, 2019, **10**, 677.
22. M.-Y. Lee, K. T. Park, W. Lee, H. Lim, Y. Kwon and S. Kang, *Critical Reviews in Environ. Sci. Technol.*, 2019, **50**, 769-815.
23. P. G. Jessop, T. Ikariya and R. Noyori, *Chem. Rev.*, 1995, **95**, 259-272.
24. W. H. Wang, Y. Himeda, J. T. Muckerman, G. F. Manbeck and E. Fujita, *Chem. Rev.*, 2015, **115**, 12936-12973.
25. T. C. Whitner, *Oil & Soap*, 1939, **16**, 39-44.
26. A. M. Smith and R. Whyman, *Chem. Rev.*, 2014, **114**, 5477-5510.
27. A. Stanislaus and B. H. Cooper, *Catal. Rev.*, 1994, **36**, 75-123.
28. L. Zhang, M. Zhou, A. Wang and T. Zhang, *Chem. Rev.*, 2020, **120**, 683-733.
29. W. Tang and X. Zhang, *Chem. Rev.*, 2003, **103**, 3029-3070.
30. T. Zell and D. Milstein, *Acc. Chem. Res.*, 2015, **48**, 1979-1994.
31. K. Sordakis, C. Tang, L. K. Vogt, H. Junge, P. J. Dyson, M. Beller and G. Laurenczy, *Chem. Rev.*, 2018, **118**, 372-433.
32. J. Eppinger and K.-W. Huang, *ACS Energy Let.*, 2016, **2**, 188-195.
33. G. H. Gunasekar, K. Park, K.-D. Jung and S. Yoon, *Inorg. Chem. Front.*, 2016, **3**, 882-895.
34. A. Alvarez, A. Bansode, A. Urakawa, A. V. Bavykina, T. A. Wezendonk, M. Makkee, J. Gascon and F. Kapteijn, *Chem. Rev.*, 2017, **117**, 9804-9838.
35. <https://www.statista.com/statistics/1065891/global-methanol-production-capacity/>.
36. J. Ott, V. Gronemann, F. Pontzen, E. Fiedler, G. Grossmann, D. B. Kersebohm, G. Weiss and C. Witte, in *Ullmann's Encyclopedia of Industrial Chemistry*, 2012, DOI: 10.1002/14356007.a16_465.pub3.
37. C. Li, M. Negnevitsky and X. Wang, *Energy Procedia*, 2019, **160**, 324-331.
38. G. J. Millar and M. Collins, *Ind. Eng. Chem. Res.*, 2017, **56**, 9247-9265.
39. G. A. Olah, *Angew. Chem. Int. Ed. Engl.*, 2005, **44**, 2636-2639.
40. G. A. Olah, G. K. Prakash and A. Goepfert, *J. Am. Chem. Soc.*, 2011, **133**, 12881-12898.
41. J. Zhong, X. Yang, Z. Wu, B. Liang, Y. Huang and T. Zhang, *Chem. Soc. Rev.*, 2020, **49**, 1385-1413.
42. J. C. J. Bart and R. P. A. Sneed, *Catal. Today*, 1987, **2**, 1-124.
43. K. C. Waugh, *Catal. Today*, 1992, **15**, 51-75.
44. C. H. Bartholomew and R. J. Farrauto, *Fundamentals of Industrial Catalytic Processes*, 2005.
45. S. Lee, J. G. Speight and S. K. Loyalka, *Handbook of Alternative Fuel Technologies*, 2014.
46. E. Alberico and M. Nielsen, *Chem. Commun. (Camb)*, 2015, **51**, 6714-6725.
47. F. Marocco Stuardi, F. MacPherson and J. Leclaire, *Curr. Opin. Green Sustain. Chem.*, 2019, **16**, 71-76.
48. X. Jiang, X. Nie, X. Guo, C. Song and J. G. Chen, *Chem. Rev.*, 2020, **120**, 7984-8034.
49. K.-i. Tominaga, Y. Sasaki, K. Hagihara, T. Watanabe and M. Saito, *Chem. Let.*, 1994, **23**, 1391-1394.
50. K.-i. Tominaga, Y. Sasaki, M. Kawai, T. Watanabe and M. Saito, *J. Chem. Soc., Chem. Commun.*, 1993, 629-631, DOI: 10.1039/c39930000629.
51. Y. Hayashi, *Chem Sci*, 2016, **7**, 866-880.
52. When everything is occurring in 'one pot' without further manipulation a tandem reaction is occurring. If the second step only occurs by performing specific manipulations to the reaction mixture such as addition of additional reagents, catalysts, ... the term 'one pot two steps' applies. Other labels can also be used for such a process such as 'telescoping reaction'. Finally, when the product of the first step is isolated and subsequently further reduced in a next reaction, a classical 'two step' process applies.
53. P. A. Dub and T. Ikariya, *ACS Cat.* 2012, **2**, 1718-1741.
54. M. Ito, T. Ootsuka, R. Watari, A. Shiibashi, A. Himizu and T. Ikariya, *J. Am. Chem. Soc.*, 2011, **133**, 4240-4242.
55. E. S. Wiedner, M. B. Chambers, C. L. Pitman, R. M. Bullock, A. J. Miller and A. M. Appel, *Chem. Rev.*, 2016, **116**, 8655-8692.
56. A. P. C. Ribeiro, L. M. D. R. S. Martins and A. J. L. Pombeiro, *Green Chem.*, 2017, **19**, 4811-4815.
57. J. Schneidewind, R. Adam, W. Baumann, R. Jackstell and M. Beller, *Angew. Chem. Int. Ed.*, 2017, **129**, 1916-1919.
58. F. K. Scharnagl, M. F. Hertrich, G. Neitzel, R. Jackstell and M. Beller, *Adv. Synth. Catal.*, 2018, **361**, 374-379, DOI: 10.1002/adsc.201801314.
59. X. Yan, H. Ge and X. Yang, *Inorg. Chem.*, 2019, **58**, 5494-5502.
60. S. Kar, A. Goepfert, J. Kothandaraman and G. K. S. Prakash, *ACS Catal.*, 2017, **7**, 6347-6351.
61. S. C. Mandal, K. S. Rawat, S. Nandi and B. Pathak, *Catal. Sci. Technol.*, 2019, **9**, 1867-1878.
62. S. Wesselbaum, T. Vom Stein, J. Klankermayer and W. Leitner, *Angew. Chem. Int. Ed. Engl.*, 2012, **51**, 7499-7502.
63. S. Wesselbaum, V. Moha, M. Meuresch, S. Brosinski, K. M. Thenert, J. Kothe, T. V. Stein, U. Englert, M. Holscher, J. Klankermayer and W. Leitner, *Chem. Sci.*, 2015, **6**, 693-704.
64. M. Everett and D. F. Wass, *Chem. Commun. (Camb)*, 2017, **53**, 9502-9504.
65. S. Kar, A. Goepfert and G. K. S. Prakash, *ChemSusChem*, 2019, **12**, 3172-3177.
66. F.-H. Zhang, C. Liu, W. Li, G.-L. Tian, J.-H. Xie and Q.-L. Zhou, *Chin. J. Chem.*, 2018, **36**, 1000-1002.
67. A. Yoshimura, R. Watari, S. Kuwata and Y. Kayaki, *Eur. J. Inorg. Chem.*, 2019, **2019**, 2375-2380.

68. V. Tripkovic, M. Vanin, M. Karamad, M. E. Björketun, K. W. Jacobsen, K. S. Thygesen and J. Rossmeisl, *J. Phys. Chem. C*, 2013, **117**, 9187-9195.
69. K. Kamada, J. Jung, T. Wakabayashi, K. Sekizawa, S. Sato, T. Morikawa, S. Fukuzumi and S. Saito, *J. Am. Chem. Soc.*, 2020, **142**, 10261-10266.
70. S. Fukuzumi, T. Kobayashi and T. Suenobu, *ChemSusChem*, 2008, **1**, 827-834.
71. A. J. Miller, D. M. Heinekey, J. M. Mayer and K. I. Goldberg, *Angew. Chem. Int. Ed. Engl.*, 2013, **52**, 3981-3984.
72. A. Tsurusaki, K. Murata, N. Onishi, K. Sordakis, G. Laurenczy and Y. Himeda, *ACS Catal.*, 2017, **7**, 1123-1131.
73. R. R. Schrock and J. A. Osborn, *J. Chem. Soc. D: Chem. Commun.*, 1970, 567-568, DOI: 10.1039/c29700000567.
74. I. Ojima and T. Kogure, *J. Organomet. Chem*, 1980, **195**, 239-248.
75. R. R. Schrock and J. A. Osborn, *J. Am. Chem. Soc.* 1976, **98**, 2134-2143.
76. J. A. Osborn, F. H. Jardine, J. F. Young and G. Wilkinson, *J. Chem. Soc. A. Inorg. phys. theor.*, 1966, 1711-1732, DOI: 10.1039/j19660001711.
77. R. Crabtree, *Acc. Chem. Res.*, 2002, **12**, 331-337.
78. S. E. Clapham, A. Hadzovic and R. H. Morris, *Coord. Chem. Rev.*, 2004, **248**, 2201-2237.
79. J. S. Samec, J. E. Backvall, P. G. Andersson and P. Brandt, *Chem. Soc. Rev.*, 2006, **35**, 237-248.
80. R. Malacea, R. Poli and E. Manoury, *Coord. Chem. Rev.*, 2010, **254**, 729-752.
81. W. A. Herrmann and B. Cornils, *Angew. Chem. Int. Ed. Engl.*, 1997, **36**, 1048-1067.
82. P. A. Dub, B. L. Scott and J. C. Gordon, *J. Am. Chem. Soc.*, 2017, **139**, 1245-1260.
83. F. M. Geilen, B. Engendahl, M. Holscher, J. Klankermayer and W. Leitner, *J. Am. Chem. Soc.*, 2011, **133**, 14349-14358.
84. M. Meuresch, S. Westhues, W. Leitner and J. Klankermayer, *Angew. Chem. Int. Ed. Engl.*, 2016, **55**, 1392-1395.
85. T. vom Stein, M. Meuresch, D. Limper, M. Schmitz, M. Holscher, J. Coetzee, D. J. Cole-Hamilton, J. Klankermayer and W. Leitner, *J. Am. Chem. Soc.*, 2014, **136**, 13217-13225.
86. J. R. Cabrero-Antonino, I. Sorribes, K. Junge and M. Beller, *Angew. Chem. Int. Ed. Engl.*, 2016, **55**, 387-391.
87. X. Cui, Y. Li, C. Topf, K. Junge and M. Beller, *Angew. Chem. Int. Ed.*, 2015, **54**, 10596-10599.
88. F. Ferretti, F. K. Scharnagl, A. Dall'Anese, R. Jackstell, S. Dastgir and M. Beller, *Catal. Sci. Technol.* 2019, **9**, 3548-3553.
89. J. R. Cabrero-Antonino, R. Adam, K. Junge and M. Beller, *Chem. Sci.*, 2017, **8**, 6439-6450.
90. R. Adam, J. R. Cabrero-Antonino, K. Junge, R. Jackstell and M. Beller, *Angew. Chem. Int. Ed. Engl.*, 2016, **55**, 11049-11053.
91. I. Sorribes, J. R. Cabrero-Antonino, C. Vicent, K. Junge and M. Beller, *J. Am. Chem. Soc.*, 2015, **137**, 13580-13587.
92. C. Bianchini, A. Meli, M. Peruzzini, F. Vizza and F. Zanobini, *Coord. Chem. Rev.*, 1992, **120**, 193-208.
93. H. A. Mayer, H. Otto, H. Kühbauch, R. Fawzi and M. Steimann, *J. Organomet. Chem.*, 1994, **472**, 347-354.
94. A. J. Canty, N. J. Minchin, P. C. Healy and A. H. White, *J. Chem. Soc., Dalton Trans.*, 1982, 1795-1802, DOI: 10.1039/dt9820001795.
95. B. G. Schieweck, P. Jüriling-Will and J. Klankermayer, *ACS Catal.*, 2020, **10**, 3890-3894.
96. W.-Y. Chu, Z. Culakova, B. T. Wang and K. I. Goldberg, *ACS Catal.*, 2019, **9**, 9317-9326.
97. M. Behrens, F. Studt, I. Kasatkin, S. Kuhl, M. Havecker, F. Abild-Pedersen, S. Zander, F. Girgsdies, P. Kurr, B. L. Kniep, M. Tovar, R. W. Fischer, J. K. Nørskov and R. Schlögl, *Science*, 2012, **336**, 893-897.
98. S. T. Bai, V. Sinha, A. M. Kluwer, P. R. Linnebank, Z. Abiri, P. Dydio, M. Lutz, B. de Bruin and J. N. H. Reek, *Chem. Sci.*, 2019, **10**, 7389-7398.
99. S. T. Bai, C. B. Bheeter and J. N. H. Reek, *Angew. Chem. Int. Ed. Engl.*, 2019, **58**, 13039-13043.
100. S. T. Bai, A. M. Kluwer and J. N. H. Reek, *Chem. Commun. (Camb)*, 2019, **55**, 14151-14154.
101. S. T. Bai, V. Sinha, A. M. Kluwer, P. R. Linnebank, Z. Abiri, B. Bruin and J. N. H. Reek, *ChemCatChem.*, 2019, **11**, 5322-5329.
102. L. Ackermann, *Chem. Rev.*, 2011, **111**, 1315-1345.
103. T. J. Korstanje, J. I. van der Vlugt, C. J. Elsevier and B. de Bruin, *Science*, 2015, **350**, 298-302.
104. T. Ohkuma, H. Ooka, S. Hashiguchi, T. Ikariya and R. Noyori, *J. Am. Chem. Soc.*, 1995, **117**, 2675-2676.
105. T. Ohkuma, H. Ooka, T. Ikariya and R. Noyori, *J. Am. Chem. Soc.*, 1995, **117**, 10417-10418.
106. T. Ikariya and M. Shibasaki. *Bifunctional Molecular Catalysis*, 2011.
107. T. Ikariya, *Bull. Chem. Soc. Jpn.*, 2011, **84**, 1-16.
108. R. Noyori, T. Ohkuma, M. Kitamura, H. Takaya, N. Sayo, H. Kumobayashi and S. Akutagawa, *J. Am. Chem. Soc.*, 1987, **109**, 5856-5858.
109. M. Kitamura, T. Ohkuma, S. Inoue, N. Sayo, H. Kumobayashi, S. Akutagawa, T. Ohta, H. Takaya and R. Noyori, *J. Am. Chem. Soc.*, 1988, **110**, 629-631.
110. R. Noyori and T. Ohkuma, *Angew. Chem. Int. Ed.*, 2001, **40**, 40-73.
111. R. Noyori, M. Kitamura and T. Ohkuma, *Proc. Natl. Acad. Sci. U. S. A.*, 2004, **101**, 5356-5362.
112. B. Zhao, Z. Han and K. Ding, *Angew. Chem. Int. Ed. Engl.*, 2013, **52**, 4744-4788.
113. J. Zhang, G. Leitius, Y. Ben-David and D. Milstein, *J. Am. Chem. Soc.*, 2005, **127**, 10840-10841.
114. G. van Koten, K. Timmer, J. G. Noltes and A. L. Spek, *J. Chem. Soc., Chem. Commun.*, 1978, 250-252, DOI: 10.1039/c39780000250.
115. C. J. Moulton and B. L. Shaw, *J. Chem. Soc., Dalton Trans.*, 1976, 1020-1024, DOI: 10.1039/dt9760001020.
116. W. S. J. Kelly, G. H. Ford and S. M. Nelson, *J. Chem. Soc. A. Inorg. phys. theor.*, 1971, 388-396, DOI: 10.1039/j19710000388.
117. W. V. Dahlhoff and S. M. Nelson, *J. Chem. Soc. A. Inorg. phys. theor.*, 1971, 2184-2190, DOI: 10.1039/j19710002184.
118. K. S. Rawat, A. Mahata, I. Choudhuri and B. Pathak, *J. Phys. Chem. C*, 2016, **120**, 16478-16488.
119. S. C. Mandal, K. S. Rawat and B. Pathak, *Phys. Chem. Chem. Phys.*, 2019, **21**, 3932-3941.
120. K. S. Rawat and B. Pathak, *Phys. Chem. Chem. Phys.*, 2018, **20**, 12535-12542.
121. S. Kar, A. Goepfert and G. K. S. Prakash, *Acc. Chem. Res.*, 2019, **52**, 2892-2903.

122. S. Kar, R. Sen, J. Kothandaraman, A. Goepfert, R. Chowdhury, S. B. Munoz, R. Haiges and G. K. S. Prakash, *J. Am. Chem. Soc.*, 2019, **141**, 3160-3170.
123. U. Jayarathne, N. Hazari and W. H. Bernskoetter, *ACS Catal.*, 2018, **8**, 1338-1345.
124. F. Wang, X. Tan, H. Lv and X. Zhang, *Chem. Asian J.*, 2016, **11**, 2103-2106.
125. J. Chen, J. Wang and T. Tu, *Chem. Asian J.*, 2018, **13**, 2559-2565.
126. A. Kaithal, M. Holscher and W. Leitner, *Angew. Chem. Int. Ed. Engl.*, 2018, **57**, 13449-13453.
127. D. Spasyuk, C. Vicent and D. G. Gusev, *J. Am. Chem. Soc.*, 2015, **137**, 3743-3746.
128. N. T. Fairweather, M. S. Gibson and H. Guan, *Organometallics*, 2014, **34**, 335-339.
129. A. Satapathy, S. T. Gadge and B. M. Bhanage, *ChemSusChem.*, 2017, **10**, 1356-1359.
130. J. M. John and S. H. Bergens, *Angew. Chem. Int. Ed. Engl.*, 2011, **50**, 10377-10380.
131. M. Trincado, D. Banerjee and H. Grützmacher, *Energy Environ. Sci.*, 2014, **7**, 2464-2503.
132. E. M. Lane, Y. Zhang, N. Hazari and W. H. Bernskoetter, *Organometallics*, 2019, **38**, 3084-3091.
133. L. M. M. de A. Martins, G. Arbilla and E. C. da Silva, *J. Phys. Chem. A*, 1998, **102**, 10805-10812.
134. Z. Han, L. Rong, J. Wu, L. Zhang, Z. Wang and K. Ding, *Angew. Chem. Int. Ed. Engl.*, 2012, **51**, 13041-13045.
135. L. Zhang, Z. Han, X. Zhao, Z. Wang and K. Ding, *Angew. Chem. Int. Ed. Engl.*, 2015, **54**, 6186-6189.
136. N. M. Rezayee, C. A. Huff and M. S. Sanford, *J. Am. Chem. Soc.*, 2015, **137**, 1028-1031.
137. J. Kothandaraman, A. Goepfert, M. Czaun, G. A. Olah and G. K. Prakash, *J. Am. Chem. Soc.*, 2016, **138**, 778-781.
138. S. Kar, R. Sen, A. Goepfert and G. K. S. Prakash, *J. Am. Chem. Soc.*, 2018, **140**, 1580-1583.
139. J. M. Hanusch, I. P. Kerschgens, F. Huber, M. Neuburger and K. Gademann, *Chem. Commun. (Camb)*, 2019, **55**, 949-952.
140. R. Sen, A. Goepfert, S. Kar and G. K. S. Prakash, *J. Am. Chem. Soc.*, 2020, **142**, 4544-4549, DOI: 10.1021/jacs.9b12711.
141. N. Yadav, F. Seidi, D. Crespy and V. D'Elia, *ChemSusChem.*, 2019, **12**, 724-754.
142. P. H. Dixneuf, *Nat. Chem.*, 2011, **3**, 578-579.
143. S. Fukuoka, I. Fukawa, T. Adachi, H. Fujita, N. Sugiyama and T. Sawa, *Org. Process Res. Dev.*, 2019, **23**, 145-169.
144. <https://www.shell.com/business-customers/chemicals/factsheets-speeches-and-articles/factsheets/omega.html>.
145. C. Alberti, S. Eckelt and S. Enthaler, *ChemistrySelect.*, 2019, **4**, 12268-12271.
146. X. Liu, J. G. de Vries and T. Werner, *Green Chem.*, 2019, **21**, 5248-5255.
147. J. Kothandaraman, A. Goepfert, M. Czaun, G. A. Olah and G. K. Surya Prakash, *Green Chem.*, 2016, **18**, 5831-5838.
148. A. Goepfert, M. Czaun, R. B. May, G. K. Prakash, G. A. Olah and S. R. Narayanan, *J. Am. Chem. Soc.*, 2011, **133**, 20164-20167.
149. B. Dutcher, M. Fan and A. G. Russell, *ACS Appl. Mater. Interfaces*, 2015, **7**, 2137-2148.
150. B. Lv, B. Guo, Z. Zhou and G. Jing, *Environ. Sci. Technol.*, 2015, **49**, 10728-10735.
151. S. Kim, H. Shi and J. Y. Lee, *Int. J. Greenh. Gas Control.*, 2016, **45**, 181-188.
152. B. Yu, H. Yu, Q. Yang, K. Li, L. Ji, R. Zhang, M. Megharaj and Z. Chen, *Energy Fuels*, 2019, **33**, 7500-7508.
153. F. A. Chowdhury, H. Yamada, T. Higashii, K. Goto and M. Onoda, *nd. Eng. Chem. Res.*, 2013, **52**, 8323-8331.
154. D. J. Tindall, M. Menche, M. Schelwies, R. A. Paciello, A. Schafer, P. Comba, F. Rominger, A. S. K. Hashmi and T. Schaub, *Inorg. Chem.*, 2020, **59**, 5099-5115.
155. V. Sinha, N. Govindarajan, B. de Bruin and E. J. Meijer, *ACS Catal.*, 2018, **8**, 6908-6913.
156. J. Wahlen, D. E. De Vos and P. A. Jacobs, *Org. Lett.*, 2003, **5**, 1777-1780.
157. P. J. Dyson and P. G. Jessop, *Catal. Sci. Technol.*, 2016, **6**, 3302-3316.
158. C. Gunanathan and D. Milstein, *Acc. Chem. Res.*, 2011, **44**, 588-602.
159. C. Gunanathan and D. Milstein, *Chem. Rev.*, 2014, **114**, 12024-12087.
160. E. Balaraman, B. Gnanaprakasam, L. J. Shimon and D. Milstein, *J. Am. Chem. Soc.*, 2010, **132**, 16756-16758.
161. G. A. Filonenko, R. van Putten, E. J. M. Hensen and E. A. Pidko, *Chem. Soc. Rev.*, 2018, **47**, 1459-1483.
162. Y.-N. Li, R. Ma, L.-N. He and Z.-F. Diao, *Catal. Sci. Technol.*, 2014, **4**, 1498-1512.
163. E. Balaraman, Y. Ben-David and D. Milstein, *Angew. Chem. Int. Ed. Engl.*, 2011, **50**, 11702-11705.
164. E. Balaraman, C. Gunanathan, J. Zhang, L. J. Shimon and D. Milstein, *Nat. Chem.*, 2011, **3**, 609-614.
165. A. Kumar, T. Janes, N. A. Espinosa-Jalapa and D. Milstein, *Angew. Chem. Int. Ed. Engl.*, 2018, **57**, 12076-12080.
166. U. K. Das, A. Kumar, Y. Ben-David, M. A. Iron and D. Milstein, *J. Am. Chem. Soc.*, 2019, **141**, 12962-12966.
167. J. R. Khusnutdinova, J. A. Garg and D. Milstein, *ACS Catal.*, 2015, **5**, 2416-2422.
168. C. A. Huff and M. S. Sanford, *J. Am. Chem. Soc.*, 2011, **133**, 18122-18125.
169. W. Li, J.-H. Xie, M.-L. Yuan and Q.-L. Zhou, *Green Chem.*, 2014, **16**.
170. C. A. Huff and M. S. Sanford, *ACS Catal.*, 2013, **3**, 2412-2416.
171. M. Vogt, A. Nerush, Y. Diskin-Posner, Y. Ben-David and D. Milstein, *Chem. Sci.*, 2014, **5**, 2043-2051.
172. H. Li, M. Wen and Z. X. Wang, *Inorg. Chem.*, 2012, **51**, 5716-5727.
173. X. Yang, *ACS Catal.*, 2012, **2**, 964-970.
174. F. Hasanayn and A. Baroudi, *Organometallics*, 2013, **32**, 2493-2496.
175. F. Hasanayn, A. Baroudi, A. A. Bengali and A. S. Goldman, *Organometallics*, 2013, **32**, 6969-6985.
176. K. W. Ting, T. Toyao, S. M. A. H. Siddiki and K.-i. Shimizu, *ACS Catal.*, 2019, **9**, 3685-3693.
177. J. Zeng, K. Fujimoto and N. Tsubaki, *Energy Fuels*, 2002, **16**, 83-86.
178. C. Reller, M. Poge, A. Lissner and F. O. Mertens, *Environ. Sci. Technol.*, 2014, **48**, 14799-14804.
179. J. Kothandaraman, R. A. Dagle, V. L. Dagle, S. D. Davidson, E. D. Walter, S. D. Burton, D. W. Hoyt and D. J. Heldebrant, *Catal. Sci. Technol.*, 2018, **8**, 5098-5103.
180. R. Yang, X. Yu, Y. Zhang, W. Li and N. Tsubaki, *Fuel*, 2008, **87**, 443-450.

181. T. Toyao, S. Kayamori, Z. Maeno, S. M. A. H. Siddiki and K.-i. Shimizu, *ACS Catal.*, 2019, **9**, 8187-8196.
182. A. V. Mironenko and D. G. Vlachos, *J. Am. Chem. Soc.*, 2016, **138**, 8104-8113.
183. S. Bai, Q. Shao, Y. Feng, L. Bu and X. Huang, *Small*, 2017, **13**.
184. Y. Chen, S. Choi and L. T. Thompson, *J. Catal.*, 2016, **343**, 147-156.
185. C. Wu, P. Zhang, Z. Zhang, L. Zhang, G. Yang and B. Han, *ChemCatChem.*, 2017, **9**, 3691-3696.
186. S. D. Senanayake, P. J. Ramírez, I. Waluyo, S. Kundu, K. Mudiyansele, Z. Liu, Z. Liu, S. Axnanda, D. J. Stacchiola, J. Evans and J. A. Rodriguez, *J. Phys. Chem. C*, 2016, **120**, 1778-1784.
187. G. Bonura, M. Cordaro, C. Cannilla, F. Arena and F. Frusteri, *Appl. Catal. B: Environ.*, 2014, **152-153**, 152-161.
188. E. S. Gutterød, A. Lazzarini, T. Fjermestad, G. Kaur, M. Manzoli, S. Bordiga, S. Svelle, K. P. Lillerud, E. Skulason, S. Oien-Odegaard, A. Nova and U. Olsbye, *J. Am. Chem. Soc.*, 2020, **142**, 999-1009.
189. E. S. Gutterød, S. Øien-Ødegaard, K. Bossers, A.-E. Nieuwelink, M. Manzoli, L. Braglia, A. Lazzarini, E. Borfecchia, S. Ahmadigoltapeh, B. Bouchevreau, B. T. Lønstad-Bleken, R. Henry, C. Lamberti, S. Bordiga, B. M. Weckhuysen, K. P. Lillerud and U. Olsbye, *Ind. Eng. Chem. Res.*, 2017, **56**, 13206-13218.
190. E. S. Gutterød, S. H. Pulumati, G. Kaur, A. Lazzarini, B. G. Solemsli, A. E. Gunnaes, C. Ahoba-Sam, M. E. Kalyva, J. A. Sannes, S. Svelle, E. Skulason, A. Nova and U. Olsbye, *J. Am. Chem. Soc.*, 2020, **142**, 17105-17118, DOI: 10.1021/jacs.0c07153.
191. L. Wang, W. Zhang, X. Zheng, Y. Chen, W. Wu, J. Qiu, X. Zhao, X. Zhao, Y. Dai and J. Zeng, *Nat. Energy*, 2017, **2**, 869-876.
192. Y. Li, S. H. Chan and Q. Sun, *Nanoscale*, 2015, **7**, 8663-8683.
193. S. Bai, Q. Shao, P. Wang, Q. Dai, X. Wang and X. Huang, *J. Am. Chem. Soc.*, 2017, **139**, 6827-6830.
194. J. A. Rodriguez, P. Liu, D. J. Stacchiola, S. D. Senanayake, M. G. White and J. G. Chen, *ACS Catal.*, 2015, **5**, 6696-6706.
195. Y. Peng, L. Wang, Q. Luo, Y. Cao, Y. Dai, Z. Li, H. Li, X. Zheng, W. Yan, J. Yang and J. Zeng, *Chem.*, 2018, **4**, 613-625.
196. D. E. Fogg and E. N. dos Santos, *Coord. Chem. Rev.*, 2004, **248**, 2365-2379.
197. Y. Chen, S. Choi and L. T. Thompson, *ACS Catal.*, 2015, **5**, 1717-1725.
198. J. Chen, X. Gong, J. Li, Y. Li, J. Ma, C. Hou, G. Zhao, W. Yuan and B. Zhao, *Science*, 2018, **360**, 1438-1442.
199. B. An, Z. Li, Y. Song, J. Zhang, L. Zeng, C. Wang and W. Lin, *Nat. Catal.*, 2019, **2**, 709-717.
200. T. M. Rayder, E. H. Adillon, J. A. Byers and C.-K. Tsung, *Chem.*, 2020, **6**, 1742-1754.
201. G. A. Filonenko, R. van Putten, E. N. Schulpen, E. J. M. Hensen and E. A. Pidko, *ChemCatChem.*, 2014, **6**, 1526-1530.
202. J. Zhang, G. Leitus, Y. Ben-David and D. Milstein, *Angew. Chem. Int. Ed. Engl.*, 2006, **45**, 1113-1115.
203. J. V. Morabito, L. Y. Chou, Z. Li, C. M. Manna, C. A. Petroff, R. J. Kyada, J. M. Palomba, J. A. Byers and C. K. Tsung, *J. Am. Chem. Soc.*, 2014, **136**, 12540-12543.
204. J. Kothandaraman and D. J. Heldebrant, *Green Chem.*, 2020, **22**, 828-834.
205. J. S. Wang, F. Z. Jin, H. C. Ma, X. B. Li, M. Y. Liu, J. L. Kan, G. J. Chen and Y. B. Dong, *Inorg. Chem.*, 2016, **55**, 6685-6691.
206. Y. Yan, B. Y. Xia, B. Zhao and X. Wang, *J. Mater. Chem. A*, 2016, **4**, 17587-17603.
207. S. Shylesh and W. R. Thiel, *ChemCatChem.*, 2011, **3**, 278-287.
208. A. M. Robinson, J. E. Hensley and J. W. Medlin, *ACS Catal.*, 2016, **6**, 5026-5043.
209. P. Sudarsanam, R. Zhong, S. Van den Bosch, S. M. Coman, V. I. Parvulescu and B. F. Sels, *Chem. Soc. Rev.*, 2018, **47**, 8349-8402.
210. K. T. Mahmudov, A. V. Gurbanov, F. I. Guseinov and M. F. C. Guedes da Silva, *Coord. Chem. Rev.*, 2019, **387**, 32-46.
211. H. J. Davis and R. J. Phipps, *Chem. Sci.*, 2017, **8**, 864-877.
212. F. D. Toste, M. S. Sigman and S. J. Miller, *Acc. Chem. Res.*, 2017, **50**, 609-615.
213. P. Dydio and J. N. H. Reek, *Chem. Sci.*, 2014, **5**, 2135-2145.
214. C. Sambiagio, D. Schonbauer, R. Blicke, T. Dao-Huy, G. Pototschnig, P. Schaaf, T. Wiesinger, M. F. Zia, J. Wencel-Delord, T. Besset, B. U. W. Maes and M. Schnurch, *Chem. Soc. Rev.*, 2018, **47**, 6603-6743.
215. K. Murugesan, T. Senthamarai, V. G. Chandrashekar, K. Natte, P. C. J. Kamer, M. Beller and R. V. Jagadeesh, *Chem. Soc. Rev.*, 2020, **49**, 6273-6328.
216. D. Formenti, F. Ferretti, F. K. Scharnagl and M. Beller, *Chem. Rev.*, 2019, **119**, 2611-2680.
217. S. Zhang, H. Neumann and M. Beller, *Chem. Soc. Rev.*, 2020, **49**, 3187-3210.
218. A. E. C. Collis and I. T. Horváth, *Catal. Sci. Technol.* 2011, **1**.
219. X. Cui, W. Li, P. Ryabchuk, K. Junge and M. Beller, *Nature Catal.*, 2018, **1**, 385-397.
220. B. Qiao, A. Wang, X. Yang, L. F. Allard, Z. Jiang, Y. Cui, J. Liu, J. Li and T. Zhang, *Nat. Chem.*, 2011, **3**, 634-641.
221. X. F. Yang, A. Wang, B. Qiao, J. Li, J. Liu and T. Zhang, *Acc. Chem. Res.*, 2013, **46**, 1740-1748.
222. L. Zhang, Y. Ren, W. Liu, A. Wang and T. Zhang, *Natl. Sci. Rev.*, 2018, **5**, 653-672.
223. R. T. Hannagan, G. Giannakakis, M. Flytzani-Stephanopoulos and E. C. H. Sykes, *Chem. Rev.*, 2020, **120**, 12044-12088.
224. A. Wang, J. Li and T. Zhang, *Nat. Rev. Chem*, 2018, **2**, 65-81.
225. T. B. Bonenkamp, L. M. Middelburg, M. O. Hosli and R. F. Wolfenbittel, *Renew. Sust. Energ. Rev.*, 2020, **120**, 109667.